

# **Passive Hydro-Actuated Unfolding of Ice Plant Seed Capsules as a Concept Generator for Autonomously Deforming Devices**

vorgelegt von  
M.Sc.  
Khashayar Razghandi  
geb. in Teheran

von der Fakultät III - Prozesswissenschaften  
der Technischen Universität Berlin  
zur Erlangung des akademischen Grades

Doktor der Ingenieurwissenschaften  
- Dr.-Ing. –

genehmigte Dissertation

Promotionsausschuss:

Vorsitzender: Prof. Dr. Manfred Wagner  
Gutachterin: Prof. Dr.-Ing. Claudia Fleck  
Gutachter: Prof. Dr. Ingo Burgert

Tag der wissenschaftlichen Aussprache: 20. November 2014

Berlin 2015

This thesis was prepared from February 2010 to February 2014

at the

Max Planck Institute of Colloids and Interfaces,

Biomaterials Department

and

ETH Zürich, Institute for Building Materials,

Wood Materials Science Group

To my parents...

پیدر و مادرم

## Abstract

Numerous examples of actuated-movements with specific responses of the structure to external stimuli can be found in biological systems, which can be a potential source of inspiration for the design of energy-efficient “smart” devices. From the hydro-driven rapid snapping of the Venus fly trap leaves to simple hydro-responsive bending of wheat awns, various plants have evolved different mechanisms to utilize water as an actuator to undergo a desired deformation via sophisticated architecture at different hierarchical levels of their systems. Some species of the family Aizoaceae, also known as ice plants, show an ingenious example of such passive actuation systems, as they evolved a smart mechanism to open their protective seed capsules and release their seeds only in the presence of liquid water (rain).

The scope of the first phase of the thesis was to investigate the underlying mechanism and the structural and compositional basis of the hydro-actuated movement of the ice plant seed capsules (*Delosperma nakurense*) at several hierarchical levels. Five hygroscopic keels were found to be the active muscles responsible for the reversible origami-like unfolding of the seed capsule upon wetting. Each keel consists of two honeycomb-like tissues made up of highly swellable hexagonal/elliptical shape cells running along an inert backing tissue. The significant swelling of a highly swellable cellulosic inner layer (CIL) inside the lumen of these cells was found to be the main engine of the actuation. The morphology and physicochemical response of the CIL to water was studied using a variety of techniques and it was shown that the entropic changes during water absorption were the main driving force for swelling of the cells. The translation of such relatively small available energy to the complex movement at a macro scale was explained by an optimized design at different hierarchical levels of the system. The cooperative anisotropic swelling of the cells in the hygroscopic tissue is translated into a flexing movement of the structure via simple Timoshenko’s bilayer bending principle, which then results in an unfolding of the seed capsules.

Inspired by the underlying mechanism in ice plant, two different strategies were developed to translate small strains at micro scale into a pre-programmed macro movement of a honeycomb structure. Through a clever application of the same simple concepts, one can “mimic” the biological model system in a broader engineering sense, with potential applications of such passive switches in biomedicine, agricultural engineering or architectural design.

# Table of content

<b>Abstract</b> .....	<b>i</b>
<b>Table of content</b> .....	<b>ii</b>
<b>1 Introduction</b> .....	<b>1</b>
1.1 Nature as a source of inspiration .....	1
1.1.1 <i>Biomimetics</i> .....	4
1.2 Hydro-actuated movement and stress generation in the plant kingdom .....	5
1.2.1 <i>Water as an actuator</i> .....	7
<i>Inflation vs. Swelling</i> .....	8
<i>Water in plant cells</i> .....	10
1.2.2 <i>Actuation based on inflation/deflation of living turgid cell</i> .....	16
<i>Differential Growth; Plastic deformation of primary cell wall</i> .....	16
<i>Deformation by an elastic response of the cell wall upon turgor pressure</i> .....	16
<i>Venus flytrap; a turgor-based rapid movement</i> .....	17
1.2.3 <i>Passive actuation based on anisotropic swelling/shrinkage of dead tissue</i> .....	18
<i>Passive hydro-actuation based on bending bi-layer structures</i> .....	19
<i>Passive hydro-actuation based on differential swelling of secondary cell wall layers</i> .....	23
1.3 Ice plant hydro-actuated seed dispersal.....	24
1.4 Objectives of the thesis .....	26
<b>2 Materials and Methods</b> .....	<b>28</b>
2.1 Analysis of the ice plant hydro-actuated movement .....	28
<i>Sample preparation</i> .....	28
<i>Cell dimension measurements</i> .....	28
<i>Raman spectroscopy</i> .....	28
<i>Confocal microscopy</i> .....	29
<i>Enzymatic removal of cellulosic inner layer</i> .....	29
<i>Cryo Scanning Electron Microscopy (Cryo SEM)</i> .....	29
<i>Measuring keel's water uptake</i> .....	30

	<i>Thermogravimetric analysis (TGA)</i> .....	30
	<i>Keel opening in water-PEG solution</i> .....	31
2.2	<b>Biomimetic design</b> .....	31
	<i>Super porous hydrogel in 3D printed honeycomb frame</i> .....	31
	<i>Hydro-actuated bilayer-cell prototype</i> .....	32
	<i>Modulus of elasticity of spruce veneers and paper</i> .....	33
	<i>Swelling properties of spruce and paper</i> .....	33
	<i>Bilayer-cell hydro-actuated movement</i> .....	34
	<i>Bilayer-cell hydro-actuated force generation</i> .....	34
<b>3</b>	<b>Investigation of the ice plant hydro-actuated seed dispersal</b> .....	<b>36</b>
3.1	Ice plant hierarchical structure and basic movements.....	36
3.2	Characterization of Hygroscopic keel cells.....	40
3.2.1	<i>Keel's cells morphology and composition</i> .....	40
3.2.2	<i>Morphology of the cellulosic inner layer (CIL)</i> .....	43
3.2.3	<i>Enzymatic removal of the cellulosic inner layer</i> .....	46
3.3	Physicochemistry of keel's actuation .....	47
3.3.1	<i>Thermogravimetric analysis (TGA)</i> .....	48
	<i>Sorption isotherm</i> .....	48
	<i>Desorption experiment</i> .....	48
3.3.2	<i>Keel's actuation at various concentration of PEG-water solutions</i> .....	50
3.3.3	<i>Actuation in different swelling agents</i> .....	52
<b>4</b>	<b>The underlying mechanisms of the hydro-actuated movement</b> .....	<b>54</b>
4.1	The cellulosic inner layer (CIL) as an actuator .....	54
4.2	CIL water uptake and swelling mechanism .....	54
4.3	Swelling-Inflation: a coupled strategy .....	57
4.4	Unidirectional expansion and flexing of the keels .....	58
4.5	Chemo-mechanical model for actuation .....	60
4.6	Origami-like folding/unfolding of the seed capsules .....	65
4.7	Ecological adaptation .....	68
<b>5</b>	<b>Biomimetic design</b> .....	<b>69</b>

5.1	Abstraction of the principles behind ice plant’s hydro-actuated movement.....	71
	‘Swelling-inflation’ strategy .....	72
	Tailoring the anisotropy of swelling .....	72
	From anisotropic expansion to more sophisticated movements.....	73
5.2	Bio-inspired hydro-responsive hydrogel-filled honeycomb actuators.....	73
5.3	Hydro-actuated bilayer-honeycomb prototype.....	75
5.3.1	Principle of the design at various hierarchical levels .....	75
5.3.2	Material selection and characterization.....	76
5.3.3	Passive hydro-actuation of bilayer-cells and honeycomb .....	78
<b>6</b>	<b>Summary and conclusion .....</b>	<b>84</b>
<b>7</b>	<b>Outlook.....</b>	<b>86</b>
	<b>Bibliography .....</b>	<b>88</b>
	<b>List of Figures.....</b>	<b>v</b>
	<b>Acknowledgements .....</b>	<b>vii</b>
	<b>Curriculum Vitae .....</b>	<b>viii</b>

# 1 Introduction

## 1.1 Nature as a source of inspiration

Humans as a species capable of tool making, have always been curious and in search for better and more suitable material to make the necessary tools satisfying the variety of their needs, from early housing constructions and simple hunting tools to today's space shuttles. One of the available resource from the early ages was the biological materials in human's environments like wood, wool, bone, etc. which would to some extent satisfy the basic needs of the time by being utilized more or less in the same area of function they were designed for in the natural system. Beside some exceptions, the only processing needed from the human part was basic processing of the material with defined structure and properties, into the desired shape and form like weaving, carving etc. By further advancement of the societies the need for better and more complex tools led to further development of both "material" and "structural" aspects of human engineering. However, there are fundamental differences between the biological materials and structures and human engineered systems.

One of the main differences between natural and engineered materials comes from the basic building blocks used in their structure (Figure 1). Being restricted to the available resources in the environment, natural systems utilize only a few basic elements from the periodic table, while human engineering makes use of a huge variety of elements from carbon and nitrogen to more scarce elements like titanium etc. Natural structures are mainly made up of composite materials which depending on the function, can be almost completely organic (skin, hair, tendon, cartilage, plant cell walls etc.), or organic-inorganic hybrid materials (tooth, bone, crustacean cuticle etc.). Besides, natural materials are more or less heterogeneous which enables them to preserve a local adaptation of their physical, chemical or mechanical properties suitable for the required local function.

Biological material grow according to their genetic recipe, which itself is a result of an incremental change through 3.8 billion years of blind evolutionary R&D, which has given nature enough time to come up with more or less optimized design solutions to satisfy a variety of functions in need. Hence, these structures have evolved to be multifunctional, efficient in respect to the available resources and flexible in terms of adaptation in response to the changing environmental conditions. Human fabrication on the other hand, is based on a secure and exact design, fulfilling a specific function, mainly achieved through a not so efficient process which can be shortly described as "heat, beat, treat"; usually using high



energy (heat, pressure etc.) to extract, shape and adjust the required properties of the material into a quasi-final product, and ending with yet again costly finishing processes. The growth process also enables the biological systems to build up hierarchical structure from nano to macro scale. Although engineered structure can also show two to three levels of hierarchical design, the extent of this multi-level architecture in natural material can go as high ten levels of hierarchy, with composition and architecture at each hierarchical level preserving a specific function at that specific scale and in overall properties and function of the system in macro (Thompson 1992; Lakes 1993; Tirrell 1994; Jeronimidis and Atkins 1995; Elices 2000; Fratzl 2003; Fratzl 2007; Fratzl and Weinkamer 2007; Aizenberg and Fratzl 2009; Bhushan 2009; Fratzl and Barth 2009; Dunlop and Fratzl 2010; Knippers and Speck 2012).

Moreover, nature has a quite different set of boundary condition as opposed to those faced in human engineering, and any of those multitudes of boundary conditions might play a crucial role in the development of the structure. Biological materials are made through a bottom-up growth process where both material (microstructure) and the final form have to be designed simultaneously through self-assembly with regard to the required function. The whole growth process can be influenced by external environmental conditions (force, light, available resource, etc.), which makes it in essence a dynamic and adaptive process, completely different from the static top-down human fabrication where the possible external influences have to be considered and brought into an exact design in advance. Hence, in studying the natural systems, special attention has to be given to those limiting biological and physical conditions and the context in which that feature has developed (Thompson 1992; Jeronimidis and Atkins 1995; Fratzl 2007; Aizenberg and Fratzl 2009; Bhushan 2009; Knippers and Speck 2012).

<b>Biological Material</b>	<b>Engineering Materials</b>
Small number of light elements: C, N, O, H, Ca, P, S, Si,...	Large variety of elements: Fe, Cr, Ni, Al, Si, C, N, O,...
Growth Biologically controlled Self-assembly	Fabrication "Heat, Beat, Treat", melt, powders, solutions, etc.
Approximate Design	Exact design

Hierarchical structuring at various scales	Forming (parts) and microstructuring (material)
Adaptation of form & structure to the function	Material selection according to function
Adaptation to changing environmental conditions Healing; self-repair Modeling and remodeling	Secure desing consideration of the possible extreme condition in function; (maximum load, fatigue, etc.)

**Figure 1. Natural vs. Engineering materials.** *Difference between biological and engineering materials on environmental conditions, basic available elements as building blocks and modes of fabrication, results in different strategies to achieve the desired function (re-sketched with permission after; Fratzl 2007).*

However, considering all these conditions and constrains, nature has come up with smart solutions to deal with the environmental challenges faced over long evolutionary history. Few examples of such solutions that can be used as a source of inspiration for development and improvement of human engineering can be categorized as follow;

- Variety of different surface properties such as super hydrophobicity, high/ low or reversible adhesion etc. (Barthlott and Neinhuis 1997; Arzt, Gorb et al. 2003; Federle, Barnes et al. 2006; Bhushan and Sayer 2008; Gorb 2009; Gorb 2012)
- Self-healing and self-repair capacity (Mattheck and Bethge 1998; Thompson, Kindt et al. 2001; Keckes, Burgert et al. 2003; Fratzl, Burgert et al. 2004; Currey 2006; Fantner, Oroudjev et al. 2006; Gupta, Seto et al. 2006; Zwaag 2007)
- Special photonic features like structural coloration etc. (Aizenberg, Tkachenko et al. 2001; Sundar, Yablon et al. 2003; Vukusic and Sambles 2003; Michielsen and Stavenga 2008; Mäthger, Denton et al. 2009)
- Outstanding mechanical properties in combination with light weight etc. (Vincent 1990; Thompson 1992; Lakes 1993; Jeronimidis and Atkins 1995; Mattheck 1998; Mattheck and Bethge 1998; Rho, Kuhn-Spearing et al. 1998; Weiner and Wagner 1998; Elices 2000; Kamat, Su et al. 2000; Collins 2004; Fratzl, Burgert et al. 2004; Fratzl, Gupta et al. 2004; Wegst and Ashby 2004; Raabe, Sachs et al. 2005; Burgert 2006; Currey 2006; Fratzl 2007; Fratzl and Weinkamer 2007; Meyers, Chen et al.

2008; Ortiz and Boyce 2008; Bhushan 2009; Dunlop and Fratzl 2010; Keckes, Burgert et al. 2003).

- Metabolism dependent or material-based sensory systems for actuated motion and stress generation (Barth 1998; Fratzl and Barth 2009, Haupt 1977; Forterre, Skotheim et al. 2005; Skotheim and Mahadevan 2005; Burgert and Fratzl 2009; Fratzl and Barth 2009; Martone, Boller et al. 2010).

### 1.1.1 *Biomimetics*

The term biomimetic (bionic, bio-inspiration etc.) refers to the science of learning and transferring such optimized solutions observed in nature into the technical application in science, engineering, design etc., with the field covering a wide range of researches from the study of biologically produced materials and structures and the structure-function relation in the biological system, to understand a specific biological process, synthesis or mechanisms etc. The topic is in its essence an interdisciplinary field where researchers from various disciplines from biology, physics, chemistry, mathematics, materials science and engineering etc. work together to understand and extract the underlying principles behind the specific feature/property of interest and translate them into more abstract, simpler models applicable to technical problems (Vincent and Mann 2002; Fratzl 2007; Speck and Speck 2008; Aizenberg and Fratzl 2009; Bhushan 2009; Fratzl and Barth 2009; Martone, Boller et al. 2010; Paris, Burgert et al. 2010; Shimomura 2010).

Most biomimetic research gets initiated in the biology discipline, with a particular feature of a biological system attracting the attention of researchers as a source of inspiration with the potential to be transferred into technical application (bottom-up approach). In the first step, a thorough multidisciplinary analysis of a biological system with a special feature of interest (e.g. outstanding mechanical behavior), helps to have a better understanding of the underlying principles responsible for that property (e.g. structure-function relationships). In next steps, by detaching from the biological system, the research focuses on the abstraction of the discovered principles into simpler models, which are more amenable for technical implementation. However, the motivation can also come from the engineering side (top-down approach), where the need for the development of a new system or improvement of an already existing product can start a systematic investigation of various biological systems with the potential to offer a suitable solution to the problem in hand (Figure 2) (Vincent and Mann 2002; Speck and Speck 2008; Bhushan 2009; Paris, Burgert et al. 2010).

Throughout the whole process, one has to look at the biological model as a concept generator rather than a direct blueprint, and consider the difference between the specific context (boundary conditions) in which the biological system has developed and the constraining factors in human fabrication (the existing engineering capabilities, safety issues, cost etc.).

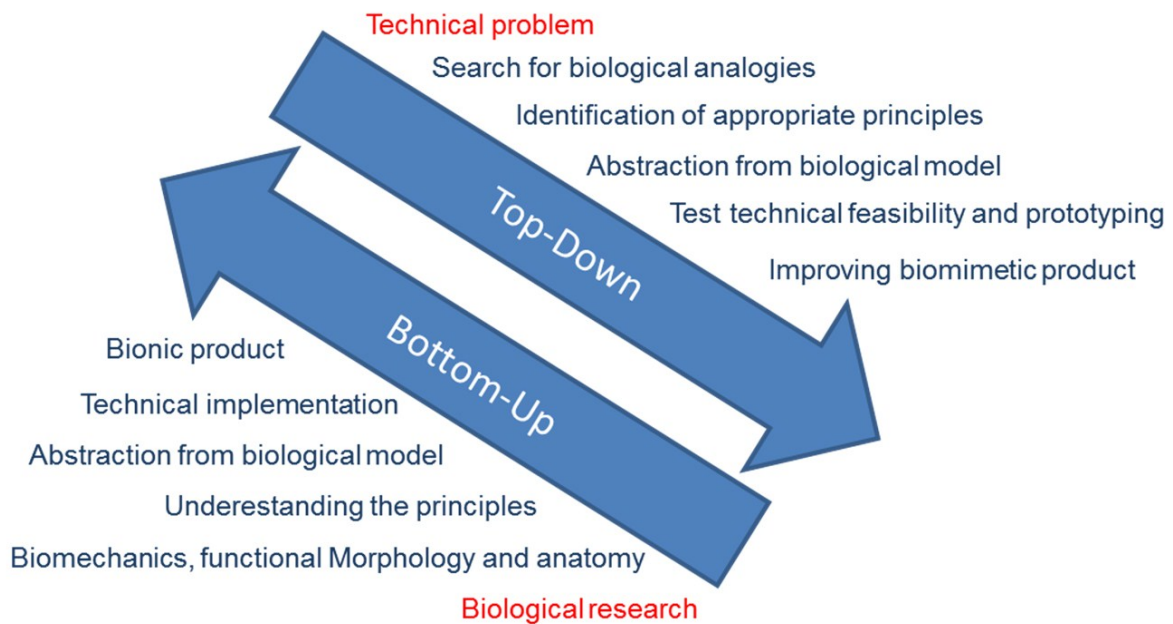


**Figure 2. Biomimetic approaches.** Bottom-up process; starting from the biological model system. Top down process; driven from the technological demands (re-sketched after Speck and Speck 2008).

One of the research fields which has gained a rising interest in recent years as a rich source for bio-inspired design of “smart” systems, is the actuated movement and stress generation in plant kingdom.

## 1.2 Hydro-actuated movement and stress generation in the plant kingdom

Plants are commonly reflected to be stationary living organisms and are not as much known for their ability to move in a detectable time scale for human eyes. Nevertheless, movement is an essential part of plant life, from movements associated to plant growth and acquiring nutrition, to spatial reorientation, seed dispersal, defense, etc. (Hart 1990; Burgert and Fratzl 2009). To satisfy such needs, plants have evolved a variety of mechanisms for stress generation and organ actuations. In all those stress generation or movement related mechanisms water plays a crucial role. The interaction of water with the plant material at

the nanoscale of the cell walls gets transferred to a response in macro scale through a sophisticated structural hierarchy of the plant body (Burgert and Fratzl 2009). Skotheim and Mahadevan (Skotheim and Mahadevan 2005) categorize different plant movements according to their speed in three basic groups (Figure 3).

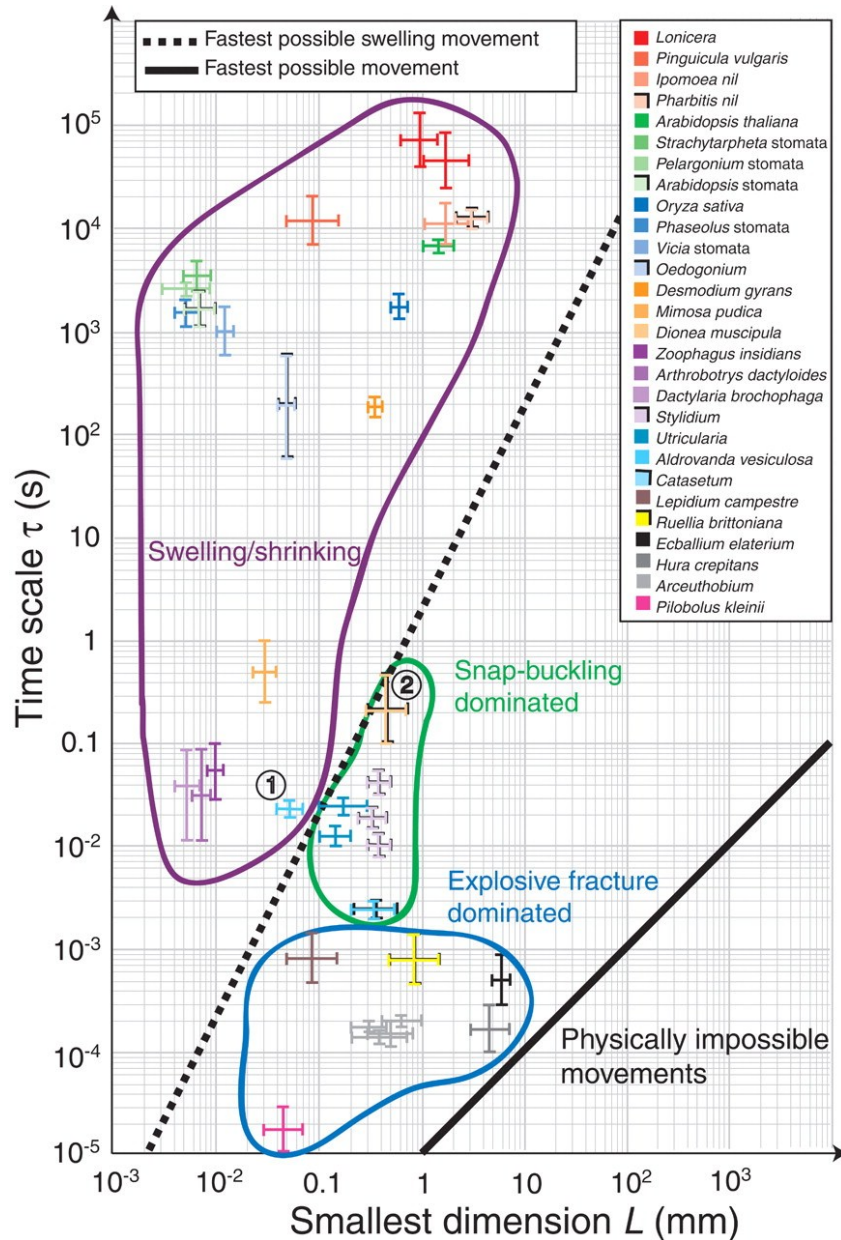


**Figure 3. Classification of plant and fungal movements.** The duration of the movement ( $\tau$ ) is plotted against the smallest macroscopic dimension of the moving part ( $L$ ). Different actuated movements are categorized into two modes of motion; slow (swelling/shrinkage) and fast (snap-buckling, explosive fracture), (Reprinted with permission from; Skotheim and Mahadevan 2005).

The slow deformations limited by the speed of fluid transport categorized as swelling/shrinking movements can be found above the dotted line in figure 3. The relatively faster ones are based on the storage and sudden release of elastic energy via

geometrical constraints and are shown in between the dotted line and above the limit of the physically possible movements. The two subcategories of the fast movements, snap-buckling and explosive fracture are only different in the mechanism of how the stored energy is released.

In general, two basic categories of plant-water interactions that induce stresses and plant movements can be distinguished. The first category is based on variation of the inner pressure and volume of the living plant cells due to active influx/efflux of water into the cells (Hodick and Sievers 1989; Sibaoka 1991; Fromm and Lautner 2007; Moran 2007; Uehlein and Kaldenhoff 2008). Actuations based on variation of the turgor pressure are commonly slow movements like stomatal movements (Hetherington and Woodward 2003; Roelfsema and Hedrich 2005). However, faster movements can also be achieved when the turgor pressure based mechanisms are combined with geometrical instabilities to go beyond the speed limitation of fluid transport, as in case of the snap-buckling movement of Venus flytrap (Hodick and Sievers 1989; Forterre, Skotheim et al. 2005; Volkov, Adesina et al. 2008). In some cases, an explosive seed dispersal is achieved through the release of the stored elastic energy accompanied by sudden rupture of pre-stressed tissues (Levin, Muller Landau et al. 2003). In contrast, the second category is passive hydro-actuation based on the swelling/shrinkage of thick and rigid dead cell walls, which can result in the generation of internal stresses or an organ movement. The required structural information for passive actuation is embedded at different hierarchical levels of the system, which allows even dead organs to be actuated by various environmental stimuli to perform a targeted deformation. As a consequence, these latter systems are independent of any control or energy input from the plant metabolism (Burgert and Fratzl 2009). Adjustments of the spatial orientation of organs such as leaning stems or branches is a wide spread example of extremely slow movements in this category (Okuyama, Yamamoto et al. 1994; Burgert, Eder et al. 2007; Goswami, Dunlop et al. 2008; Burgert and Fratzl 2009), while opening and closing of pine cone scales (Dawson, Vincent et al. 1997) or moisture dependent bending of wild wheat awns (Elbaum, Zaltzman et al. 2007) are examples of relatively faster but still rather slow passive hydro-actuated deformation.

### 1.2.1 Water as an actuator

Water possesses a large dipole moment that enables it to participate in a wide range of reactions, with a special one being the ability to build up hydrogen bonds with itself and other available solutes. The energy of a hydrogen bond lies in between the strong covalent

bonds and relatively loose Van der Waals forces, which makes a suitable compromise to have a degree of dynamism as well as stability. The ability to form hydrogen bonds with a large variety of biomolecules gives water the ability to be utilized as an ‘inflating’ or ‘swelling’ agent and provide the energy required for the movement or stress generation.

### ***Inflation vs. Swelling***

***Inflation*** can be defined as a change in the volume of a confined geometry due to the variation of pressure of the gas/liquid inside the cell. Changes in the water/gas pressure inside a confined geometry (sphere, cylinder, etc.) can exert stress on the walls. The generated stresses in the walls of a sphere or cylinder are illustrated in Figure 4.

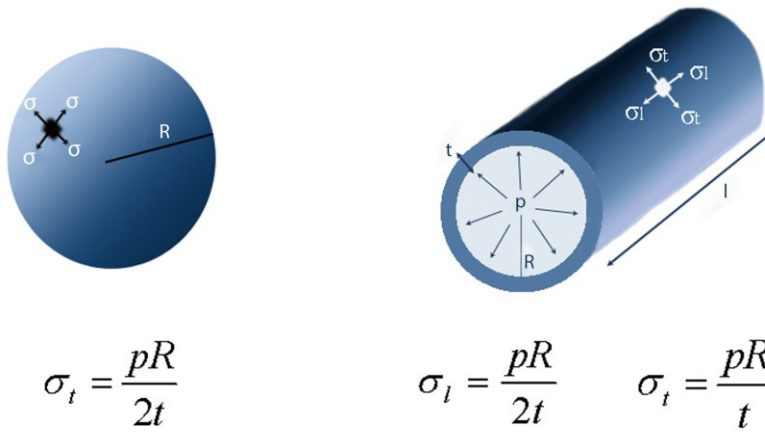


***Figure 4. Inflation’s principle.*** Variation in the pressure of a gas/liquid inside a close sphere or cylinder leading to the generation of stress in the cell walls. (*p* is the internal pressure, *R* the radius and *t* the thickness of the cylinder or sphere and  $\sigma_t$  and  $\sigma_l$  are the hoop and longitudinal stress respectively).

The hoop or tangential stress in a vessel under pressure equilibrates the internal pressure resulting from the water uptake in the cell. Hence, influx/efflux of water in such a thin-walled cell can provide the required energy for deformation or stress generation in the confined system.

***Swelling*** is referred to the uptake of a liquid by a solid upon which the solid dimensions change while maintaining the macroscopic homogeneity. Flory-Huggins theory describes the swelling pressure ( $\Pi$ ) for a polymer-liquid solution and its relation to the Gibbs free energy of mixing ( $\Delta G_{mx}$ ) as (Teraoka 2002; Treloar 2005):

$$\Pi = -\frac{\partial \Delta G_{mx}}{\partial V} + \Pi_e = -\frac{RT}{V_s} \left( \ln(1-\nu) + \left(1 - \frac{1}{r}\right)\nu - \chi\nu^2 \right) + \Pi_e \quad (\text{Eq. 1})$$

The  $\Pi_e$  term corresponds to the counteracting elastic force associated with elastic expansion of the polymer chains, the  $-\chi v^2$  part corresponds to the enthalpic term and the  $\ln(1-v) + (1-\frac{1}{r})v$  part represents the entropic contribution, where  $V_s$  is the solvent molar volume,  $\chi$  is the apparent interaction parameter depending on the specific properties of the particular polymer-liquid mix,  $r$  is the number of repeating unit in a polymer chain,  $v$ , the polymer volume fraction,  $R$ , the gas constant and  $T$ , the absolute temperature.

According to this theory, the water uptake and swelling of polymer networks in general can be described in a stepwise process: first the enthalpy driven hydration of the most polar hydrophilic groups occurs, and then after saturation of all bonding sites, the further adsorption is mainly entropy driven with adsorbed water filling the spaces between the network chains and centers of larger pores etc. (Hansen 1969; Teraoka 2002; Treloar 2005).

In the enthalpy driven stage, the interaction parameter  $\chi$  defines the affinity of a macromolecule to water and is related to the polymer solubility parameters. Hansen described the solubility of a solute in a solvent in three distinct parts; a non-polar part coming from the energy of dispersion bonds between molecules ( $\delta_d$ ), a polar part showing the energy from dipolar intermolecular force ( $\delta_p$ ) and a component representing the energy from hydrogen bonds between molecules ( $\delta_h$ ). Total solubility parameter  $\delta_T$  is expressed as (Hansen 1969):

$$\delta_T^2 = \delta_h^2 + \delta_p^2 + \delta_d^2 \quad (\text{Eq. 2})$$

In the final step, when all bonding sites are occupied, the main mechanism for further water uptake is entropy-driven with the entropy of the mixing being related to polymer volume fraction ( $v$ ) and number of repeating units in polymer chains ( $r$ ) (Teraoka, 2002, Treloar 2005):

$$\Delta S_{mix} = -R \left[ \ln(1-v) + \left(1 - \frac{1}{r}\right)v \right] \quad (\text{Eq. 3})$$

The infinite dilution at this stage is restricted by counteracting force due to the associated elastic expansion of the chain network and swelling continues only to the point where the entropic gain of the mixing and the elastic entropy of the network reach an equilibrium level.



### ***Water in plant cells***

A special feature of the plant cells in comparison to animal cells is that plant cells have an extracellular matrix called ‘cell wall’ which encapsulates the cell’s plasma membrane. The cell wall acts as a supportive framework giving the cell its mechanical rigidity to withstand the cell’s inner turgor pressure, protecting the cell’s inner organ from environment organs etc. The plant cell wall is a relatively dense network of various macromolecules and its architecture in general can be described as a fibre-reinforced composite with stiff cellulose microfibrils being embedded in a much softer matrix which can consist of hemicelluloses, lignin, pectin etc. (Fengel 1984; McCann 1991; Carpita and Gibeaut 1993; Bacic 1998; Kerstens, Decraemer et al. 2001; Salmén 2002; Fratzl, Burgert et al. 2004).

The two basic “swelling” and “inflation” mechanisms discussed above can be found in hydro-actuation systems in plants;

Plants can utilize the basic ‘inflation’ principle to induce volume changes in the living cells, through active change of the pressure inside the cells. An increase in osmotic potential of the cells results in a decrease in water potential, and to maintain the equilibrium, water flows into the cells and results in either reversible or irreversible change of cell volume (Nobel 1970).

On the other hand, cell wall behavior upon water adsorption can be understood and described as water uptake and swelling of a composite of polymeric chains, depending on the properties and architecture of the cell wall. This principle can be utilized for directing the response of the cell to humidity changes, or translate the changes in the cell’s inner pressure into a reversible elastic deformation of the cell wall and cell volume change, or an irreversible inflation with a permanent volume change.

#### **Cell wall components**

Natural cellulose (cellulose I) is a macromolecule made up of a linear chain of (1,4)-linked  $\beta$ -D-glucan which can be found in various organisms such as higher plants, algae etc. It is basically a composite of two polymorphs, I $\alpha$  and I $\beta$  which can coexist at different ratios, with I $\beta$  being the more dominant one in the cell walls of higher plants (Kovalenko 2010). The intermolecular hydrogen bonding and Van der Waals forces between the neighboring chains result in a packing of the cellulose chains into relatively ordered aggregates (Moon, Martini et al. 2011). These cellulose fibrils are partly crystalline consisting of crystalline regions with highly ordered parallel arrangement of cellulose chains and more disordered amorphous regions. Depending on the species, fibrils can possess a diameter of 3–5 nm but their exact length is not clearly determined yet though it is estimated to be about 10  $\mu$ m

(Cosgrove 2005). Covalent bonds between the glucose units along the chain and the dense network of hydrogen bonds and Van der Waals forces in and in between the chains result in a high stiffness of the fibrils in the axial direction (Cosgrove 2005; Salmen 2006). The cellulose microfibrils are formed and extruded into the cell wall by complex structure called cellulose synthase complexes (Saxena and Brown 2000). The cortical microtubules can guide the movement of the cellulose synthase complexes, thus providing a degree of control over the direction of the deposition (Paredes, Somerville et al. 2006; Emons, Höfte et al. 2007; Lloyd and Chan 2008).

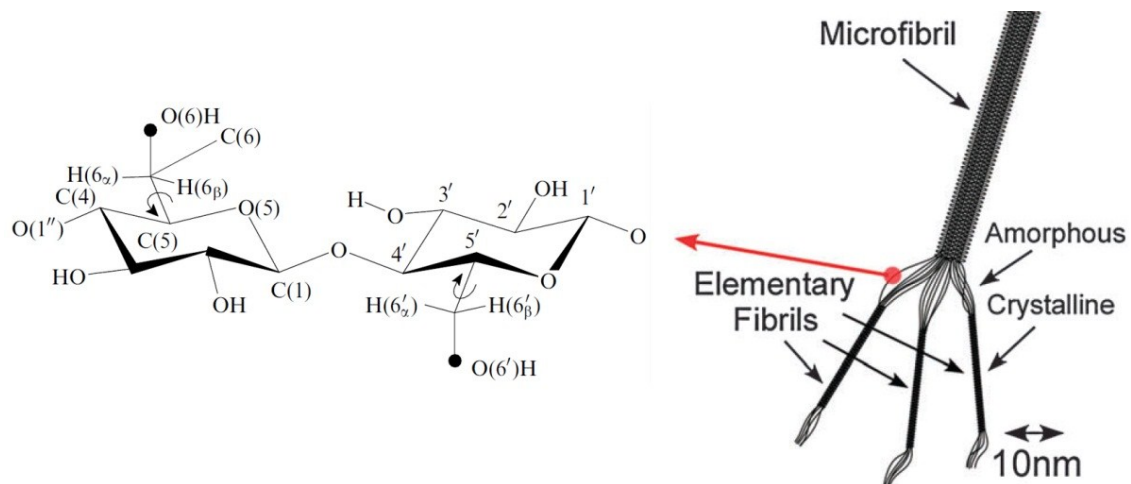


**Figure 5. Structure of the natural cellulose chains in the plant cell wall.** Schematics illustrate a cellulose microfibril (right) with the repeating unit of a cellulose chain (left). (Reprinted with permission from; Kovalenko 2010; Postek, Vladár et al. 2011).

Hemicelluloses are one of the main building blocks of the cell wall matrix. These polysaccharides consist of various sugar units and their main role is to work as binding agents, forming a strong yet resilient network with cellulose fibrils on the basis of hydrogen bond formation. Pectins make up a complex and heterogeneous family of water soluble polysaccharides which provide a relatively flexible matrix for the cellulose-hemicelluloses network. Lignin is another constituent of the cell wall matrix which contains different phenyl groups that makes it more hydrophobic than the other constituents. Pectin and lignin are also the main constituents of the middle lamella between the cells gluing the neighboring cells. The matrix-microfibril interaction is an important determining factor in cell wall properties as the mechanical response of the fibre composite largely depends on the interface between the stiff cellulose fibrils and the resilient matrix (Fengel 1984; Carpita and Gibeaut 1993; Bacic 1998; Fratzl, Burgert et al. 2004; Cosgrove 2005; Salmen 2006).

**Primary cell wall;** Growing plant cells possess a so-called primary cell wall, which consists mainly of cellulose, hemicelluloses, pectin and structural proteins. Besides protecting the cell against environmental factors such as intruding organisms etc., it also determines the structural support and shape of the cell. By resisting against the internal turgor pressure inside the cell, the primary cell walls tailor the direction and rate of the cell growth. The mechanical and chemical characteristics of primary cell walls need to be analyzed in combination with the effect of turgor pressure inside the living cells. Cellulose interactions with hemicelluloses and pectin are of specific importance during the cell growth or other functions that require elastic deformation of the cells. During these processes, the cell wall needs to be stiff enough to bare the hydrostatic pressure inside the cells and external loads, and yet compliant enough to respond to the cell turgor pressure to allow for the cell wall extension accompanied by cell enlargement (Cleland 1971; Taiz 1984; Veytsman and Cosgrove 1998).

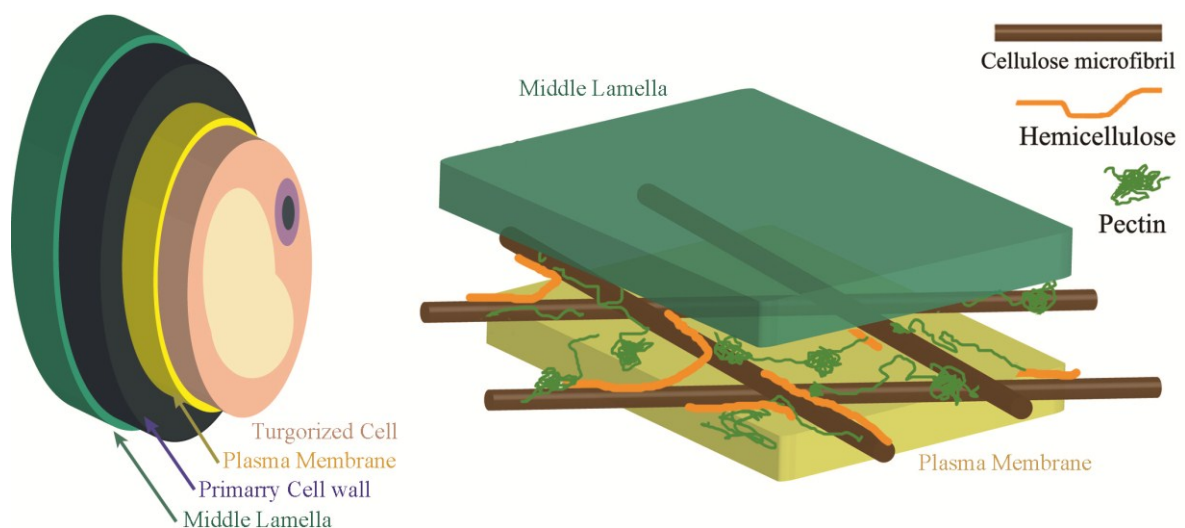


**Figure 6. Simple schematic of plant primary cell wall architecture and composition.** Left: A turgid living plant cell surrounded by plasma membrane, primary cell wall and the middle lamella. Right: Primary cell wall with the cellulose microfibrils embedded in a relatively soft polymeric matrix of hemicelluloses and pectin. To allow for plastic deformation as a consequence of turgor driven cell growth, primary cell walls should be rather flexible and must be able to loosen some of the load-bearing linkages between the fibrils while bearing the inner pressure load.

**Secondary cell wall;** Once the cell growth stops, secondary cell walls with thicker and stronger layers can be formed by the cell. These cell walls have no pectin and structural proteins but are rich in lignin as a matrix component which makes them much more rigid. Secondary cell walls have a distinct lamellar structure with a specific arrangement of

cellulose fibrils inside these layers (Figure 7). The angle between the microfibril orientation and the cell wall axis is known as microfibril angle (MFA) and is an important parameter in defining the mechanical and swelling properties of the cell wall as a whole. In wood cell walls, S1 and S3, the inner and outer layers of the secondary cell wall, have a relatively large MFA almost perpendicular to the cell axis. The middle layer (S2) is the thickest and the dominant layer determining the stiffness and the anisotropy of the cell wall. In “normal” wood cell walls cellulose fibrils in the S2-layer are laid almost parallel to the cell axis (MFA 0-10°), while specific reaction tissues in trees such as compression wood can possess an MFA of up to almost 60° (Reiterer A. 1999; Burgert, Keckes et al. 2002; Burgert and Fratzl 2009). The cellulose orientation dictates an anisotropic deformation of cells and tissues upon water uptake and release, which is utilized in the plant kingdom for directed actuation (more detail in chapter 1.2.3).

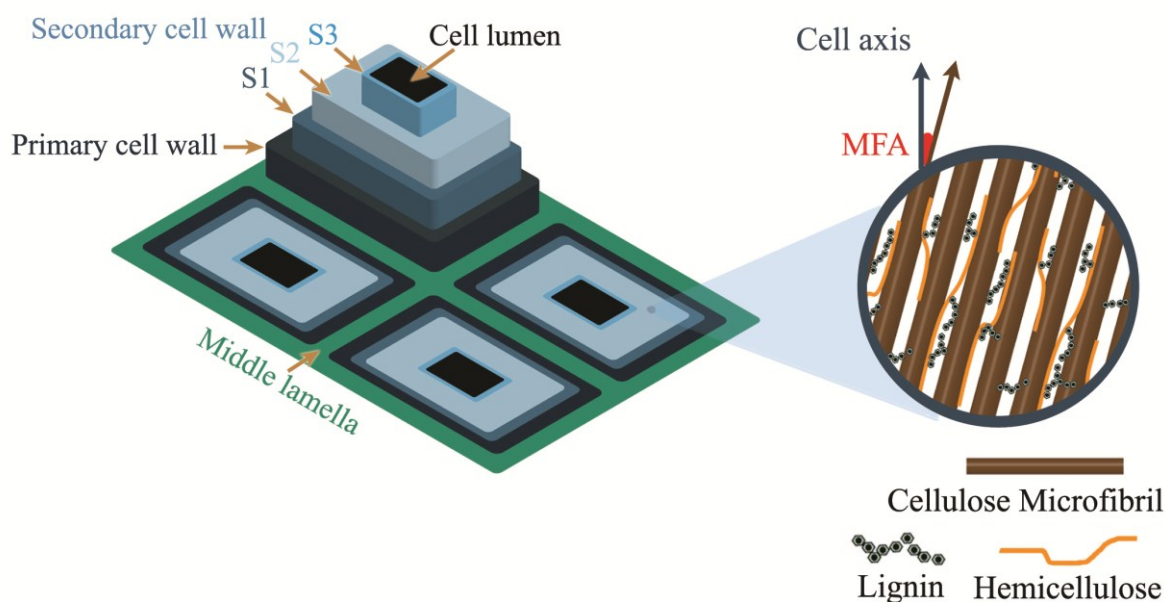


**Figure 7. Simple schematic of secondary cell wall architecture and composition.** Wood cell wall with primary cell wall and different layers of the secondary cell wall (S1, S2 and S3) are depicted schematically separating the cell lumen (black) from the intercellular middle lamella (green). Hemicelluloses and lignin work as a cross-linking and filling agent in the secondary cell wall. The orientation of the cellulose fibrils towards the cell axis is known as microfibril angle (MFA) and is one of the crucial factors determining the anisotropy of the cell wall swelling (right).

### Cell wall-water interaction

Adsorption of water results in the swelling of the cell wall matrix and the amorphous cellulose with the consequent effect on the bulk plant tissue. This applies to primary and secondary cell walls, but commonly the latter are studied in this regard from a wood

science perspective. To investigate the interaction of water with cell walls, the equilibrium moisture content of the tissue is usually monitored upon increasing/decreasing relative humidity at a given temperature. The result is a sorption isotherm that provides an entire picture of the different stages of interaction with water (Figure 8).

Various models have been developed to understand the different adsorption stages in cell wall-water interaction with each stage corresponding to a different state of water in the cell wall. Due to various interpretations of the results the true nature of each state is still under debate. However, studies suggest that water can exist in two different states in freshly cut samples; as free water in the porous systems such as the lumen of the cells and as bound water inside the cell walls. From the chemical point of view the hydroxyl groups of the wood constituents are the main target for attracting water molecules. Hence, starting from low relative humidity, the initial adsorption of water into the cell wall is a hydration process where the first layer of water is adsorbed and fixed on the sorption sites mainly consisting of free hydroxyl groups of hemicelluloses and the amorphous regions of cellulose (Wallenberger 2003; Engelund 2013). The reaction is exothermic and the enthalpic gain of the system is the main driving force for adsorption of the first few layers.

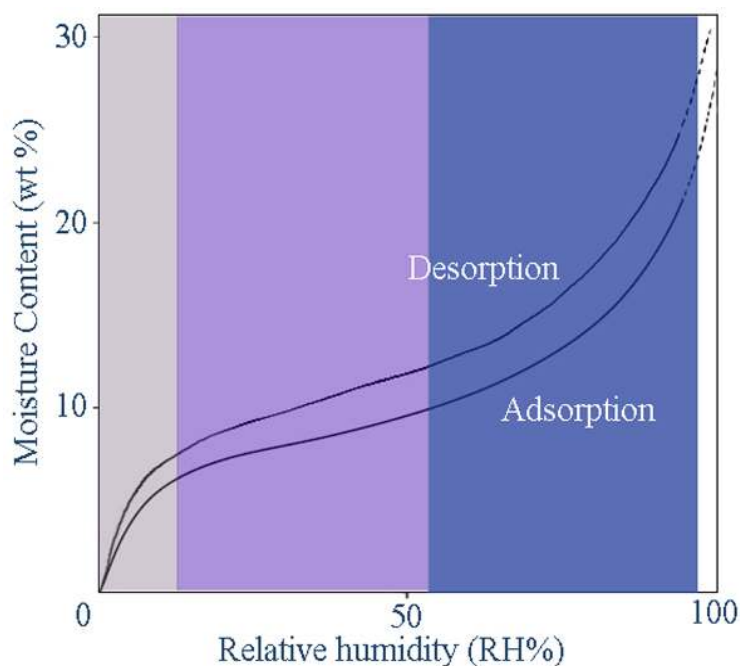


**Figure 8.** A typical sorption isotherm for wood. The equilibrium moisture content (the weight of the adsorbed water per weight of the dry wood) is plotted against the relative humidity (RH %). In the initial adsorption region, the first layer of water is adsorbed into the cell wall and makes strong bonds with the accessible hydroxyl groups of the cell wall polymers. The sorption continues by adsorption of further water molecule into and in between each available sorption sites (Skaar 1998; Engelund 2013).

Up to 40-50 % RH, the enthalpy of the sorption is constant and could be related to binding of one water molecule per glucose unit (Engelund 2013). At higher relative humidity from 50 up to 85% RH, the enthalpy of the interaction was found to decrease which is contributed to the adsorption of a second and third water molecule on each sorption site or in between them (Çarçabal, Jockusch et al. 2005; Engelund 2013). A modified version of the BET sorption theory (Brunauer et al. 1938) combined with the Dent sorption model (Dent 1977) was suggested to be able to cover the whole range of the sorption (Engelund 2013). Further adsorption of water into the system helps to open up the intermolecular hydrogen bonds between the polysaccharides and ease the conformational changes and mobility of the chains (Kimura, Hatakeyama et al. 1974). Above approximately 70% RH the sorption isotherm exhibits an increase in the slope of adsorption (Engelund 2013), which was formerly explained as sorption of free water in capillaries (Sheppard 1933). However, recently it was shown both theoretically and experimentally that the capillary sorption is not that significant at this RH and the change in the slope cannot be contributed to the capillary sorption alone (Engelund 2010; Thygesen 2010; Engelund 2013).

The sorption hysteresis is a common feature for porous polymeric materials (e.g. wood, Figure 8) and can be related to the difference between the adsorption and desorption process; In adsorption the water molecules have to be adsorbed into a relatively dense structure, thus requiring a greater external pressure to re-open the structure which was collapsed during the prior drying and desorption process. While in desorption, water molecules have to escape from an already opened porous structure, thus requiring a relatively lower vapor pressure to maintain a specific moisture content (Engelund 2011).

Upon drying of the fresh samples, the water inside the cell lumen is the first to leave, till the point where the main water in the tissue is the water saturated inside the cell wall. The amount of water contained within the saturated cell wall is known as fibre saturation point (FSP) (Skaar 1988; Engelund 2013). Water uptake/loss above this point has barely any influence on the dimension of secondary cell walls. However, adsorption/ desorption of water into the cell wall below this point results in anisotropic swelling/ shrinkage of the bulk tissue, and if restricted can exert huge stresses (Skaar 1988).

In analogy, more sophisticated anisotropic deformation or stress generation in bulk tissues can be understood and explained through the work of water (swelling/inflation mechanism) on a structure elaborately designed at different hierarchical levels.

## 1.2.2 Actuation based on inflation/deflation of living turgid cell

### *Differential Growth; Plastic deformation of primary cell wall*

Differential growth movements are probably the simplest way for a plant to perform a specific deformation in its organ. Cell growth is achieved through an irreversible plastic deformation of the primary cell wall, caused by an increase in the cell volume via water uptake. In normal state, the internal stress in the cell wall and the turgor pressure are in mechanical equilibrium. To allow the plastic deformation of the cell wall for growth, stress relaxation occurs via selective loosening of the load-bearing connection between microfibrils, which results in a drop in the turgor pressure and further water uptake and expansion of the cell (Lockhart 1965; Firn and Myers 1989; Fry, Smith et al. 1992; Cosgrove 2000; Cosgrove 2005; Burgert and Fratzl 2009). The unequal irreversible differential growth of the cells on opposite sides of an organ can lead to an in-balance volumetric change and the consequent organ deformation. Growth-induced bending of coleoptiles of grasses is one of the most prominent examples of plant movement related to the differential irreversible growth of cells (Firn and Myers 1989; Hart 1990; Burgert and Fratzl 2009).

### *Deformation by an elastic response of the cell wall upon turgor pressure*

To utilize a reversible movement, plants need an elastic response of the primary cell wall to changes in the cell's inner pressure (Toriyama and Jaffe 1972; Morillon, Liénard et al. 2001). The most abundant reversible turgor-based systems in plants are the stomatal movements for controlling the gaseous exchange between the plant interior and its environment.

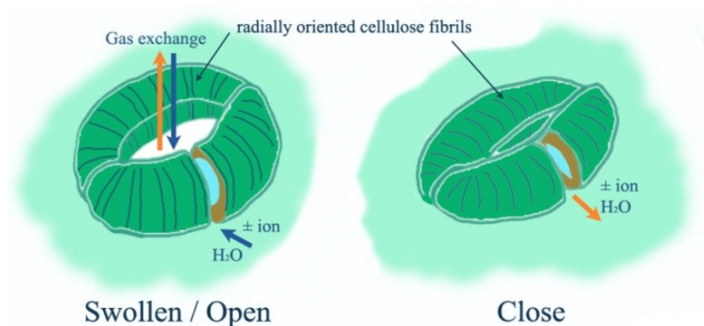


**Figure 9. Stomatal movement.** Left. Schematic illustration of the guard cells during stomatal movements. Cell volume increases during the opening and causes the cells to bend. The cross section of the cells changes from flat oval in close state to circular in the open state (Roelfsema and Hedrich 2005).

Plants can regulate the size of the small pores on their leaves by changing the volume and shape of their so called ‘guard cells’ through active variation of the cells turgor pressure (Figure 9) (Toriyama and Jaffe 1972; Morillon, Liénard et al. 2001; Hetherington and Woodward 2003; Roelfsema and Hedrich 2005; Burgert and Fratzl 2009).

Light-induced or circadian movements of the leaves of many species are controlled by such variation of the inner pressure of special motor-cells in the joint-like hinges at the base of the stalk of the leaves called pulvini (Iino 2001; Moran 2007). The same principle can also be found in relatively rapid leaf folding of mimosa upon external stimuli (Campbell 1977; Haupt 1977; Levin, Muller Landau et al. 2003; Moran 2007).

### ***Venus flytrap; a turgor-based rapid movement***

The carnivorous *Dionaea muscipula* leaves, better known as Venus flytrap uses a similar turgor based mechanism combined with a special metastable geometry of its leaves to perform one of the fastest plant organ movements (Hodick and Sievers 1989; Hart 1990; Fagerberg 1991; Forterre, Skotheim et al. 2005; Volkov, Adesina et al. 2008; Burgert and Fratzl 2009). The biochemical response of the plant to the external stimuli results in water flow and swelling of specific cells which leads to a significant volume change of the leaf’s tissue on adaxial and abaxial sides. Yet, the process based on simple water flow in the leaf tissue would be relatively slow and can’t explain the astonishing speed of the leaf folding (Toriyama and Jaffe 1972; Hodick and Sievers 1989; Fagerberg 1991; Fagerberg 1996). The fascinating translation of the small and slow cellular movement based on water flow to a much faster macro scale movement of the organ in Venus flytrap is achieved by coupling the cell turgor pressure variation with instabilities in the geometry of the entire organ (Forterre, Skotheim et al. 2005).

In the open state, the leaf is curved outwards (concave) holding the leaves in an intermediate mechanically meta-stable phase through a high turgor pressure inside the responsive motor cells (Figure 10). Stimulation of hair sensors by a prey triggers the leaf volume change through the water flow between the inner and outer face of the leaf, which consequently instabilize the metastable folding state. To release the stress, the leaf goes through an elastic relaxation via a sudden curvature conversion to a convex (inward) folding, which results in a rapid closure and snapping of the trap (Forterre, Skotheim et al. 2005; Burgert and Fratzl 2009; Fratzl and Barth 2009).



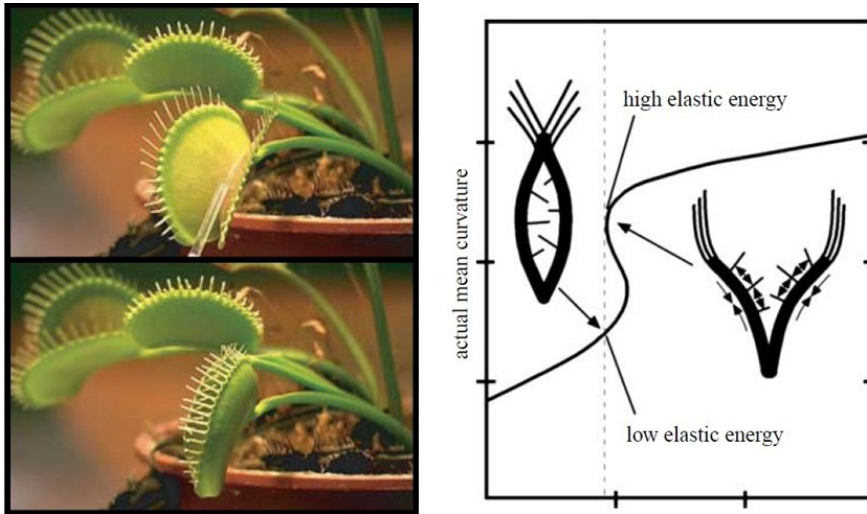


**Figure 10. The Venus flytrap hydro-actuated movement.** The leaves of Venus flytrap close in a fraction of a second when triggered by a prey (Adapted with permission from; Forterre et al. 2005). Right: Schematic of the Venus flytrap leaf in open and closed states, with the mechanical metastable curve separating the two forms. The high elastic energy stored in the metastable folding state can easily switch into the low elastic energy state upon trigger, resulting in the rapid snapping of the leaves (Reprinted with permission from; Burgert and Fratzl 2009).

### 1.2.3 Passive actuation based on anisotropic swelling/shrinkage of dead tissue

Some plants make use of basic swelling principles for generating internal stresses and organ movement. The principle can be well illustrated in a simple model of a composite consisting of almost undeformable stiff fibrils in a much softer swellable matrix (Figure 11). The significant difference between the swelling/shrinkage capacity and stiffness of the reinforcing cellulose fibrils and the soft matrix, results in an anisotropic swelling of the cell wall perpendicular to the fibrils orientation. Hence, the orientation of the microfibrils in the cell wall is the main controlling factor to determine the directionality of the swelling. By having control over the architecture of the cell wall via controlling the orientation of the cellulose microfibrils in the cell-wall formation process in the living cell, plants can control the directionality of the swelling/shrinkage after cell death to generate relatively huge compressive or tensile stresses or perform a desired movement (Dawson, Vincent et al. 1997; Reiterer 1999; Burgert, Eder et al. 2007; Elbaum, Zaltzman et al. 2007; Fratzl, Elbaum et al. 2008; Burgert and Fratzl 2009).

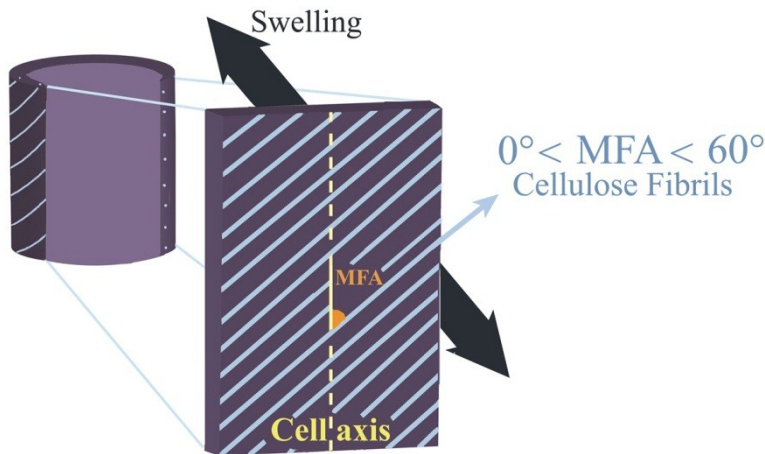


**Figure 11. Anisotropy of swelling in the secondary cell wall.** Schematic model of the secondary cell wall composite structure with stiff cellulose microfibrils embedded in the swellable soft matrix of hemicellulose, lignin etc. The main swelling occurs in direction perpendicular to the cellulose microfibrils, hence the variation of the microfibril angle (MFA) respect to the cell axis in the dominating secondary cell wall layer S2 ( $0-60^\circ$ ) can determine the anisotropy of the swelling/expansion in the cell wall (Burgert and Fratzl 2009).

### ***Passive hydro-actuation based on bending bi-layer structures***

One of the simple yet ingenious strategies used by various plants is to use a bilayer structure to perform various movements. When two elements with different mechanical response to an external stimulus (temperature, humidity etc.) are connected to each other, the extension/compression of one side is hindered or resisted by the more passive part. The compromise for the element with more extensibility (active part) is to satisfy the elongation through bending (Figure 14a).

A well-known example of passive hydro-actuated movement based on this principle is the pine cone seed dispersal, with the pine cone scales being closed in wet state and open upon drying to unveil the seeds. The reversible hydro-responsive bending movement of the scales is realized through a sophisticated architecture of the cell wall (Figure 12). Each scale is made up of two layers on the upper and lower sides with different structure regarding the cellulose MFA. The specific orientation of the cellulose microfibril in the cell wall during the plant growth, results in different shrinking responses of the two layers. On the upper side fibrils are almost parallel to the cell's axis, which restricts the upper side to shrink only in the direction perpendicular to the scale. The lower side on the other hand, has a MFA of about  $90^\circ$ , thus water desorption of the cell wall matrix results in the shrinkage of the cells along the longitudinal direction. The combined material response of the two sides with different swelling response leads to the bending of the scale upon humidity changes (Dawson, Vincent et al. 1997; Burgert and Fratzl 2009).

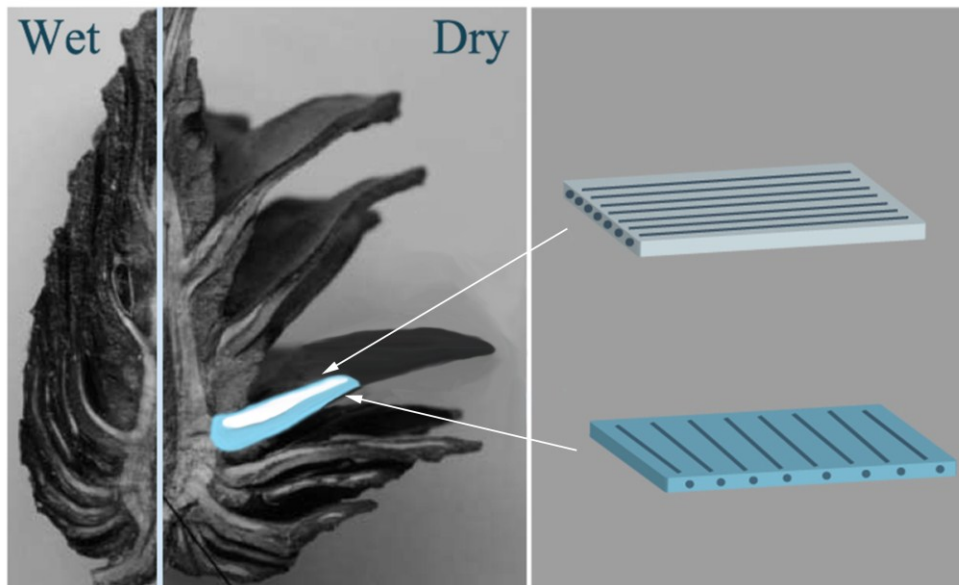


**Figure 12. Passive hydro-actuated bending of the pine cone scales.** A cross-section of a pine cone along its longitudinal axis in wet and dry state is shown with schematic of the two layers on upper (white) and lower (blue) side of a scale. In the upper layer fibrils are oriented along the longitudinal direction while in the lower part fibrils are more perpendicular to the cell axis. The different swelling properties of the two layers result in the bending and opening of the scales upon drying (Re-sketched with permission after; Burgert and Fratzl 2009).

A similar mechanism enables the wild wheat awns to actuate seed dispersal units via a swimming-like movement upon natural day-night humidity cycles. The seed dispersal unit consists of two antenna-like awns which land the seed in helical-descending movement to the ground (Figure 13). Each awn consists of two layers with different swelling properties. On the inner side of the awns (cap) the cellulose microfibrils are laid almost parallel to the cell axis which restricts the swelling/shrinkage in the direction perpendicular to the cell axis. The cells on the ridge (the outer part of the awns) have multi-layered cell walls with alternating MFA, which leads to a more isotropic shrinkage/swelling of the tissue upon humidity changes which is in general larger than the longitudinal swelling at the cap. As a result, the difference in the swelling/shrinkage of the inner and outer part of the awns results in a slow bending movement of the awns upon ambient humidity changes (Elbaum, Zaltzman et al. 2007). The cyclic changes between the relatively dry air during the day and higher humidity at night, can lead to a very slow swimming movement of the seed dispersal unit, while small spike-like silica hairs on the outside of the awns ensure a progressive forward movement by preventing the unit to move backwards and out of the soil (Elbaum, Zaltzman et al. 2007).

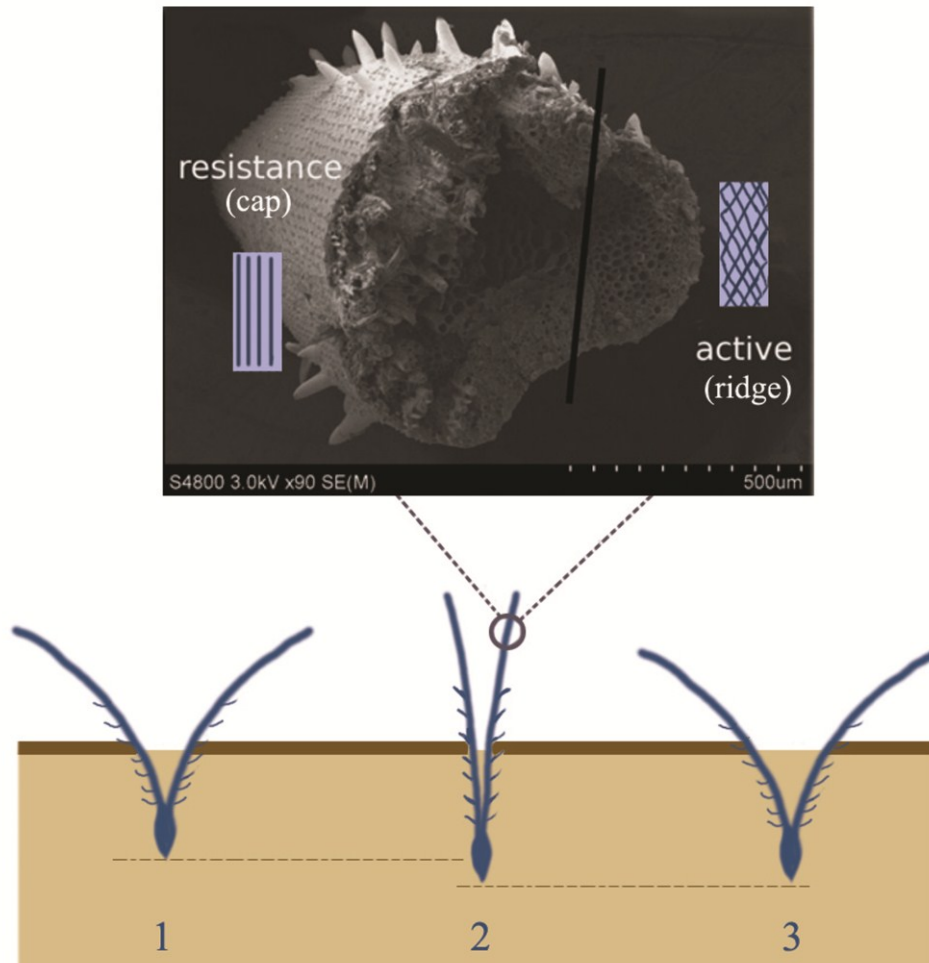


**Figure 13. Hydro-driven movement of wild wheat awns.** The swimming movement of the wild wheat awns is shown schematically. A SEM- micrograph of the cross-section of the wheat awn depicts the active (ridge) and resistive (cap) part. The cellulose fibrils are oriented parallel to cell axis in the cell walls of the passive part (inner side), preventing the swelling of the cells in the longitudinal direction. The random orientation of the microfibrils in the cell walls of the cells in the outer ridge makes the active part swell more than the inner tissue. This leads to a periodic bending movement of the awns upon the humidity changes during day (1, 3) and night (2), which pushes the seed case into the soil. (Adapted with permission from; Elbaum, Zaltzman et al. 2007).

The curvature of such bending-bilayer structure can be derived from the analogy of bending of bimetallic strip derived by Timoshenko (Timoshenko 1925), and in simple form is proportional to the difference in swelling strains between the two layers and inversely related to the thickness of the bilayer. In the absence of an external load, both force and torque are balanced, so that;

$$\frac{F_1 h_1}{2} + \frac{F_2 h_2}{2} = \kappa(E_1 l_1 + E_2 l_2) \quad (\text{Eq. 4})$$

Where,  $F_1 = \varepsilon_1 E_1 h_1 t$  and  $F_2 = \varepsilon_2 E_2 h_2 t$  are the forces in each layer,  $I_1 = \frac{th_1^3}{12}$  and  $I_2 = \frac{th_2^3}{12}$  the moments of area and  $t$  the width,  $h_1$  and  $h_2$  the thickness of the lower and upper layer,  $E_1$  and  $E_2$  the respective Young modulus and  $\kappa$  the curvature.

In addition the strain at the interface between the two layers must be equal.

$$\varepsilon_1^* + \frac{F_1}{E_1 h_1 t} + \frac{\kappa h_1}{2} = \varepsilon_2^* + \frac{F_2}{E_2 h_2 t} + \frac{\kappa h_2}{2} \quad (\text{Eq. 5})$$

Where,  $\varepsilon_1^*$  and  $\varepsilon_2^*$  are the swelling strains in the two layers.

Solving these equations for the curvature  $\kappa$  results in:

$$\kappa = \frac{6(\varepsilon_2^* - \varepsilon_1^*)(1+m)^2}{(h_1 + h_2)(3(1+m)^2 + (1+mn)(m^2 + \frac{1}{mn}))} \quad (\text{Eq. 6})$$

Where,  $m = \frac{h_1}{h_2}$  and  $n = \frac{E_1}{E_2}$ .

In the simplified case of  $m=n=1$ , the curvature can be calculated as:

$$\kappa = \frac{3(\varepsilon_2^* - \varepsilon_1^*)}{2(h_1 + h_2)} \quad (\text{Eq. 7})$$

Where, the curvature is proportional to the difference in swelling strains between the two layers and inversely proportional to the thickness of the bilayer.

More sophisticated movements such as twisting can also be achieved if the contraction/expansion mismatch between the two layers occurs at an angle with the main line (Figure 14b). Just by changing this angle, the layered structure performs a bending, coiling or twisting movement (Chen et al. 2011; Forterre and Dumais 2011).

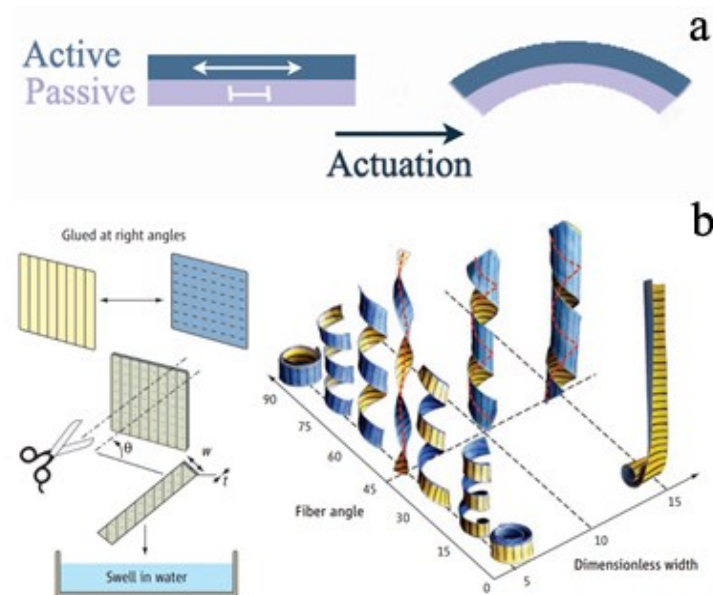


**Figure 14. Principles behind actuated-deformation of bi-layer structures.** The top image illustrates the bending of a bilayer made up of two materials with different strain response to a specific stimulus. The less responsive or passive layer resists the more pronounced expansion/ contraction of the active layer and the system bends to reach a compromise between the different response of the two layers (a). The schematic on the bottom (b) shows a simple paper-bilayer model where the dimensionless width and the fibre angle control the actuation pattern from simple bending to more complicated twisting movements (Adapted with permission from; Forterre and Dumais 2011).

### ***Passive hydro-actuation based on differential swelling of secondary cell wall layers***

Another sophisticated stress generation strategy is due to the formation of a highly swellable cellulosic layer inside the cell lumen of some species. Presence of these so called G-layers (gelatinous layers) in the cell lumen of the reaction wood of some hardwood species and some contractile roots etc. were found to generate high tensile stresses in the tissues, with the underlying mechanism of the stress generation being still under debate (Clair 2003; Clair, Ruelle et al. 2006; Burgert, Eder et al. 2007; Clair, Gril et al. 2008; Goswami, Dunlop et al. 2008; Mellerowicz, Immerzeel et al. 2008; Bowling and Vaughn 2009; Burgert and Fratzl 2009; Schreiber, Gierlinger et al. 2010; Clair, Alm eras et al. 2011; Mellerowicz and Gorshkova 2012).

Based on one theory, the suitable arrangement of the cellulose microfibrils in the surrounding secondary cell wall enables the cell wall to translate the tangential stress from the transverse swelling of the G-layer into a maximum axial contractile stress in the cell wall and the bulk tissue as depicted in Figure 15 (Burgert, Eder et al. 2007; Goswami, Dunlop et al. 2008; Burgert and Fratzl 2009; Schreiber, Gierlinger et al. 2010).

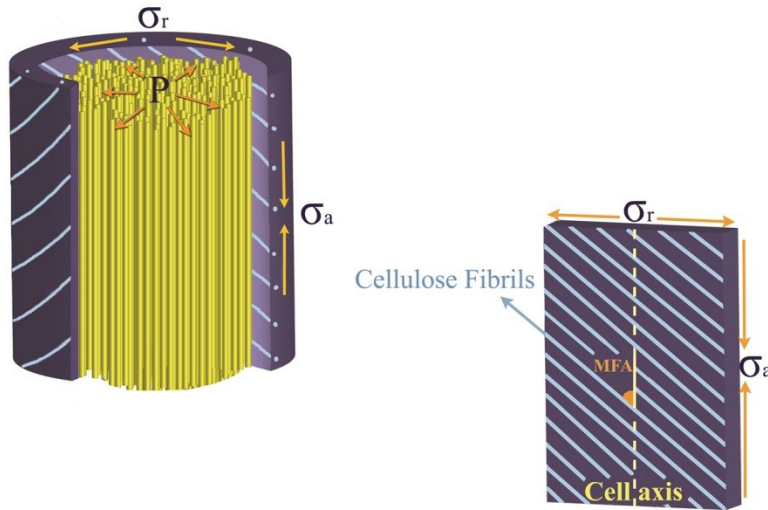


**Figure 15. Proposed mechanisms for tensile stresses generation in tension wood fibres.** The lateral swelling of the cellulose rich G-layer inside the cell lumen (yellow fibres) exert a tangential pressure ( $P$ ) on the secondary cell wall which results in a circumferential stress  $\sigma_r$  within the cell wall. The specific orientation of the cellulose fibrils in the cell wall translates this stress into an axial tensile stress  $\sigma_a$ , so that the microfibril angle (MFA) determines the  $\sigma_a/\sigma_r$  ratio and leads to the shortening of the tension wood fibres (re-sketches with permission after; Goswami, Dunlop et al. 2008).

Other models on the active role of the G-layer in tension wood fibres have proposed different stress generation mechanisms with relation to various features such as, the role of xyloglucan in the stress generation process, a honeycomb model for cellulose structure in the G-layer, or variations in the cellulose fibril orientation in the surrounding secondary cell wall layers etc. (Clair B. 2003; Clair, Ruelle et al. 2006; Clair, Gril et al. 2008; Mellerowicz, Immerzeel et al. 2008; Mellerowicz and Gorshkova 2012).

### 1.3 Ice plant hydro-actuated seed dispersal

One of the more ingenious examples of passive actuation in plant kingdom and the subject of this thesis, is the hydro-responsive unfolding of the ice plant seed capsules. Aizoaceae also known as ice plants grow in semi-arid areas and some of its species have evolved a sophisticated seed dispersal mechanism in which their seed containing fruit opens only upon sufficient hydration. The earliest mention of the hydro-responsive movement in Aizoaceae family in literature was from Steinbrinck who suggested that the ice plant fruits are primarily a protective carrier for the seeds that only open and relieve the seeds when wetted in rain thus enabling the germination of their seeds under these favorable conditions (Steinbrinck 1883). A systematic anatomical study of ice plant hydro-responsive seed capsules was first done by Kerner and Oliver (Kerner A. 1894). Preliminary studies mainly

aimed at simulation of the seed dispersal under rain by falling water droplets on the open capsules and suggested that the weight of the falling drops cause the seeds to eject up to half a meter away from the seed compartments (Berger 1908; Schmid 1925). Yet many researchers suggested that the specific structure of the seed capsule prevents the seeds to disperse rapidly and concluded that the seeds get initially washed away to the upper side of the capsule and then get splashed out by the falling droplets (Brown 1921; Huber 1924; Bolus 1928). It was also observed that, upon repeated wetting/drying cycle only a few seeds would fall out from the open capsules and it was suggested that it could be an adaptation to dry climate to not waste all the seeds at once in case of insufficient rainfalls (Brown 1921). The most recent thorough investigation of ice plant hydro-actuated seed dispersal goes back to Lockyer and Garside (Garside and Lockyer 1930; Lockyer 1932). In their studies on the seed dispersal mechanism, they could show that all seeds could be ejected and dispersed through the center of the capsule within 20 minutes of dropping water experiment and concluded that falling of the rain drops is an efficient mechanism for ejection of the seeds (Garside and Lockyer 1930; Lockyer 1932).

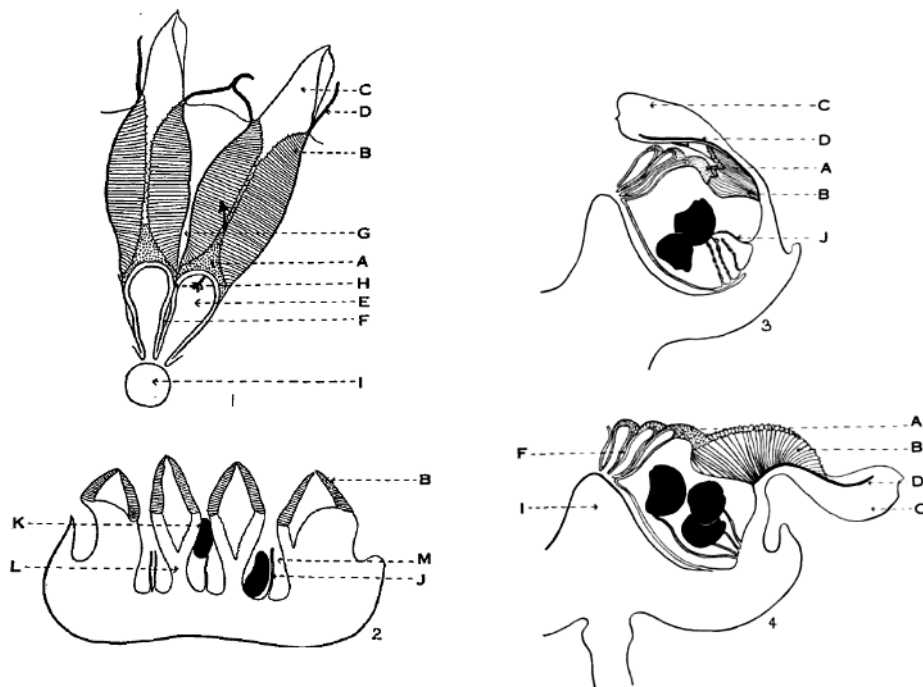


**Figure 16. First anatomical illustration of the ice plant seed capsule.** Surface view of an ice plant seed capsule (*carpanthea pomeridiana* N. E. Br.) depicts the two hygroscopic valves (1). The tangential section of an open fruit is illustrated in figure 2. Vertical and radial cross sections of the valve in closed and open capsules are depicted in figure 3 and 4 respectively. A. An arch which keeps the two halves of the septum apart, B. Hygroscopic keel, C. Valve, I. Central axis of the capsule, K. Seed, L. Septum (Reprinted with permission from; Garside and Lockyer 1930).



In their study of the anatomical features of the ice plant fruits, Garside and Lockyer (1930) reported that each seed capsule can consist of 10-20 seed containing valves, each with two “fan-shaped” hygroscopic tissues responsible for the opening/closing of the capsules (Figure 16). In the dry state, the keels were found to be hard and folded toward the central axis of the capsule resulting in a closed configuration of the seed capsules. Upon wetting the hygroscopic keel absorbs water and expands and unfolds outward about the capsules surrounding wall (Garside and Lockyer 1930; Lockyer 1932). Various studies have reported the ice plant hygroscopic keels to be made up of a rhomboidal shape cells with each cell having a secondary deposit of mucilage which can readily absorb water and swell the keel’s cells (Huber 1924; Garside and Lockyer 1930; Lockyer 1932).

#### **1.4 Objectives of the thesis**

Earlier studies on the ice plant seed dispersal were mainly based on pure anatomical examination of the system at the macro and micro scale and investigations on the seed dispersal efficiency. The underlying mechanism for the complex hydro-actuated movement was not in the focus of these studies. The biomimetic potential of such sophisticated passive actuation system called for a more detailed thorough analysis of the underlying mechanism and was the primary motivation to study the biomechanical and physiochemical principles behind the hydro-actuated unfolding mechanism of ice plant seed capsules in more detail.

In this thesis the seed capsules of ice plant species *Delosperma nakurense* (Engl.) Herre., were taken as the biological model system, with three main objectives:

- To utilize a multidisciplinary approach to investigate the underlying mechanism of ice plant hydro-actuated seed dispersal to gain insight into the biomechanics of the actuation and the role of material structure at different hierarchical levels in the global function of the system as a hydro-responsive deformable structure.
- To understand the physicochemical basis behind the water adsorption and the resultant swelling using a variety of experiments to extract a simple theoretical model for the chemo-mechanics of the actuation.
- To abstract the underlying principles behind the hydro-actuated movement to design biomimetic passive actuation demonstrator as a proof of concept.

The experimental procedures and a general background on the materials and main techniques that were applied through the three different phases of the project are presented

in chapter 2 “Materials and Methods”. The results of the experiment that were followed to pursue the answer to the questions proposed in the first and second objectives are presented in chapter 3 “Investigation of the ice plant hydro-actuated seed dispersal”. A discussion and comprehensive interpretation of the results in chapter 3 were put together in chapter 4 “The underlying mechanisms of the hydro-actuated movement“. The 5<sup>th</sup> chapter “Biomimetic design”, starts with a brief summary and abstraction of the discovered principles that can be used in the process of the biomimetic design, followed by two basic bio-inspired design ideas to develop biomimetic actuators as a proof of concept. The last chapter covers the conclusion of the whole project with a brief outlook on the potential future works.

## 2 Materials and Methods

### 2.1 Analysis of the ice plant hydro-actuated movement

#### *Sample preparation*

Ripe seed capsules of ice plant species *Delosperma nakurense*, grown at the Botanical Garden of the Technical University of Dresden, accession nr. 009255-21, were collected and kept in dry conditions. Wet hygroscopic keels were dissected from the valve and other covering tissues with tweezers and scalpel. For some cell investigations keels were embedded in polyethylene glycol 2000 (PEG, MW = 2,000) and cut in 10–30  $\mu\text{m}$  thick slices with a rotary microtome (Leica, RM2255, Wetzlar). Later, samples were washed with distilled water to remove PEG and were used for light, confocal or scanning electron microscopy and Raman spectroscopy. Further staining with a solution of fuchsin-chrysoïdin-astrablue mixture (FCA) was used when contrast and compositional analysis were needed. Staining with 0.1% aqueous safranin was used for confocal microscopy. In both cases, samples were immersed in the staining solution for 5–10 min and then washed three times in distilled water.

#### *Cell dimension measurements*

To quantify changes in the cell shape during wetting and drying cycles, the light microscopy was used for wet measurements and scanning electron microscopy for dry measurements. Both wet and dry measurements were made from the same region of a single piece of keel. Measurements were made using ImageJ v1.43 l and a computer drawing tablet to determine the length of cells along the X- and Y-directions, as well as their perimeter, and area. Analysis of the cell size at various parts of the keels was done by measuring the size of the cells in a fully open wet keel by live videos in a Nikon eclipse Microscope (Nikon Digital sight DS-2MV camera, NIS-elements D 3.1 software). The difference in cell size was compared along the keel length; from keel's back connected to the capsule, to keel's free tip, and keel height; from the keel's base connected to the backing, to the free ridge of the keels (Figure 21).

#### *Raman spectroscopy*

Thin sections of keel tissue were fixed under a glass coverslide in distilled water or  $\text{D}_2\text{O}$ . Raman spectra were collected with a confocal Raman microscope (alpha300; WITec) equipped with a piezoelectric scan stage (P-500, Physik Instrumente) and a Nikon objective

(100x oil immersed, NA = 1.25) (Gierlinger and Schwanninger 2006). A laser of  $\lambda = 532$  nm was focused onto the sample and Raman scattering was detected with a CCD camera (DV401-BV; Andor) behind a spectrometer (UHTS 300; WITec) with a spectral resolution of  $3 \text{ cm}^{-1}$ . Samples were mapped in  $0.33 \text{ }\mu\text{m}$  steps using an integration time of 0.5 s. Data were analyzed and images were produced using ScanCtrlSpectroscopyPlus software (WITec).

### ***Confocal microscopy***

Laser scanning confocal microscopic imaging was performed with a Zeiss LSM 510 scanning system (Zeiss MicroImaging GmbH) equipped with a  $\times 40$  objective (NA = 1.25) on small pieces of the keel using natural lignin fluorescence for contrast to observe cell shape (Donaldson et al. 2004) and using fluorescence from safranin staining for contrast between the cell wall and CIL (Bond et al. 2008). For safranin-stained samples,  $10 \text{ }\mu\text{m}$  were microtomed away from the top of cells to allow safranin to infiltrate the cell. For all samples, the laser excitation wavelength was 488 nm. Emissions were collected with the filter set to 530–600 nm for lignin autofluorescence and with two channels set to 515–545 nm and 590–700 nm for safranin stained samples.

### ***Enzymatic removal of cellulosic inner layer***

To investigate the role of the cellulosic inner layer (CIL) in keel actuation, the CIL was removed by enzymatic treatment as described previously (Schreiber 2010). Briefly, FCA-stained sections of a keel ( $30 \text{ }\mu\text{m}$ ) were treated with Cellulase ONOZUKA RS from *Trichoderma viride* (EC 3.2.1.4) (2.3 enzyme units per mg) (Yakult Pharmaceutical Industry.). Samples were placed in Eppendorf tubes filled with a 1 ml of solution of  $100 \text{ mg ml}^{-1}$  enzyme in ammonium formate buffer (pH 5) and were placed in shaking water bath ( $40 \text{ }^\circ\text{C}$ , 60 r.p.m.) for 10 h. As a control, two samples were prepared and stained the same way but were treated only in 1 M ammonium formate (pH 5). The swelling behavior of the cells was measured as described before.

### ***Cryo Scanning Electron Microscopy (Cryo SEM)***

To investigate the morphology of the cellulosic inner layer (CIL), scanning electron micrographs in cryo conditions were obtained Cryo SEM (Jeol JSM7500F) equipped with a cryo preparation system (Gatan Inc., ALTO-2500, Abingdon). Common sample preparation methods such as microtome cutting turned out to be troublesome here, as upon

slightest wetting, some of the CIL spongy tissues tended to come out of the lumen and cover and conceal the inner structure. To avoid the problem, sample preparation was done inside the cryo-stage of the preparation chamber. Wet keels were frozen in liquid nitrogen, transferred into the cryo-stage of the preparation chamber ( $-130^{\circ}\text{C}$ ), and sublimated at a temperature difference of  $-90^{\circ}\text{C}$  and  $-130^{\circ}\text{C}$  for few minutes to remove contamination by condensed ice crystals. Afterward the specimens were cryo-fractured to expose the inner cellulosic layer, subjected to palladium magnetron sputter coating (3 nm thickness) in the frozen condition and finally transferred from the cryo-preparation chamber to the gas cooled SEM stage and observed at a temperature of  $-130^{\circ}\text{C}$  and accelerating voltage of 1-3 kV.

### *Measuring keel's water uptake*

The dissected keels were soaked in water until they fully opened. A fully wet open keel was placed on a precision laboratory balance (Sartorius, ME5) with a camera mounted on top. Keel weight loss was monitored upon drying and the point at which the keel's closing started was taken as the weight of the fully wet open keel. The keel weight was also measured in complete dry state at room temperature. The keel's moisture content at room temperature ( $\sim 50\%$  RH) was measured using TGA data and was subtracted from the dry weight measured at room temperature, to gain the keel's dry weight. The keel water uptake till full opening was calculated as follows:

$$\text{Keels Water uptake}(\text{mg mg}^{-1}) = \frac{\text{keels water content in open state}}{\text{Dry keel weight}} = \frac{\text{Wet Open keel weight} - \text{Keel's Dry weight}}{\text{Keel's Dry weight}}$$

### *Thermogravimetric analysis (TGA)*

The keel's water adsorption-desorption was measured with a Thermogravimetric analysis device (SETARAM, SENSYS evo TG-DSC), connected to a humidity generator (SETARAM, WETSYS, Lyon). For a better gas circulation, 10 symmetric holes were punched into the wall of the aluminum sample holders. About 15 dissected keels with dry weight of about 3.8 mg were put in the prepared sample holder and placed in TGA furnace for thermo-gravimetric analysis. The water adsorption-desorption isotherms of the keels were measured at  $31^{\circ}\text{C}$  by applying a step-by-step humidity program with 10% RH steps and equilibrium time of 3h to get the equilibrium moisture content. Further a continuous adsorption-desorption ramp with 3% RH change per hour was obtained. Each experiment was repeated at least 2 times.

To gain the overall water uptake and also investigate the adsorption-desorption mechanism, the keel's weight loss from the fully wet open state to the completely dry state was monitored at 31°C and 0% RH.

### ***Keel opening in water-PEG solution***

To study the keel's water adsorption-desorption in higher ranges of water activity, keel opening was monitored in different concentrations of water- polyethylene glycol 2000 (Carl Roth, PEG, MW = 2,000, Karlsruhe) solutions. Keels were fixed and secured from their passive septum on a holder, standing freely in a beaker with cell's side (XY plane) facing the microscope. A thermostat (LAUDA, Tich-Kältethermostat RM6 T) was utilized to control the solvents temperature. A 50 wt.% water-PEG solution was prepared and was used as a stock solution. Samples were placed in the stock solution or pure water and by gradual addition of water to the stock solution (or the stock solution to water), keel opening state was monitored in different PEG-water concentration. For each concentration the solution was left to reach the equilibrium temperature and opening state. Images of the keels in different opening stages were taken by light microscopy. By choosing and tracking three fixed points at the keel center (where the maximum bending takes place), the corresponding opening angle ( $\alpha$ ) was measured and normalized according to the keels opening angle in completely dry and completely open wet states ( $\alpha_d$  and  $\alpha_w$  respectively). Keel opening states were calculated by means of an 'opening factor' (OF) defined as:

$$OF = \frac{(\alpha - \alpha_d)}{(\alpha_w - \alpha_d)} \quad (\text{Eq. 8})$$

With OF values ranging between 0 in dry and 1 in fully wet state.

Keels opening factor was plotted against water potential in the actuating medium.

## **2.2 Biomimetic design**

### ***Super porous hydrogel in 3D printed honeycomb frame***

Diamond-shaped honeycomb models based on the geometrical features of the keel's cell geometry (Guiducci 2013), were built by rapid prototyping of the a polymeric mixture of polyacrylates and polyurethanes ("VeroWhite®") with an Objet® Connex 500 multimaterial 3D printer by the group of Dr. James Weaver at Wyss Institute, Boston. Super porous poly-acryl-co-acrylamide hydrogels were synthesized following the protocol for the radical polymerization reaction presented by Gemeinhart et al. (Gemeinhart, Chen

et al. 2000). The main monomeric precursors, acrylic acid (AA, 15% vol) and acrylamide (AM, 10 wt.%) were mixed with N,N'-methylene-bis-acrylamide (BIS, 0.25 wt.%) as the cross-linker and the pH of the stock monomer solution was adjusted to 5.1 using 50 wt.% sodium hydroxide (NaOH). For stabilization of the bubbles formed in the polymerization process, 0.5 wt.% "PLURONIC® F127" surfactant was added to the solution. The total volume of the stock solution was increased to 20ml by adding pure water. The redox initiator pair, N,N,N',N'-tetramethylene diamine (TEMED, 2 wt.% of the monomer solution) was added to the solution and the ammonium persulfate (APS) was added only at the time of polymerization. 50 mg of sodium bicarbonate powder were added to the system roughly about 210 seconds after addition of APS, and the final solution was stirred manually with a spatula to obtain a homogeneous dispersion. A rapid prototyped honeycomb was inserted in the solution as the reaction was taking place. The synthesis of the super porous hydrogel inside the honeycomb structure was left to be completed for 4-5 hours, and the extra hydrogel surrounding the honeycomb structure was trimmed and removed afterwards. Finally, hydro-actuated deformation of the hydrogel-filled honeycombs was monitored upon exposure of the prepared honeycomb-hydrogel hybrids in water.

To study the swelling behavior of the super porous hydrogels, the swelling of the separately synthesized hydrogel were measured (in water uptake %) upon swelling of the oven-dried hydrogel discs in micro pure water, acidic (HCl, pH 1.2) and basic (NaOH, pH 8) solutions.

### ***Hydro-actuated bilayer-cell prototype***

For construction of the bilayer-cells, we tested various wood veneers with different geometry and swelling properties as active layer, and various polymeric films, papers, scotch tapes, wood veneers etc. acting as the resistive passive layers. For the final experiment 0.6mm thick spruce veneers (estimated 107 years old Norway spruce *Picea abies* (L.) Karst., (Lanvermann, Evans et al. 2013), cut by a horizontal slicing machine at Technical University of Dresden, Germany), was used as the active layer, while 0.2 mm thick papers (Supersilk DCP; 222200, Fischerpapier) were used as the passive resisting layer. For single bilayers, 6×2 cm pieces of spruce veneer were cut with the spruce fibres running perpendicular to the longer axis of the rectangle, and were glued (PUR Bond HBS 309 polyurethane glue) on 6×2 cm pieces of the paper cut with the longer axis being parallel to the longer side of the paper (where fibres are more aligned due to the rolling direction in paper manufacturing). Hence upon actuation cycles the spruce veneer would expand/contract due to the swelling/shrinkage perpendicular to the fibre direction, while

the paper layer swell less along the fibre/rolling direction and resist the swelling of the spruce.

For investigation of a bilayer-cell, two of such bilayers were made with an extra 1cm longer paper tale on both sides. Each tale was attached to the tale of the other bilayer by wrapping a tape around them so that the paper sides of the two bilayers face each other with the spruce veneers making up the outer side of the final cell structure (Figure 40). To scale up the cells into a honeycomb structure, 4 active elements ( $6 \times 2 \text{ cm}^2$  spruce veneers) were glued on to  $26 \times 2 \text{ cm}^2$  paper strips with 3mm space in between them, leaving two 1cm tales on both end of the paper strip free. Two of such strips were attached together by wrapping a tape around the two tales and the space between the veneers, to have a row of four cells with the paper as their inner walls and the wood covering their outer layers. 5 to 6 of such rows of cells were connected to each other from the middle of each cell by a double-sided tape to build up a honeycomb structure. To be able to monitor the actuation of the prototype upon changes in relative humidity (or wetting/drying cycles), the resulted honeycomb was fixed at two vertical bars with two wires running through the paper tales on both sides of the rows.

### ***Modulus of elasticity of spruce veneers and paper***

The elastic modulus of the active and passive layers were measured to be used as an input for modeling the actuation of the spruce-paper bilayer and bilayer-cells. Samples of spruce veneer and paper were cut in  $3 \times 2 \text{ cm}^2$  pieces in both parallel and perpendicular direction to wood fibres and paper's rolling direction. These dimensions were chosen to have similar sample size for measurements in both directions parallel and perpendicular to the fibril orientation. Unidirectional tensile tests were performed by an in-house-built bi-directional tensile test device for 3 samples of each material and direction (100N mini load cell, ALF259-Z3923, Kelkheim, Germany; Velocity controlled mode, strain rate  $10 \mu\text{m s}^{-1}$ , room condition  $25^\circ\text{C}$ ,  $\sim 50\%$  RH). The strain upon tension were measured by monitoring the displacement of the two sets of points on sample surface by an in-situ installed camera, and the module of elasticity was obtained by measuring the slope of the linear part of the stress-strain curve ( $\sim 0.2\%$  strain). Average of measurements for 3 samples of each material and each direction were calculated and presented for finite element simulation purposes.

### ***Swelling properties of spruce and paper***

The same tensile tester was used to measure the swelling properties of the two layers required for the modeling of the actuation (Motor position controlled, room condition



25°C, ~50% RH). Samples of spruce veneer and paper were cut in  $3 \times 2 \text{ cm}^2$  pieces in both directions parallel and perpendicular to fibre directions (or rolling direction in case of the paper) and were clamped into the two gages of the instrument. The software was programmed to set the force to zero upon detection of any increase in the force upon swelling of the samples, so that the samples were free to expand upon wetting. Swelling and dimensional changes of the samples upon wetting were monitored through measuring the distance between the two set of points at two ends of the samples near the gages by an in-situ installed camera. Average of swelling measurements for 3 samples of each material and each direction were calculated and presented for finite element simulation purposes.

### ***Bilayer-cell hydro-actuated movement***

To analyze the actuation of spruce-paper bilayers and bilayer-cell, samples of bilayer and bilayer-cells ( $6 \times 2 \text{ cm}^2$ ) were fixed horizontally in the air on their tails, with the edge of the bilayer stripes facing the camera. Actuation was monitored by taking sequential images of the set, and changes in the curvature of the bilayer stripes and the opening of the cells (distance between the outer edge of the two walls of the bilayer-cells) were measured using ImageJ v1.43l and a computer drawing tablet in two different set of experiments; in the first experiment the set was placed from the initial state in room temperature (25°C, ~50% RH) into an insulated in-house-built humidity chamber with relatively constant RH of 92-95% inside ( $\sim 75 \times 50 \times 30 \text{ cm}^3$ , insulated box with the in-flow of humid air). In the second experiment liquid water was sprayed on all sides of the samples for a couple of minutes until final equilibrium opening and the actuation upon wetting and the consequent drying at room condition (25°C, ~50% RH) was monitored.

To investigate the potential of utilizing such bilayer-cell structure in a real prototype, the bilayer-honeycomb set was placed from room conditions (25°C, ~50% RH) into a climate room with 95%RH (Institute for Building Materials, ETH, Zurich), where the actuation was monitored by taking pictures of the honeycomb opening/closing structure every 10 minutes for 18 hours.

### ***Bilayer-cell hydro-actuated force generation***

For a preliminary study of the force generating capability of the bilayer-cells, a close bilayer-cell ( $6 \times 2 \text{ cm}^2$ ) was placed under a glass slide with a tip of a load cell in close contact (almost touching) to the glass slide, pointing almost exactly on the middle of the bilayer-cell wall (where maximum bending occur). The whole set were moved from the room condition (25°C, ~50% RH) into a climate room with 95%RH (Institute for Building

Materials, ETH, Zurich). The load cell on top of the glass slide would prevent the opening of the cells and measured the force exerted from the bilayer cell-walls restricted from bending. The force exerted by the single bilayer-cell after reaching the equilibrium state after 18 hours was taken as the maximum force the single bilayer-cell was able to generate.

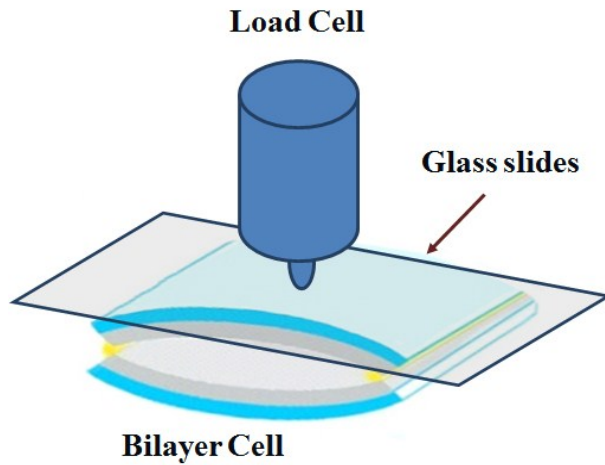


***Figure 17. Experimental set up for hydro-actuated force generation in bilayer-cells. Schematic illustration of the experimental set up for measuring the force exerted by a bilayer-cell upon actuation in 95%RH.***

### 3 Investigation of the ice plant hydro-actuated seed dispersal

Ice plants seed dispersal is an example of an ingenious evolutionary adaptation in plant kingdom, where the plant seed capsule undergo a complicated 3-dimensional movement and opens upon hydration with water to release the seeds under favorable conditions for germination. The hydro-responsive seed capsules of ice plants are non-living tissue at the point of actuation, hence unlike the turgor driven plant movements (e.g. in chapter 1.2.2), their actuation is completely independent of an active metabolism and can be categorized in passive hydro-actuation systems. However, while most of the passive hydro-actuation discussed earlier (e.g. in chapter 1.2.3), is based on simple movements such as bending, ice plants seed capsules exhibit a more complex origami-like movement upon hydration/dehydration cycles. To understand the basic principles behind this sophisticated hydro-actuated movement, seed capsules of the ice plant species *Delosperma nakurense* were taken as a biological model system and different aspects of the actuation, from the biomechanical nature of the sophisticated movement at the macro scale to the physical chemistry of the water uptake etc., were investigated at various hierarchical levels of the system.

#### 3.1 Ice plant hierarchical structure and basic movements

The hierarchical structure of the seed capsules from *Delosperma nakurense* is shown in Figure 18 in the dry and hydrated states, with the respective schematic representation of the structure at each hierarchical level. Ice plant seed capsules consist of five protective valves which are closed in the dry state and covering the seed compartments, hence preventing premature dispersion of the seeds. The valves are partitioned by five septa lying beneath the valves in closed dry state (Figure 18 a). Upon hydration with liquid water all five protecting valves flex and unfold outward over an angle of  $\sim 150^\circ$  within a couple of minutes and unveil the seeds (Figure 18 c). A 3-dimensional schematic of a seed capsule is illustrated in Figure 18b with each valve depicted at a different stage of opening from fully close to fully open state.

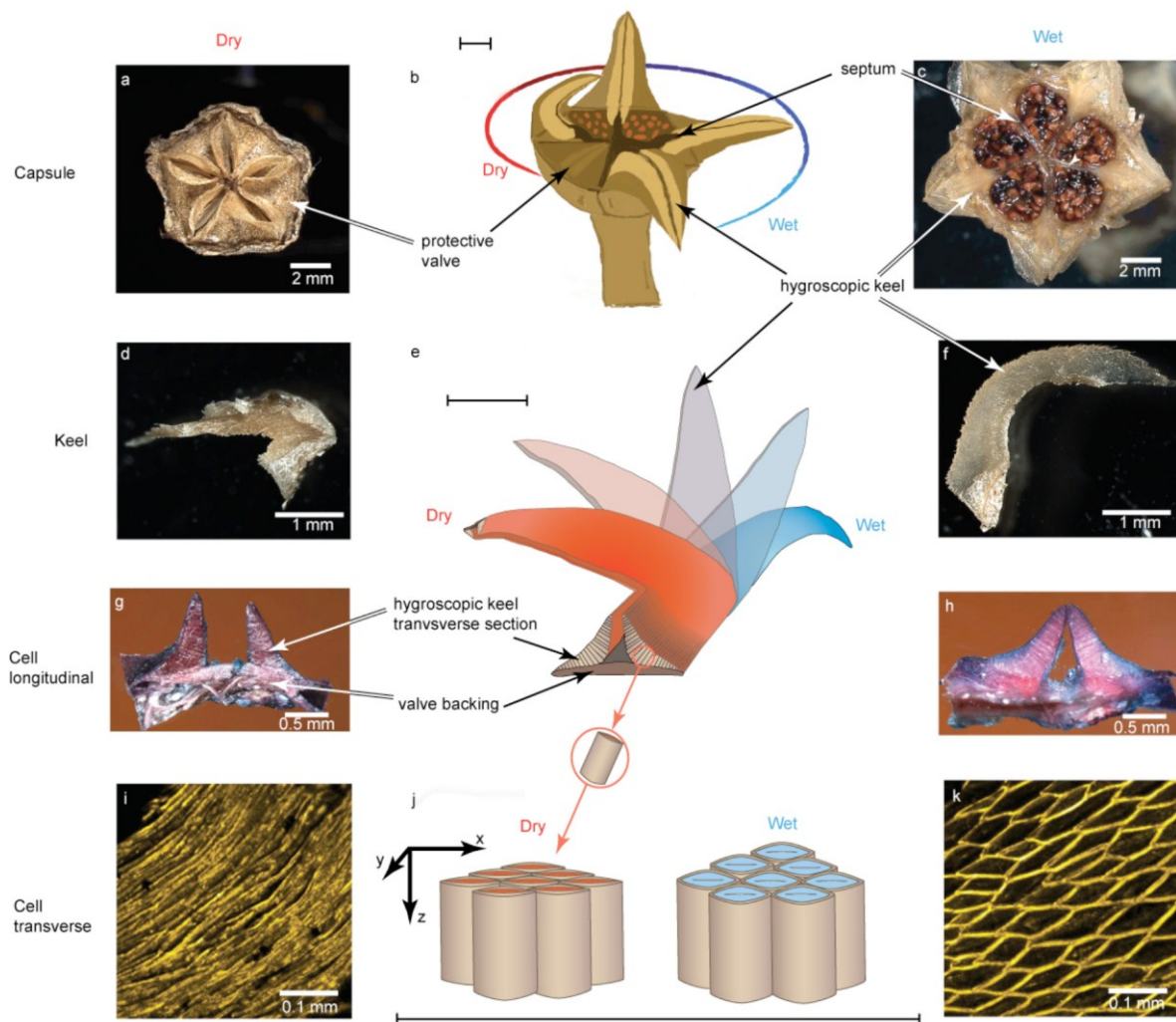


**Figure 18. Ice plant seed capsule hierarchical morphology.** The light and confocal microscopy images show the ice plant seed capsule structure at various hierarchical levels in wet (right: c, f, h, k) and dry states (left: a, d, g, i). An illustrated schematic provides a simplified representation of structures at each hierarchical level and the progressive actuation movement upon changes in the hydration states (b, e, j). Cross-section of the keel two halves (g-h) was stained with FCA to provide a contrast for depicting the longitudinal axis of the cells. Lignin autofluorescence provides the contrast in confocal microscopy images of the transverse cell cross-section (i, k) (Reprinted from; Harrington, Razghandi et al. 2011).

The active “muscles” responsible for this reversible movement was found to be a hydro-responsive tissue (hygroscopic keel) attached on a “backing tissue” along the centre of the inner valve surface (Figure 18 b, c, e). Each keel halves undergoes a deformation from a closed retracted state (Figure 18d) to an open flexed conformation (Figure 18f) upon wetting/drying cycles. Schematic in Figure 18e depicts the structure of the hygroscopic keel with the two keel halves being connected to the backing tissue at the keel base and free at their edges, and illustrates the progression of the reversible hydro-actuated flexing

movement of the keel's two halves upon wetting and drying. Each keel half was found to be made up of a network of hexagonal/elliptical shaped cells of different lengths running from the top edge of the keels towards the keel base where they are attached to the backing tissue (Figure 18i and k). Schematics in Figure 18e and j depict the orientation of the cells within the hygroscopic keel and the cell shape in wet and dry states, with the Z-direction representing the longitudinal axis of the cells, and the shorter and longer axes of the transverse cell cross-section being assigned as Y and X directions respectively. The transverse cross-sectional cut of the hygroscopic keel (XZ-plane) stained with fuchsin-chrysoidin-astra blue mixture (FCA) are shown in Figure 18 g and h. Figure 18i and k are the lignin autofluorescence confocal microscopy images of the transverse cross-sectional cut of each keel's halves honeycomb tissue (XY-plane) and shows how upon drying, the eye-like shaped cells collapse and close almost completely in the shorter axis of the transverse cell cross-section (Y-direction). The schematic illustrations of the hierarchical structure of the ice plant seed capsule in Figure 18 j, e and b, give the first impression of how anisotropic swelling of the cells in the honeycomb tissue would result in the unfolding of the ice plant seed capsules.

By monitoring the drying of a fully open wet keel the progressive closing movement of the keel was tracked (Figure 19d). The tip of the keel (point A in Figure 19a-c) undergoes a flexing movement around the keel base (point E), with the maximum bending of the keel occurring at a point between points C and D, defined as the "hinge" point of the flexing. A closer look at the transverse cut of the two halves of the keel revealed that, the free edges of the keel's two halves are touching on their ridges in wet state and move apart from each other upon drying, creating an empty space which allows for the tight packing around the middle septum upon closing of the capsule (Figure 18 g-h, insets in Figure 19a-c and Figure 20). It was also observed that the backing tissues supporting the keel's two halves is slightly curved outward in the dry state and changes its curvature to a fully straight line upon wetting (Figure 20 c, d).

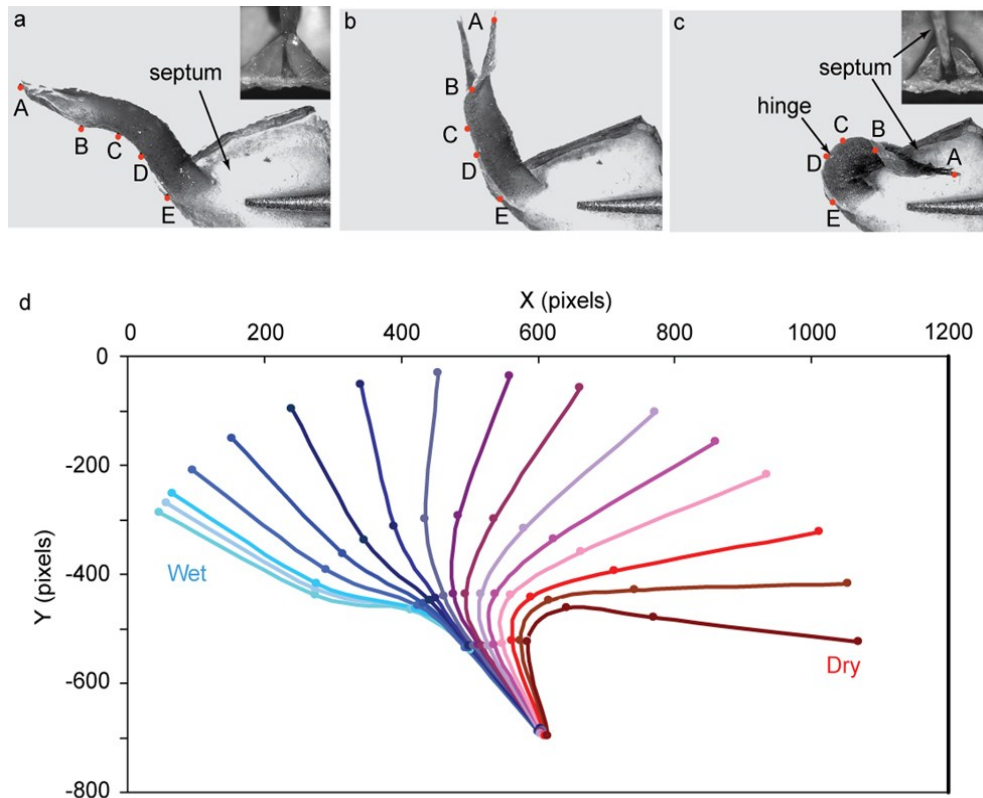


**Figure 19. Detailed analysis of keel movement.** The gradual closing of a fully open wet keel was monitored upon drying using image correlation. A dissected keel attached to the middle septum is shown in fully open wet state (a), an intermediate state (b), and the close/dry state (c). Five different spots on different parts of the keels labeled as A-E were monitored through the closing movement of the keels and the trajectory of the relative movements of each point during drying were plotted (d). The cross-sectional cut of the two keels between points D and E are shown in wet (a) and dry (c) state revealing how the two keel halves pack around the middle septum in the dry state (Reprinted from; Harrington, Razghandi et al. 2011).

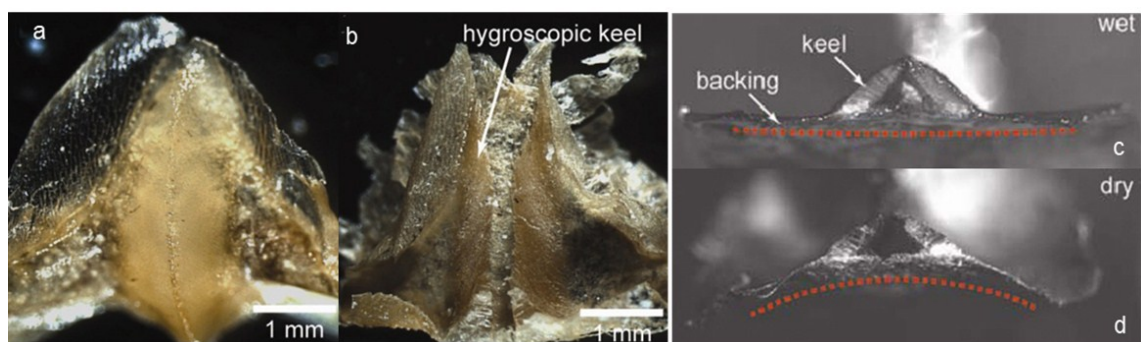


**Figure 20. Separation of the two keels upon drying.** The top view of the keels shows how the two keel's ridges are touching in wet state (a) and move apart and separate upon drying (b) allowing for a fit packing of the keels on the middle septum of the capsule. The cross-sectional cut of the two keels shows how the backing tissues curvature changes from a fully straight line in wet state (c) to a slightly outward curved (d) in the dry state (Adopted from; Harrington, Razghandi et al. 2011).

## 3.2 Characterization of Hygroscopic keel cells

### 3.2.1 Keel's cells morphology and composition

The first observations with the light and lignin autofluorescence confocal microscopy (Figure 18 i-k) revealed that the eye-like shaped cells show a large anisotropy of deformation in their cross-sectional axis upon wetting/drying cycles. The observation indicated that the origin of the observed hydro-responsive movement in macro scale must be the collaborative opening/closing of all cells in the shorter axis of their cross-section (Y-direction) resulting in the unidirectional expansion and retraction of the keels. A more systematic measurement of the short and long transverse cross section of the cells in wet and dry states showed that cell's length along the Y-direction (short cross-sectional axis) increase 4-fold upon wetting while the cell's length shows only a slight 10% changes in the long cross sectional axis of the cells along X-direction (Table 1). The cell's cross sectional area undergoes a near 4-fold change upon wetting and drying cycles, whereas the cells perimeter shows only a slight 20% increase.

*Table 1. Transverse cell shape changes during wetting and drying cycles.*

	<b>Dry</b>	<b>Wet</b>	<b>W/D</b>	<b>P values *</b>
Length X ( $\mu\text{m}$ )	77.2 $\pm$ 14.5	84.4 $\pm$ 16.5	1.09*	4.4 $\times$ 10 <sup>-4</sup>
Length Y ( $\mu\text{m}$ )	5.9 $\pm$ 1.1	24.4 $\pm$ 5.5	4.15*	4.0 $\times$ 10 <sup>-95</sup>
Perimeter ( $\mu\text{m}$ )	166.1 $\pm$ 29.7	198.1 $\pm$ 34.4	1.19*	5.4 $\times$ 10 <sup>-13</sup>
Area ( $\mu\text{m}^2$ )	394.5 $\pm$ 110.5	1477.4 $\pm$ 491.5	3.75*	4.0 $\times$ 10 <sup>-61</sup>
Y/X	0.076	0.289		
n	110	129		

All values are mean  $\pm$  s.d.  
 \* A two-sample T-test was performed for each property to determine if mean values were significantly different between wet and dry states.

The cell size and shape were also found to vary along the cell's length (Y-direction) and cell's height (Z-direction). Moving from the back of the keel toward its tip along the Y-direction (Figure 21) cells become slightly bigger in circumference and more elongated in X-direction (lower Y/X ratio).

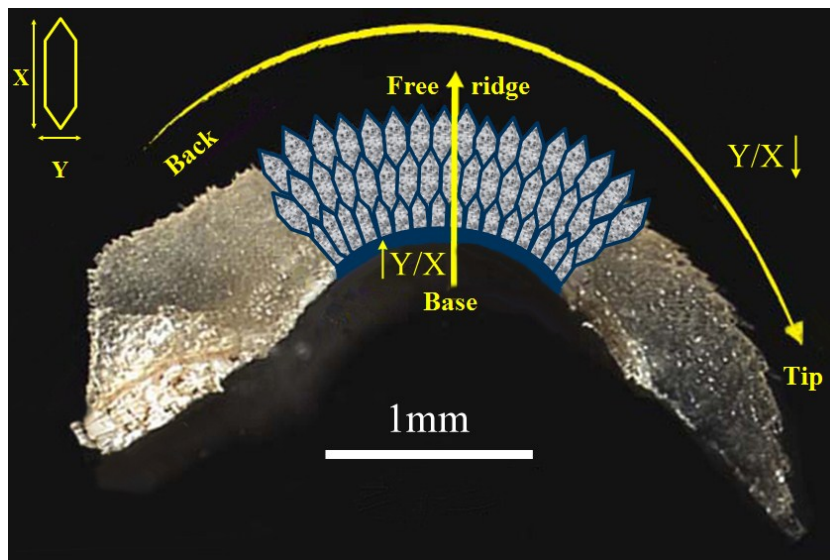


**Figure 21. Variation of the size of the keel's cells in wet open state.** Light microscopy image of a fully open wet keel with cells shape and orientation illustrated in exaggerated size on top. Free cells close to the ridge of the keels are in average 25% larger in the Y-direction (shorter axis of the cell's cross-section) than the cells near the keel's base attached to the backing tissue. Going from the back of the keels connected to the middle septa in the seed capsules to the keels tip (Y-direction), cells perimeter increases while cells become more elongated in the longer transverse cross-section (X-direction).

Further, it was observed that in the wet open state, the cells at the base of the keel attached to the backing tissue were in average about 25% shorter in the Y-direction than the cells near the ridge of the keel (T-test  $P < 0.005$ ), revealing that the free cells on the ridge of the keels open more than the cells on the keel's base, probably because they don't have the restriction of being attached to the passive backing tissue (Figure 21).

In the initial investigation of the keel's cells composition, a cross-sectional cut of network of cells was stained with a fuchsin-chrysoidin-astra blue mixture (FCA) (Figure 22a). The cell walls showed a red stain indicating presence of lignin in the cell walls. Moreover, staining revealed the presence of a non-lignified cellulosic (bright blue staining) structure filling the lumen of the keel's cells. This cellulosic inner layer (CIL) found in the lumen of the keel's cells partly resembled the 'G-layer' found in the cell lumen of the tension wood (Clair et al. 2003; Clair et al. 2006; Burgert et al. 2007; Goswami et al. 2008; Schreiber et al. 2010; Mellerowicz et al. 2008). Laser scanning confocal microscopy images of safranin-stained keel cell's depicts the cell walls in red colour and the cellulosic inner layer (CIL) in yellow, and revealed that upon drying and closing of the cells, the CIL retracts towards the cell walls suggesting an active role of the cellulosic inner layer in the reversible deformation of the cells upon wetting and drying (Figure 22 b-c).



Confocal Raman spectroscopy helped to study the composition and role of the cellulosic inner layer in water uptake and swelling of the cells in more details. The main Raman peaks for cellulose ( $1,067\text{-}1,143\text{ cm}^{-1}$ ) appear in both the cell wall and the cellulosic inner layer (shown at two different intensities in figure 22 d, e). Integration at higher intensities revealed that the CIL has an organized structure with lamellae running along the X-direction (Figure 22e). As was expected from the FCA staining, the peak representative for lignin ( $1,546\text{-}1,643\text{ cm}^{-1}$ ) appeared only in the cell walls and not in the cell lumen where the CIL was found (Figure 22f). The Raman peaks for water ( $2,223\text{-}2,725\text{ cm}^{-1}$ ) showed that the cellulosic inner layer can absorb and contain large amounts of water and contribute to the main swelling and expansion of the cells (Figure 22g).

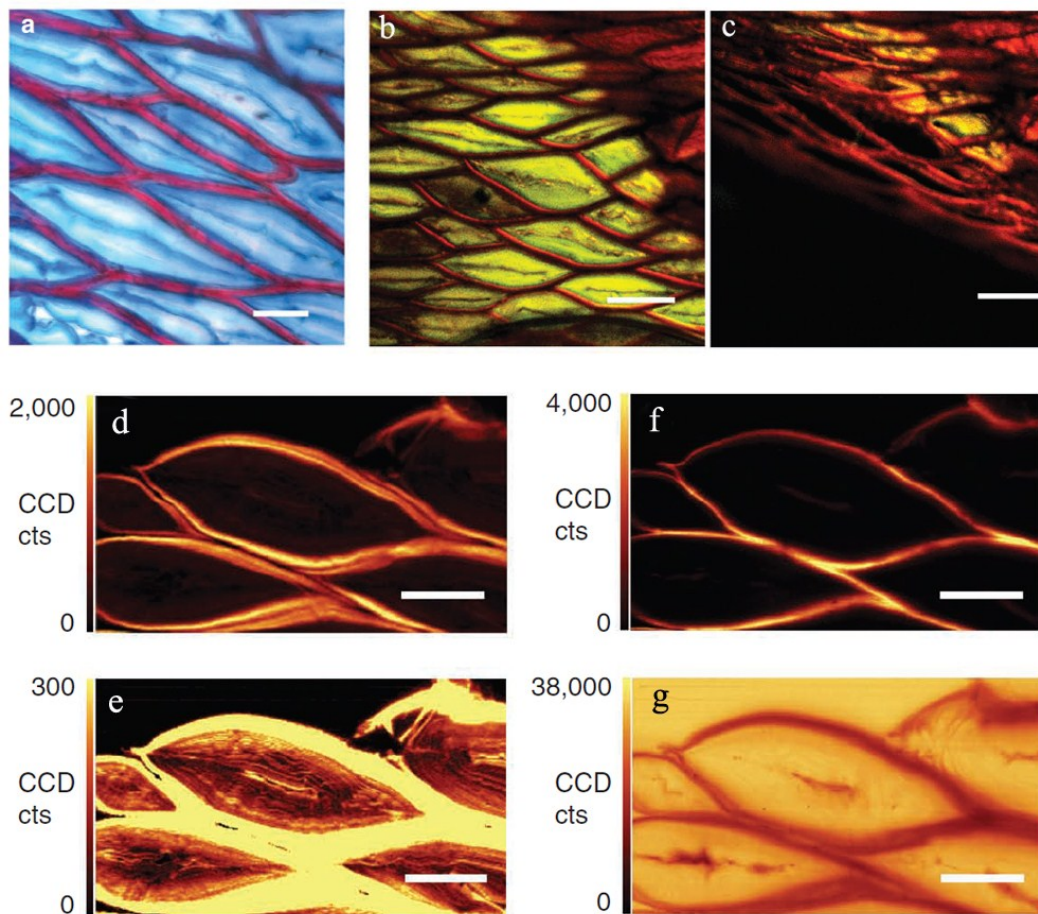


**Figure 22. Composition and morphology of hygroscopic keel cells.** FCA staining (a) shows a lignified cell wall (red) with a non-lignified cellulose inner layer (CIL) filling the lumen of the keel's cells (blue). Confocal Raman spectroscopic images of keel cells integrated for cellulose at two different intensity levels (d and e,  $1,067\text{-}1,143\text{ cm}^{-1}$ ), lignin (f,  $1,546\text{-}1,643\text{ cm}^{-1}$ ), and water (g,  $2,223\text{-}2,725\text{ cm}^{-1}$ ). Consecutive confocal microscopy images of safranin-stained keel in wet (b) and during drying (c) with cell wall colored in red and the cellulosic inner layer (CIL) in yellow. Scale bars are defined as follows: a= 25  $\mu\text{m}$ ; b-c= 50  $\mu\text{m}$ ; d-g= 20  $\mu\text{m}$ . (Adopted from; Harrington, Razghandi et al. 2011).

### 3.2.2 Morphology of the cellulosic inner layer (CIL)

To gain a better understanding of the underlying mechanism of the cell's swelling, the structure and morphology of the cellulosic inner layer (CIL) inside the keel's cell was investigated using Cryo scanning electron microscopy (Cryo-SEM).

The Cryo-SEM images of the cell's transverse cross-section (XY-plane) showed the lamellar structure of the CIL in more details (Figure 23). Since the top membrane was cut off in the XY-slices, some of the CIL material was swollen out and lost in the preparation process, which may explain the voids seen in the cell lumina.

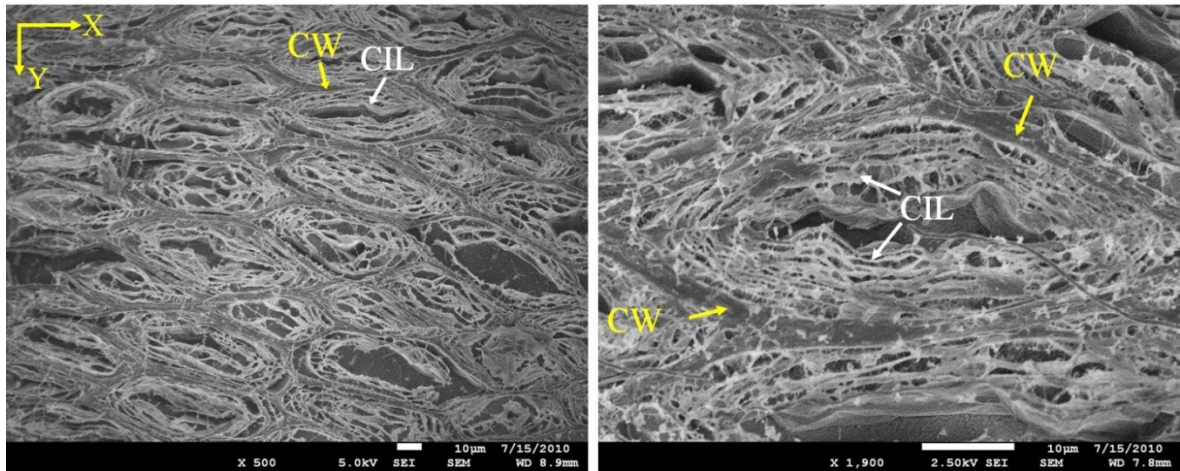


**Figure 23.** Cryo-SEM micrographs of a cell transverse cross-section in swollen state. The left micrographs show 20-30 $\mu$ m thick slices of the cell's transverse cross-section (XY-plane) in the frozen swollen state, with a magnified image of an individual cell presented on the right. The lamellar structure of the cellulosic inner layer (CIL) inside the cell wall (CW) is visible in the micrographs. The absence of the cell's top membrane in the cut slices let most of the CIL material swell out of the cells, explaining the voids observed in the cell's lumen.

To preserve the CIL material inside the cell lumen, the frozen wet keels inside the Cryo-SEM preparation chamber. The micrographs of the cryo-fractured cells frozen in the fully open wet state are presented in Figures 24-26. The colour-coded schematic in the figures illustrates a typical cell in the micrographs, with red representing the broken cell wall covering the underlying CIL lamellae depicted in blue.

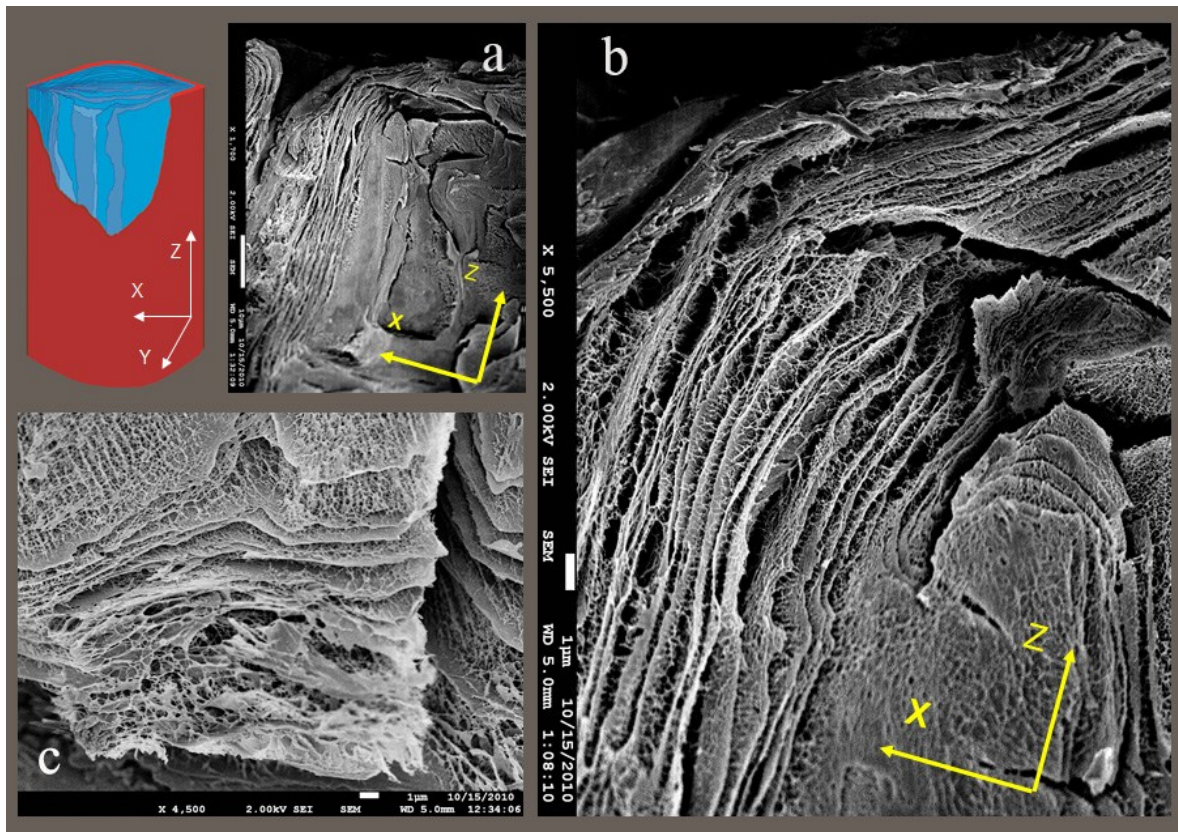


**Figure 24. Cryo-SEM micrographs of a cell in swollen state.** A frozen swollen cell fractured longitudinally along the XZ-plane is depicted in micrograph (a), with the schematic illustrating a typical fractured cell where the cell wall (red) with a broken front reveals the inner structure of the cellulose inner layer (blue). The lamellar structure of the CIL can be clearly seen in the higher magnification (b,c), where the dense sheets of cellulose nanofibres are connected with a much more porous network of cellulose nanofibres (Adopted from; Razghandi et al. 2014).

Figures 24 a, b show the XZ-plane of a cryo-fractured cell where the lamellar structure of the cellulose inner layer can be easily observed. A closer look at the lamellar structure revealed that the CIL consists of sheets of densely packed cellulose nanofibers running parallel to the cell wall, with a much more porous network of cellulose fibrils running in between them (Figure 24b-c).

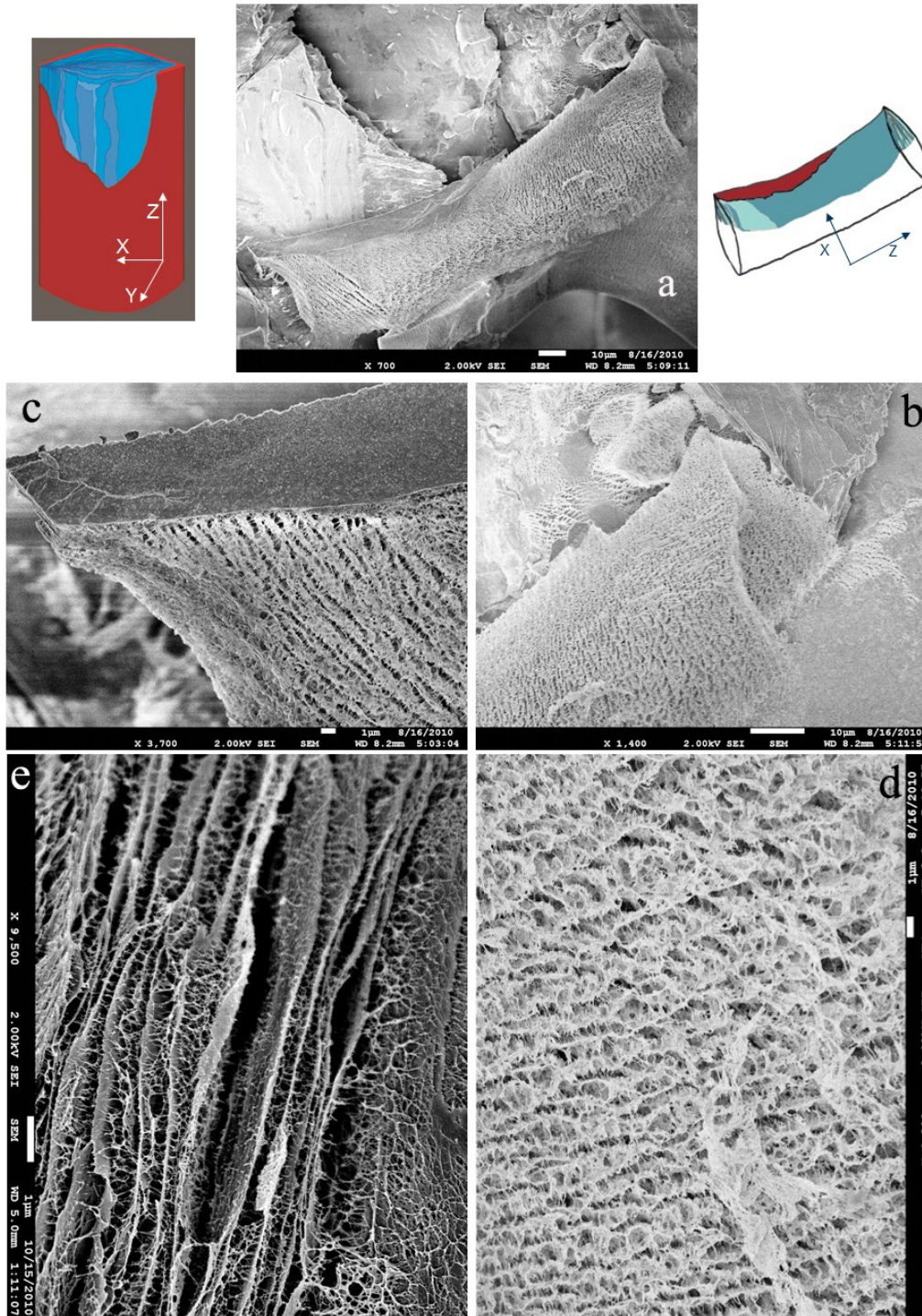


**Figure 25. Cryo-SEM micrographs of keel's cell in swollen state.** A schematic of a typical cell is illustrated on top-left; The cell wall is depicted in red with its front part broken (as in cryo-fractured cells) to reveal the lamellar structure of the cellulosic inner layer in the cell lumen (blue). A micrograph of a longitudinal view of a cryo-fractured cell is shown in figure (a), where except for a small part on the top, most of the cell wall is broken leaving some of the CIL still in contact (schematic on top-right). The structure of the CIL in left and right side of the broken cell are presented in higher magnifications in b and c. A closer look shows the lamellae of densely packed cellulosic nanofibres with a much more porous sponge-like network of cellulose fibres filling the space in between them (b:1400x, c: 3700x, d:4300x, e:9500x). (Adopted from; Razghandi et al. 2014).

A fractured part of a frozen cell in open state is depicted in Figure 25, where absence of the broken cell wall in most part of the cells reveals the structure of the inner cellulosic layer. A broken half of CIL lamellae is visible at the right side of the cell. The right and left side of the broken cell are depicted in higher magnifications in Figure 25b and c, respectively. The lamellar structure of the CIL is clearly visible in the magnified images, with the highly porous layer filling the space in between them (magnification increasing from Figure 25b to d).

Figure 26 depicts the structure of the cellulosic inner layer in higher magnification. Both the lamellae and the porous layers are clearly visible in the micrographs.

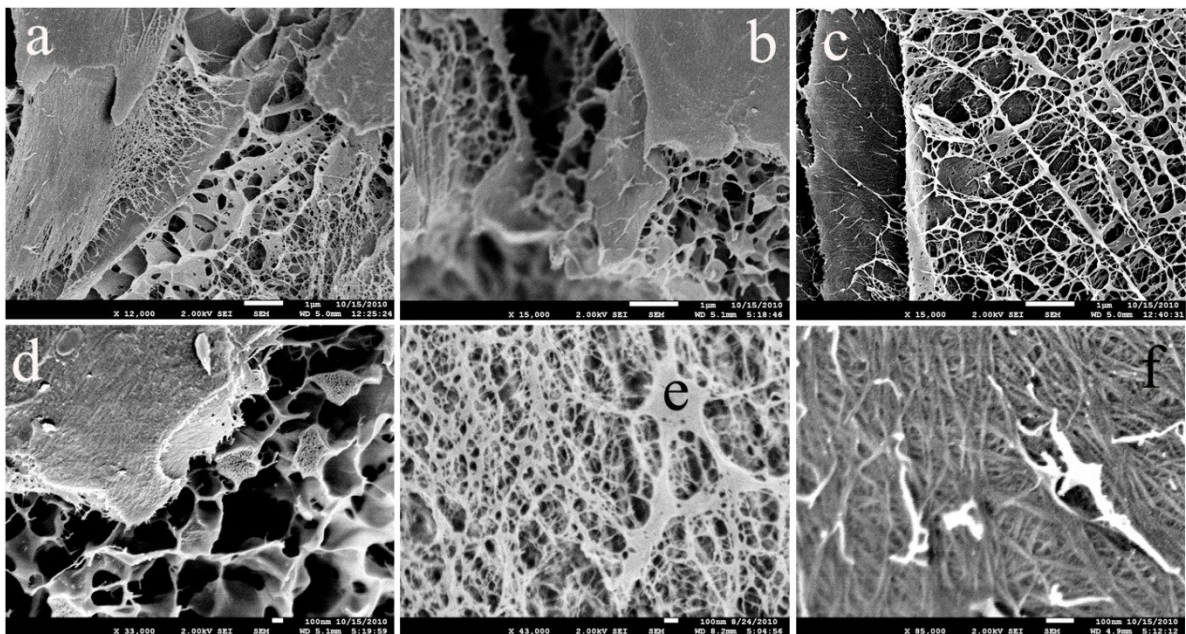


**Figure 26. Cryo-SEM micrographs of CIL in higher magnification.** Micrographs of cellulosic inner layer (CIL), with both densely packed lamellae and the sponge-like porous network of cellulosic nanofibres visible in figures (a) to (d) (magnification increased). Figure (e) depicts the structure of the sponge-like highly porous network of cellulosic inner layer, while micrograph in (f) shows the surface of a densely packed mat of cellulose nanofibres making up the lamellae.

### 3.2.3 Enzymatic removal of the cellulosic inner layer

To study the role of cellulosic inner layer in the hydro-actuated flexing movement of the keels, the non-lignified inner layer was removed enzymatically and the response of the cell's network upon wetting/drying cycles was monitored (Figure 27).

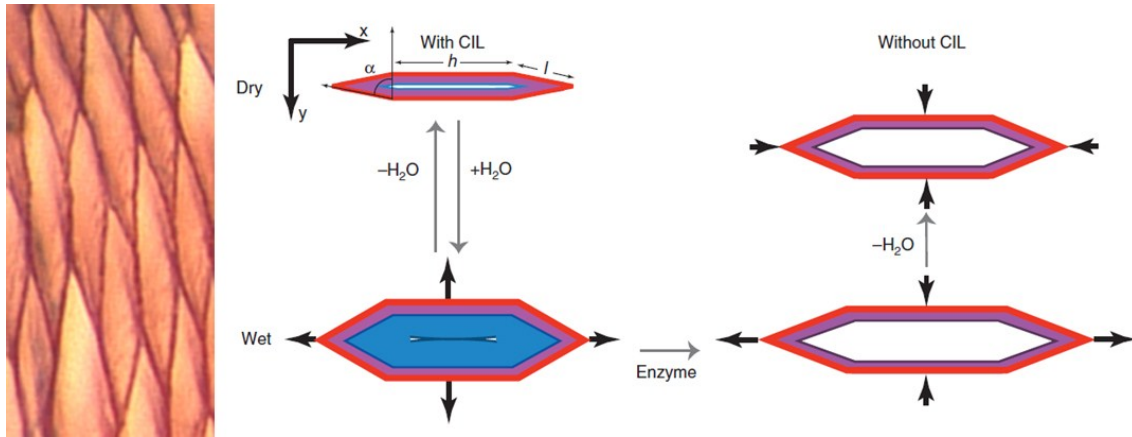


**Figure 27. Effect of enzymatic removal of cellulose inner layer (CIL) on cell's actuation.** Left: Network of keel cells after enzymatic removal of the cellulose inner layer. Right: Relative cell shapes are represented as idealized hexagons with the appropriate ratios of X to Y lengths. Thick black arrows represent the direction of change in the X and Y lengths of the cell following the respective treatment (Adopted from; Harrington, Razghandi et al. 2011).

Table 2 shows the changes in dimensions of enzyme-treated cells (without the CIL) upon wetting/drying cycles. It is clear that the cell's network without the cellulose inner layer loses its actuation response and, except a slight relaxation due to the swelling of the cell wall, does not undergo the previously observed 4-fold expansion/ retraction.

*Table 2. Relative changes in dimension of the cells with and without CIL (enzymatically removed) upon wetting/drying cycles.*

	Wet	Dry	Wet (no CIL)	Dry (no CIL)
Length X ( $\mu\text{m}$ )	100	91.6	121.4	104.3
Length Y ( $\mu\text{m}$ )	28.8	7.0	23.3	21.9
Y/X	0.288	0.076	0.191	0.210

Relative values were calculated by normalizing all values so that the length X in the wet state (with CIL) is 100. This was necessary because average cell size varies between individual keels.

### 3.3 Physicochemistry of keel's actuation

As a first step in investigating the swelling behavior of the CIL in detail, the actuation of the keels were monitored in a humidity chamber and it was observed that, the keels did not open even in relative humidity reaching up to almost 85%, and keel unfolding only occurred in the presence of liquid water. To find out the amount of water necessary for the full actuation of the keels, weight and actuation state of drying fully open keels were monitored. The water content of a fully open keel at the point where the closing started was measured to be about  $3 \pm 0.8$  mg water per milligram of the dry keel.

### 3.3.1 Thermogravimetric analysis (TGA)

#### ***Sorption isotherm***

For further investigation of CIL water interaction, keel's water adsorption-desorption isotherm was obtained by thermogravimetric analysis (TGA) (Figure 28). The sorption isotherm experiment was limited to relative humidities below 90% as working at higher relative humidity had the potential problem of water condensation and inaccurate RH in adsorption-desorption measurements. However, the keel's moisture content at the maximum reliable RH of about 85% was measured to be about 15 wt.%, which was found to be insufficient to initiate actuation.

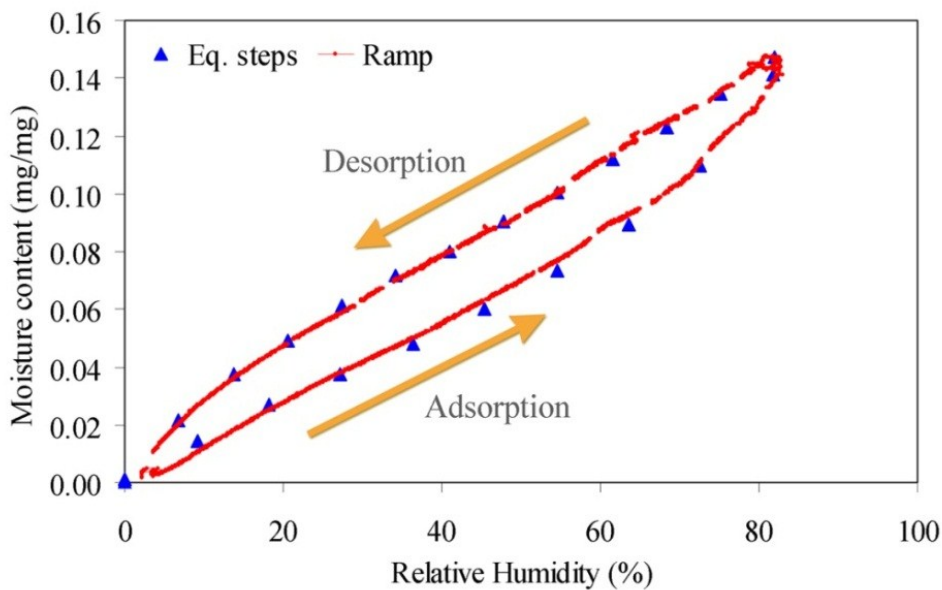


**Figure 28. Water adsorption-desorption isotherm in TGA.** Adsorption-desorption data collected during continuous ramping of relative humidity changes (red solid lines) and the equivalent data acquired from equilibrium moisture content steps (blue triangles). The maximum possible relative humidity achievable by TGA was about 85%, with the keel's maximum moisture content measured to be about 15%, which is much less than the keel's water content at fully swollen open state (300%) (Reprinted from; Razghandi et al. 2014).

#### ***Desorption experiment***

The free desorption experiment was done to provide the required information for filling the experimental gap for relative humidity above 85%. The desorption isotherm of the fully wet keels was obtained over time at 31°C and 0% RH, and is shown by means of a thick black curve on the top of Figure 29. The derivative of the water content over time ( $\frac{dWC}{dt}$ ) is also plotted at the bottom as a light-blue line.

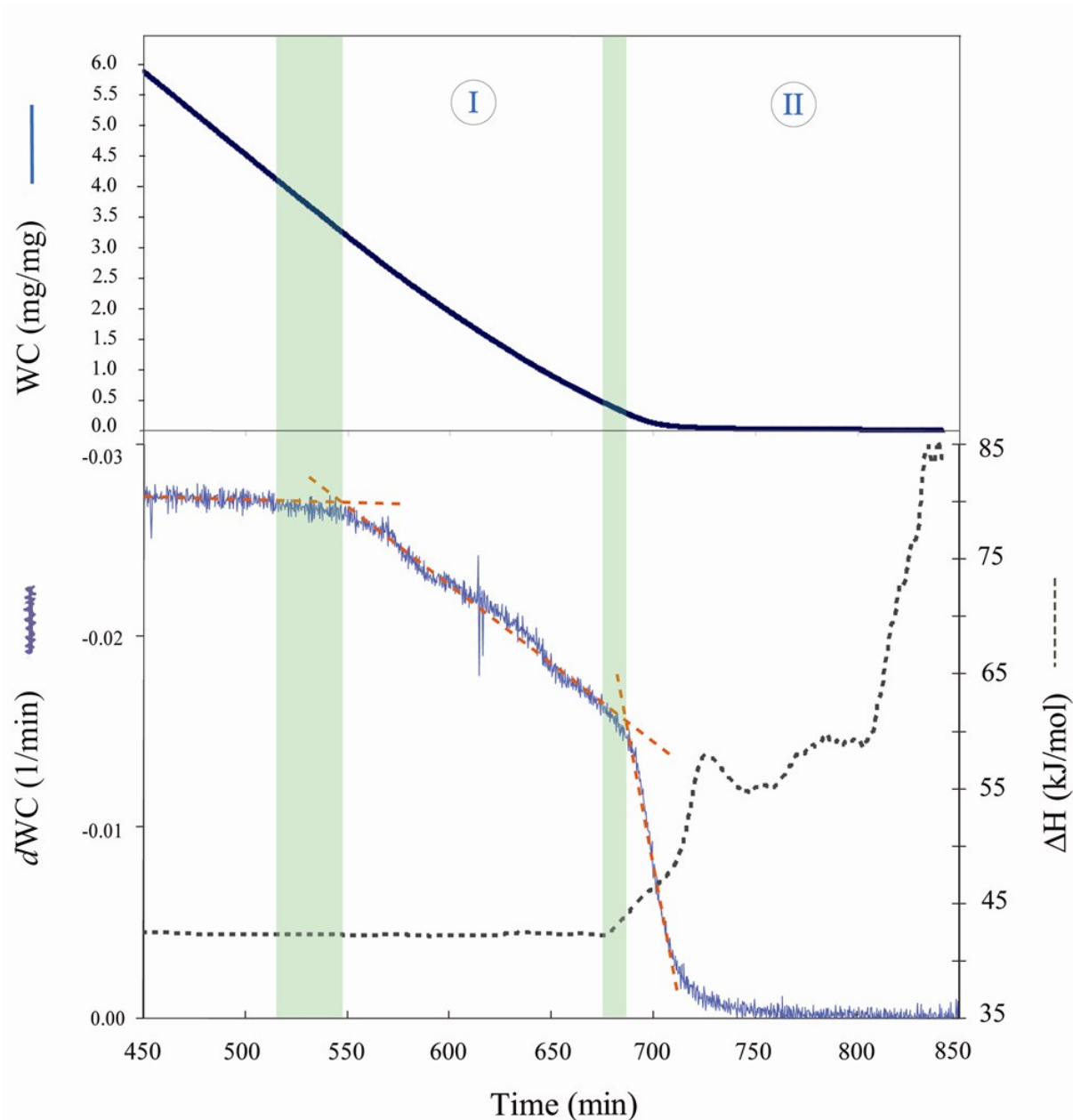


**Figure 29. Keel water loss in TGA.** The black thick curve at the top presents the keel water content ( $WC$ ) over time at  $31^{\circ}\text{C}$  and  $0\%$  RH and the light blue curve at the bottom shows the derivative of the water content over time ( $dWC$ ). The enthalpy change upon water loss is also presented by the black dotted line at the bottom. At the beginning and up to about 510 minute, the evaporation of the free water outside and adjacent to the keels occurs. From there on, two distinct desorption phases could be distinguished in the  $dWC$  graph. The onset of each desorption phase could be defined by the appearance of the first deviation in the slope of the curve (the cross-section of the two red dotted-lines), with the green windows showing the range at which the different stages start. The first decline in the desorption rate ( $dWC$ ) occurs around water content of about  $3.3\text{ mg mg}^{-1}$  (about 545 minute). Most of the water content of the keel responsible for the cell swelling is desorbed in the entropic stabilization phase (I), while the partial enthalpy of the desorption remains constant. In the second phase (II) a significant drop in the desorption rate is accompanied by sudden increase in the enthalpy of the interaction (Reprinted from; Razghandi et al. 2014).



In the first few hours, the evaporation rate was constant and evaporation of the free water inside the sample holder and on the keel's surface occurred (up to about 510-540 minute).  $\Delta H$ , the partial enthalpy of desorption (calculated from the measured heat flow), was about  $42.3 \text{ kJ mol}^{-1}$  and constant throughout this region. Considering the inherent fluctuations at zero relative humidity, this value was consistent with the enthalpy of water evaporation at this temperature (Skaar 1988).

After evaporation of the free water, two distinct desorption phases were detected in the desorption curve (Figure 29). To be able to distinguish the onset of each, the best linear fit for each region was plotted on the curve as red dotted line. The intersect of the two trend lines was taken as the onset of the first phase where the desorption rate starts to decrease, and the keel water content at this stage (about 540 minute) was measured to be about  $3.3 \text{ mg mg}^{-1}$ , consistent with the keel's water content in the fully open state measured with precision laboratory balances. Hence, this could be an indication of the beginning of desorption of the water from inside of the keels.  $\Delta H$  is still constant throughout the desorption phase (I), suggesting an entropy based desorption mechanism. An abrupt increase in the enthalpy of the interaction ( $\Delta H$ ) below water content of about  $0.4 \text{ mg mg}^{-1}$  (green window ~678-688 minute), suggests the presence of a second desorption phase, where the enthalpic term plays a significant role in the adsorption-desorption mechanism. It is also clear that the desorption rate drops significantly at this stage (Phase II in Figure 29). The significant difference between the moisture content of 15% measured at 85% RH (Figure 28) and the final water uptake of 300-350 wt.% in the completely swollen state, suggests that a boost in water uptake must occur beyond RH of 85%. This finding is corroborated by the results from the water-PEG experiments where the swelling was monitored at higher ranges of effective relative humidity.

### 3.3.2 Keel's actuation at various concentration of PEG-water solutions

To investigate the keels actuation at higher ranges of equivalent relative humidity, keel opening/closing was monitored upon changing the concentration of water-polyethylene glycol (MW= 2,000) solutions at 12, 20 and 35°C. As it was observed that FCA dye molecules could not pass through the covering membrane on top of the cells and stain the CIL, it was concluded that the much bigger PEG-2000 molecules are too spacious to pass the membrane. Hence, the PEG osmotic pressure in water solution was the determining factor whether water molecules tend to migrate to cellulose fibres or PEG chains, giving us a mean to monitor the keel's actuation at various water potentials ( $a_w$ ).

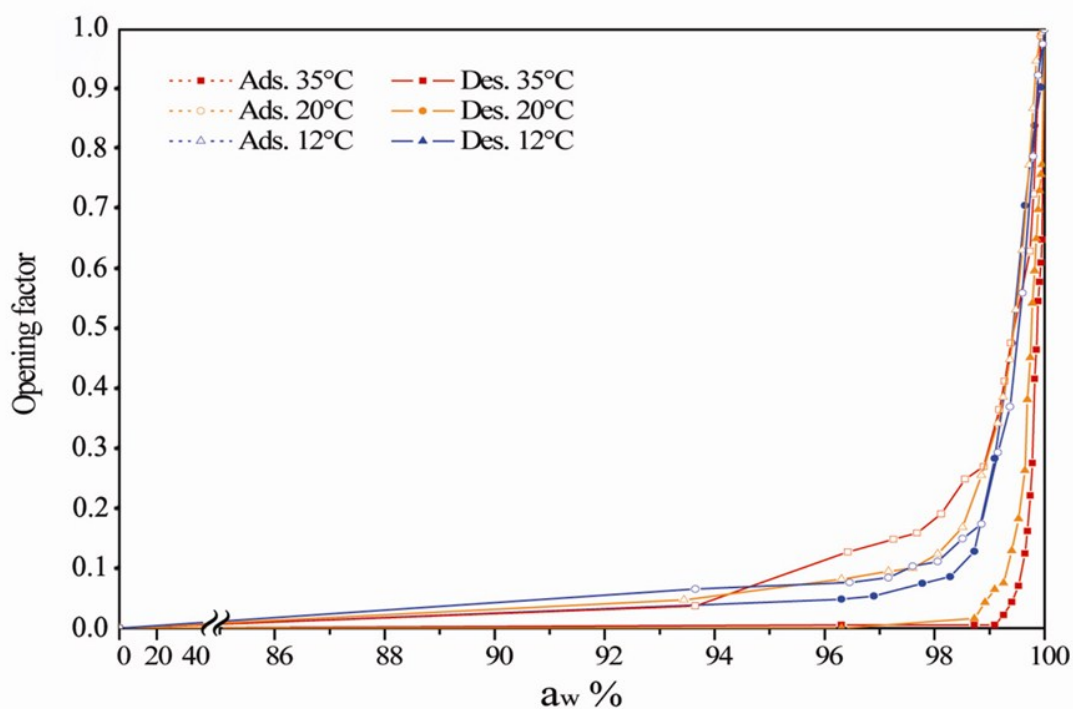
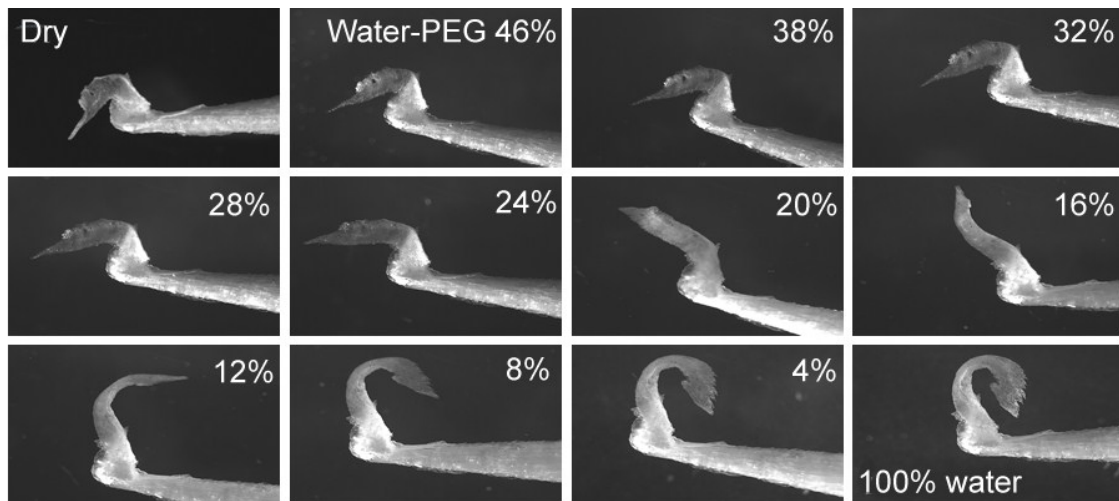


**Figure 30. Keel actuation in various PEG-water concentrations.** Image sequences depict the keels at different opening states in various concentrations of water-PEG2000 solutions; from dry keel in top-left to 50 wt.% PEG-water solution to pure water at bottom-right. The graph shows the changes in the keel opening angle monitored upon increasing/decreasing water concentration in water-PEG solutions for 12, 20 and 35°C, and were plotted against the calculated water activity in the solvent ( $a_w$ , as an equivalent of relative humidity). The opening starts only above equivalent relative humidity of about 95% (Reprinted from; Razghandi et al. 2014).

To measure the swelling pressure upon keel opening, PEG-water concentration was converted to PEG osmotic pressure using a phenomenological one-parameter equation of state proposed by Cohen et al. (Cohen, Podgornik et al. 2009). By applying the equation of vapor pressure osmometry (Teraoka 2002), the water potential  $a_w$  was calculated from the

PEG osmotic pressure as an equivalent of relative humidity. Keel opening angles ( $\alpha$ ) at different water-PEG2000 concentrations and temperatures were measured and normalized to the keel's opening angle in the completely dry and wet states ( $\alpha_d$  and  $\alpha_w$  respectively). The degree of keel opening was quantified by means of an 'opening factor' (OF) calculated as follow;

$$OF = \frac{(\alpha - \alpha_d)}{(\alpha_w - \alpha_d)} \quad (\text{Eq. 8})$$

Where OF can take values between 0 (dry) and 1 (fully wet) and increases by increasing the water to cellulose volume ratio in the cell lumen.

The opening factor vs.  $a_w$  can be interpreted as the adsorption-desorption curves for high relative humidity ranges (Figure 30). Keel opening started only above water potential ( $a_w$ , equivalent relative humidity) of about ~95%.

### 3.3.3 Actuation in different swelling agents

To investigate the influence of various features of a solvent on its actuation capability for ice plant actuation system, actuation power of water was compared to various other solvents with different characteristics. Ice plant keels were placed in different media and their actuation state at equilibrium state was measured and compared as "opening factor" (detail in methods), with the reported opening factor ranging from 0 at completely dry and close state to 100% at fully open state.

The swelling behavior of a solvent depends on different parameters such as solvent molar volume and Hansen solubility parameters (Eq. 1-2). The solubility is directly related to the internal energy of solvents and solutes. The relation between the total solubility parameter ( $\delta_T$ ) and the cohesive energy density (CED, as the energy that binds the molecules in 1 cubic centimeter) is defined as;

$$\delta_T^2 = CED = \frac{\Delta E}{V_m} = \frac{\Delta H - RT}{V_m} = \delta_h^2 + \delta_p^2 + \delta_d^2 \quad (\text{Eq. 9})$$

Where; T= absolute temperature, R = gas constant, Vm= molar volume, H= enthalpy of vaporization, E= the energy of vaporization and  $\delta_h$ ,  $\delta_d$ ,  $\delta_p$  are hydrogen bonding, non-polar and polar parts of the Hansen solubility parameter respectively (defined in Eq. 2) (Hansen 1969; Barton 1990).

Keel opening in each solvent is plotted against solvents CED, where the bubble size depicts the comparative molar volume of the solvents (Figure 31). At first glance, water was found to be the best swelling agent for CIL to actuate the keel's flexing movement.

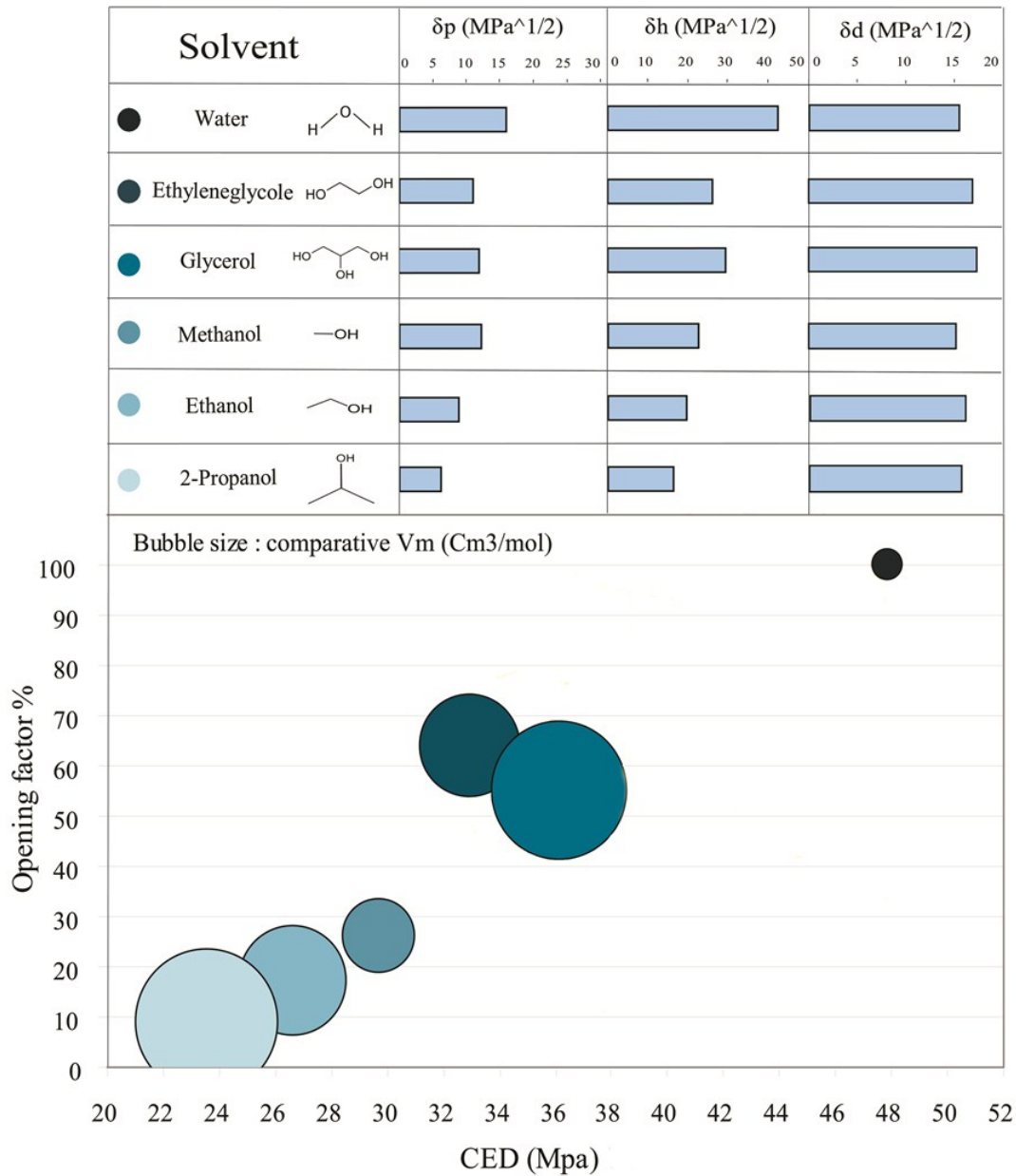


**Figure 31. Role of different solvent parameters in actuation of the ice plant keel.** The table shows the different solvents used as actuating media for the keel's actuation, with their Hansen solubility parameters shown in blue bars ( $\delta$  in MPa<sup>1/2</sup>). The three partial solubility parameters  $\delta_p$ ,  $\delta_h$  and  $\delta_d$  represent a polar interaction, hydrogen bonding component and a non-polar part of the total Hansen solubility parameter, respectively. The correlation between keel opening factor in different solvents and the solvents cohesive energy density (CED) calculated from the solubility parameters is shown at the bottom. The bubble size represents comparative solvent's molar volume (Cm<sup>3</sup>/mol).

## **4 The underlying mechanisms of the hydro-actuated movement**

### **4.1 The cellulosic inner layer (CIL) as an actuator**

The experiment with the enzymatic removal of the cellulosic inner layer (CIL) inside the lumen of the keel's cells resulted in cells losing their ability to open and close upon wetting/drying cycles, which proved the active role of the CIL in hydro-actuated movement of the ice plant keels. The removal of the CIL in the wet open cells led to relaxation of the cell walls, so that the cells length slightly decreased in the Y-direction and increased in the X-direction. The only dimensional changes observed upon wetting/drying cycles of the cells without CIL, were the slight expansion/shrinkage of the cells in X-direction, due to the swelling/shrinkage of the cell wall materials (Figure 27 and Table 2).

Initial Raman spectroscopy imaging revealed the lamellar structure of the cellulosic inner layer (CIL) with the concentric lamellas running parallel to the cell wall (Figure 22).

Further investigation of the cells frozen in open wet condition with Cryo-SEM revealed that, CIL is made up of lamellae of dense mats of cellulose nanofibres running parallel to the cell wall with a highly porous sponge-like network connecting and filling the gap between the lamellae (Figure 23-26). The highly porous sponge-like structure of the CIL resembles the structure and morphology of the cellulosic networks observed in artificial cellulose hydrogels and aerogels, which are highly porous gel-like structures made of interwoven cellulose nanofibrils (Jin, Nishiyama et al. 2004; Cai, Kimura et al. 2008). The main swelling contribution is considered to arise from this sponge-like porous structure. It was observed that the CIL morphology is not uniform through different parts of a sample, indicating that the pore size and the orientation of the fibres in the network show only a short-range local order, which can be related to the different adsorption/desorption dynamics in different regions frozen at different swelling states. One can speculate that the observed lamellar architecture most probably plays a role in determining the directionality of the swelling (Figure 22-24).

### **4.2 CIL water uptake and swelling mechanism**

In the hydro-actuated plant systems based on water-cell wall interaction (Dawson et al. 1997; Elbaum et al. 2007), an incremental change in relative humidity induces a certain level of actuation in the system, so that the movement is a direct function of the relative humidity. A remarkable peculiarity of the hydro-driven unfolding of ice plant seed capsule

was that the actuation did not occur until a surprisingly high relative humidity and needed a certain threshold for unfolding to occur (above  $\sim 95\%$  RH). It was also observed in the initial water uptake experiments, that in the fully open actuated state, keels contain  $3 \pm 0.8$  mg water per milligram of the dry keel. This was significantly more than the moisture content known for wood cell wall, indicating that the CIL adsorption mechanism might differ from that known for plant cell walls.

The TGA sorption isotherm experiment (Figure 28) was limited to RH of 0-85%, yet it revealed that even up to such high relative humidity keel adsorb only maximum water of about  $0.15 \text{ mg mg}^{-1}$  which was significantly lower than the water content measured for a fully wet open keel ( $3 \text{ mg mg}^{-1}$ ).

On the other end of the spectrum, the water-PEG experiment captured the keel's actuation above water activities of about 90% (Figure 30). To understand the relation between the two experiments, water activity in the PEG-water solution was correlated with the relative humidity in the TGA sorption experiment, while the opening factor could be correlated to the water content. The results from the osmotic experiment showed that the actuation occurred only beyond a water activity ( $a_w$ ) of about 95%. At such high equivalent relative humidity water starts to condense suggesting that actuation starts only in presence of liquid water. A trend similar to the sorption hysteresis in TGA experiment was observed in the PEG-water experiment. However, the effect of temperature on the observed hysteresis was not consistent with the known reverse effect where the sorption hysteresis decreases by increasing the temperature (Skaar 1988). Here, the desorption isotherms (obtained through decreasing the water concentration in the solution) were similar for different temperatures and slight differences were negligible compared to the errors of opening factor measurements. Adsorption curves on the other hand, were found to be temperature dependent where by going to higher temperature the keel opening was shifted to higher RH% resulting in a bigger sorption hysteresis. A possible explanation for the significant yet unusual temperature sensitivity of the adsorption curves can be that, PEG chains have less entanglement and more mobility at higher temperatures so that smaller molecules might find the chance to enter the cell lumen and sit on cellulose fibres in CIL and act as a barrier against water adsorption shifting the water adsorption and actuation to the higher water activities in the solution. This can also explain why such temperature dependency was absent in desorption curves while the starting point in the desorption experiment was always pure water covering the CIL chains, eliminating the possible effect of the small PEG molecules.

The free desorption experiment provides the required information for further speculation about the experimental gap above 85% RH (Figure 29). The sudden increase in the enthalpy of evaporation at a water content of about  $0.4 \text{ mg mg}^{-1}$  coupled with a further decline in the slope of the desorption rate, suggest a change in the adsorption-desorption mechanism at this moisture content. Initial water adsorption below this point is mainly enthalpy driven, with the first few layers of water adsorbed onto the cellulose chains. This implies that for the discussed experimental gap above 85%RH (Figure 28), adsorption would continue with the same mechanism up to about  $\sim 0.4 \text{ mg mg}^{-1}$ , which still would not be enough to trigger the actuation. The constant  $\Delta H$  above a water content of  $0.4 \text{ mg mg}^{-1}$ , suggests that the water uptake at this stage is mainly entropically driven and continues until full water uptake of about  $\sim 3.5 \text{ mg mg}^{-1}$  (Figure 29). This was in agreement with the previously measured keel water content in fully open state. Thus it could be concluded that the entropically driven adsorbed water in this region (phase I) is the mechanically working water, responsible for swelling of the CIL inside the lumen of the cells and opening of the keel.

To explain the observed difference between the actuation mechanism in ice plants and other hydro-actuated movements resulting from the swelling in the cell wall, one has to consider the observed structural spacing and morphological difference between CIL and other systems. The cell wall, as the hydro-responsive element in pine cones or wheat awns is in general a relatively compact structure. The matrix components lignin and hemicelluloses function as filling and cross-linking agent and connect the cellulose microfibrils, which results in the mechanical stability of the system and constrains the excess of water flow into the cell wall (Raven, Evert et al. 1999). In such compact structures, a few layers of adsorbed water can fill the distance between the relatively close fibrils. The enthalpic gain for this initial adsorption results in relatively small swelling strains limited to the thickness of the first layers of the adsorbed water, yet it exerts relatively large enough forces on the fibrils to actuate the movement of the organ. The network of the interconnected cellulose fibrils in CIL on the other hand, is not restricted by the surrounding matrix and shows a much more open structure than in the cell wall, making the space between the lamella-like structure more prone to water adsorption and the consequence swelling (Elbaum et al. 2008). In such an open sponge-like structure, the distance between the fibrils is too big to be filled with the first layers of adsorbed water, thus the initially adsorbed water alone could not be responsible for the swelling of the cells. At high relative humidity, when all adsorption sites have been saturated, the enthalpic gain

fades and then the entropic gain of the system is most probably the driving force for further water uptake and swelling of the cells. Here, the entropic gain of the system upon swelling of the cellulosic inner layer generates relatively low forces but leads to high swelling strains which cumulates to initiate the observed large deformation.

The experiment with keel's actuation in different media could help to gain further understanding of the cell water uptake by giving us a mean to compare the influence of various features of a solvents on the swelling of the cellulosic inner layer (Figure 31). In the first glance one can see that solvents with higher CED values showed more swelling power. On the other hand, the swelling power of a solvent is expected to decrease with increasing molar volume, as osmotic pressure (defined the ability of a network to adsorb an adsorbent) is inversely related to solvent molar volume represented by Flory-Huggins equation (Eq. 1). This can explain the comparatively minor swelling of the cells in glycerol compared to ethylene glycol. Despite slightly higher CED, glycerol's molar volume is significantly higher than ethylene glycol which makes it a weaker actuator. All three alcohols (Ethanol, Methanol and Propanol) induce only a partial swelling of the CIL, though, their minor actuation followed by the same trend of losing the swelling power by lower solubility parameters and higher molecular size. Comparison of keel's opening in glycerol and methanol put even more weight on the impact of hydrogen bonding power compared to the other solubility parameters, as despite having similar value of the polar part ( $\delta_p$ ) and relatively higher molar volume, glycerol showed double the actuation power of methanol thanks to its significantly higher hydrogen bonding power ( $\delta_h$ ). Hence, comparative studies of the swelling power of various solvent to actuate the ice plant keels illustrate how water with the highest hydrogen bonding power and dipolar intermolecular interaction, and the additional advantage of having the lowest molar volume, is the most favorable choice for swelling of ice plant CIL to fuel the actuation systems.

### **4.3 Swelling-Inflation: a coupled strategy**

It can be concluded that ice plant utilize the cellulosic inner layer (CIL) as a smart system for adjustment of their inner pressure after cell's death, providing yet another strategy for passive hydro-actuated movements. In hydro-actuated movement discussed in chapter 1.2.2, active metabolism-dependent adjustment of turgor pressure was found to control the inflation/deflation in the living cells, while for passive hydro-actuated movement discussed in chapter 1.2.3, enthalpy driven adsorption of water into the densely packed cell wall was the driving force for the passive hydro-actuated deformation of dead tissues. Through



coupling of both, the ‘swelling’ and ‘inflation’ mechanisms, ice plant can utilize passive swelling of a highly swellable inner layer (CIL) to maintain the inflation/deflation function even in the dead cells. The concept of harvesting the actuation energy from water uptake via coupling of the two mechanisms was observed before in the so called G-layers inside the cell lumen of tension wood (e.g. tension wood in chapter 1.2.3). The peculiarity of the ice plant system is that the driving force for the actuation comes from the entropic gain of the system upon adsorption of water into the porous CIL, introducing a passive mean for inducing inflation/deflation in the dead cells, which leads to a large complex movement through specific architecture of the system at higher hierarchical levels.

The difference between the underlying concept of the actuation based on the swelling of the cell wall and the one achieved through the swelling-inflation mechanism become more crucial when discussed in terms of the energy and the conditions required for achieving such large movements. In case of actuation based on the swelling of the cell wall, the chemical bonding of water as a solvent with the ability to form hydrogen bonds, and the densely packed cell wall constituents with hydroxyl sites available for adsorption of the water molecules, is crucial and the enthalpic gain of the system upon the interaction is the main energy source for the swelling and the consequent actuation. On the other hand, ‘swelling-inflation’ coupled mechanisms requires a relatively lower energy from entropic gain of the system upon swelling and can be achieved through free swelling of any suitable macromolecule in such confined cells, which will be shown with a simple chemo-mechanical model in chapter 4.5 (Razghandi et al. 2014).

#### **4.4 Unidirectional expansion and flexing of the keels**

In previously discussed examples of passive hydro-actuated movement in plants (e.g. chapter 1.3.3), tailoring the anisotropy of deformation was introduced at the cell wall level, where specific arrangement of the cellulose fibrils in the cell wall matrix (MFA) would direct the swelling and deformation. In case of the ice plant, the transaction from the simple swelling-inflation into the large directed movement comes from the architecture at cell level. It was observed that cell deformation upon swelling is not isotropic and cells swell up to 4 times in the Y-direction (shorter axis of the transverse cell cross-section), while undergo only a slight 10% expansion in X-direction (Figure 18, Table 1). The highly anisotropic deformation could be explained by the elastic deformability of the cells solely based on the anisotropy in the geometrical features of the cells. In general, the geometrical properties of cellular materials have a great influence on the mechanical properties of the

whole structure (Gibson and Ashby 1988). By simplifying the eye-like shape of the cells into an ideal cellular solid with an elongated hexagonal shape (Figure 32) the ratio between the stiffness of the cell's frame in the X- and Y-direction can be calculated by applying the following equation derived from the Gibson and Ashby model for the cellular solids (Gibson and Ashby 1988):

$$\frac{E_x}{E_y} = \frac{\left(\frac{h}{l} + \sin \alpha\right)^2 \sin^2 \alpha}{\cos^4 \alpha} \quad (\text{Eq. 10})$$

Where, h is the longer side, l the shorter side, and  $\alpha$  the opening angle in this simplified elongated hexagon model of the cells.

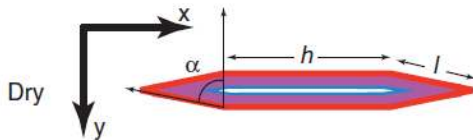


**Figure 32. Simplified model of the hygroscopic keel cells.** An ideal cellular solid with an elongated hexagonal shape representing the eye-like shape cells of the hygroscopic keel (Adopted from; Harrington, Razghandi et al. 2011).

By taking these simplified geometrical features of the cells in the dry state and assuming the cell wall material to be isotropic, the model predicts the stiffness of the keel's honeycomb tissue to be ~5,500 times stiffer in the X-direction than in the Y-direction. This ratio between the stiffness in two directions decreases to about ~30 for the cells in the wet open state. Based on this simple model, the mechanical and geometrical anisotropy observed in the cells network is the key factor in translating the swelling of the CIL inside the keel's cells into a directional deformation. It should be noted that the observed lamellar structure of the CIL (Figure 22-24) may also have a facilitating role in the observed directional swelling of the cells in Y-direction, though based on the calculation this does not seem to be a necessary requirement for the anisotropic deformation.

Although the highly anisotropic cooperative swelling at the cell level could account for the unidirectional movement of the keel's honeycomb tissue, it could not explain the flexing of the keels and the consequent unfolding of the seed capsules. To understand how the simple expansion/shrinkage of the keel honeycomb tissue can lead to unfolding/folding of the seed capsule, one has to bring the concept of bilayer bending into the account (Timoshenko 1925). Thorough study of the size and shape of the cells in fully open wet keels showed

that, compared to the free cells near the ridge of the keel, the cells connected to the inert backing tissue at the base of the keel are 25% shorter in the Y-direction. The presence of the passive backing tissue introduces a gradient in the swelling of the cells along the X-direction with two different swelling properties at the two extremities (Figure 21). To compromise between the different cooperative expansions of the cells at different distances from the backing tissue, the keel-backing structure would bend as a whole, leading to the opening/closing of the seed capsules.

#### 4.5 Chemo-mechanical model for actuation

For a better understanding of the general energetic changes that accompany the opening of the keels, the equations of thermodynamic and mechanical equilibrium of the system were considered. The keel could be treated as an ensemble of several osmotic compartments (the cells), each containing a polymer that swells in water. The amount of the macromolecules inside each cell was assumed not to change during the experiments due to the impermeability of the osmotic membrane covering the cells. The only component that could be exchanged across the membrane was assumed to be the solvent (water in this case). It was also assumed that the CIL is made of a non-cross-linked polymer so that there is no work term included to account for the elastic energy required to swell the polymeric network.

As the CIL is confined inside the cells, upon swelling it pushes against the cell walls to open the keel. At equilibrium, the partial free energy of the absorbate outside and inside the keel is identical, so that:

$$-\Pi(\alpha) = \frac{1}{\bar{v}} \frac{\partial \Delta G_{mix}(\phi_w)}{\partial n} + P(\phi_w) \quad (\text{Eq. 11})$$

Where  $\Pi$  is the osmotic pressure of the solvent outside the keel cells (i.e. in the gas phase or in the PEG solution), which depends on the activity,  $\alpha$ .  $\bar{V}$  is the molar volume of the solvent,  $n$  is the number of water moles,  $\phi_w$  the water volume fraction in the cells and  $p$  the mechanical internal pressure due to the elastic response of the structure to the strains imposed by the swelling.

Equation 11 defines an implicit relation between the water activity (through the osmotic pressure) and the amount of water molecules inside the cells at equilibrium. As this equation describes the sorption behavior of the keels, it could be applied to model their opening. To do so, a model for the partial free energy of the solvent and a model for the mechanical work as a function of the water content were defined as follows.

**Chemical model:** As the molecular structure of the CIL is partly unknown, there is no precise thermodynamic model for the partial free energy of the solvent. Nevertheless, a semi-quantitative treatment could be done considering that the CIL consists of polysaccharide macromolecules and the Flory-Huggins relation could express the chemical potential of the solvent. For several water-polysaccharides solutions, the first term of the Eq.11 can be approximated by (Treloar 2005):

$$\frac{\partial \Delta G_{mix}(\phi_w)}{\partial n} = RT \left( \ln(\phi_w) + 1 - \phi_w + \chi(1 - \phi_w)^2 \right) \quad (\text{Eq. 12})$$

Where  $\chi$  is the Flory interaction parameter.

In principle the equation describes the chemical potential of the solvent in the whole dilution range, provided that the value  $\chi$  is known at every volume fraction. For concentrated polymeric solutions,  $\chi$  depends on the nature of the macromolecule, but in the dilution ranges we are interested in ( $\phi_w$  higher than 0.2), a constant value for  $\chi$  of about 0.5 was taken to approximate the chemical potential of water (Eckelt et al. 2008; van der Sman and Meinders 2011).

**Mechanical model:** Upon actuation, the valve flexes from a closed configuration with a convex curvature to an open one with reversed curvature. From a mechanical perspective and given the morphology of the actuating system, each actuating unit was considered as a bilayer of two materials (keel honeycomb tissue + backing layer), with different thickness, stiffness and expansion coefficient. An approximate estimation of the change of curvature due to hindered keel expansion against a non-expanding backing could then be provided by the theory of Timoshenko (Timoshenko 1925):

$$\Delta \alpha = \frac{6l\Delta\varepsilon(1+m)^2}{t_{tot} \left( 3(1+m)^2 + (1+mn) \left( m^2 + \frac{1}{mn} \right) \right)} \quad (\text{Eq. 13})$$

Where,  $\Delta \alpha$  is the increment of the curvature angle of the bilayer;  $m = \frac{t_k}{t_b}$  and  $n = \frac{E_k}{E_b}$  are

respectively the thickness and stiffness ratios between the keel (k) and the backing tissue (b);  $l$  is the length of the portion of bilayer that is actually flexing;  $\Delta\varepsilon$  is the keel-backing differential swelling strain and depends on the internal pressure (resulting from the swelling of the model macromolecules inside the confined cells), leading to the expansion of the keel cells (the backing is assumed not to swell).

Mechanical testing on dissected keels and backing specimens has proven to be unviable due to the small dimensions of the specimens. Hence, their mechanical properties were extrapolated from geometrical features of their microstructure (Table 3), and were utilized as input for the finite element simulation of the keel's flexing, where the keels were modeled as a regular two-dimensional cellular structure with highly anisotropic diamond shaped cells. The geometrical data of keel and backing microstructure were collected from the representative samples. The stiffness of the keel in a direction parallel to the cells short axis has been calculated with the Gibson-Ashby formula for 2D cellular materials (Gibson and Ashby 1988):

$$E_k = \left( \frac{t_{wall}}{l_{wall}} \right)^3 \frac{\sin \alpha}{\cos \alpha^3} \quad (\text{Eq. 14})$$

The backing layer is a foam material with thicker lignified cell walls. Mechanical properties are extrapolated by using a closed cells foam model with rhombic dodecahedra topology:

$$E_b = f^2 \left( 1.9 \frac{t_{wall}}{l_{wall}} \right)^2 + (1-f)(1.9) \frac{t_{wall}}{l_{wall}} \quad (\text{Eq. 15})$$

Where,  $f$  is the fraction of material contained in the cell's edges, while  $1-f$  is the fraction contained in the faces.

*Table 3. Geometrical data of ice plant hygroscopic keel and backing tissue.*

	Keel	Backing
<b>Microstructural data</b>		
Microstructure type	2D cellular, diamond-shaped cells	Closed cells foam, rhombic dodecahedra cells
Cell wall thickness ( $\mu\text{m}$ )	2.15	5.71
Cell parameters	$X_{\text{cell}}=83.16$	$l_{\text{wall}}=17.24$
	$Y_{\text{cell}}=6.36$	
<b>Bilayer data</b>		
Layer thickness ( $\mu\text{m}$ )	720	44.4
Swelling strain	(from FE simulation)	0.

Through a simple 2D finite element simulation (performed by Guiducci L., Razghandi et al. 2014), the final configuration of keel's microstructure upon exposure to hydraulic pressure inside the cells could be predicted. In this way the keel's extension along the Y-axis was derived as a function of the internal pressure. The simulations revealed that a value of pressure  $p^*=150$  kPa is sufficient to open the model cells up to about 4-fold that was observed in the fully actuated keel cells (Figure 33a-d).

On the curve in Figure 33d, the transition from the initial wet state (where only the walls are swollen) to the full swollen state (where the keels has expanded 4-fold) corresponds to the portion of curve delimited by the dotted line. It is worth noticing that the value of pressure is in the order of hundreds of kPa, hence only a relatively small mechanical work is needed to reach the fully swollen state.

Finally, to describe qualitatively the opening of the keel with the chemo-mechanical model, we had to relate the opening factor with the water volume fraction inside the cells. This was done by considering that the volume of the cell's lumen relates to the keel's strain ( $\Delta\varepsilon$ ), which itself is proportional to the curvature (opening angle) of the keel. Taking the volume of the CIL as the volume of the lumen of the closed cell, the volume fraction of water was calculated at every strain as the volume increase with respect to the dry state divided by the actual volume of the lumen.

Considering that the  $X_{cell}$  and cell height do not change significantly while opening, the CIL volume fraction was estimated as:

$$\phi_{CIL} = \frac{V_{CIL}}{V_{tot}} = \frac{\varphi(y_{cell} - 2t_{wall})x_{cell}h_{cell}}{[(1 + \Delta\varepsilon)y_{cell} - 2t_{wall}]x_{cell}h_{cell}} = 1 - \phi_w \quad (\text{Eq. 16})$$

Where,  $V_{CIL}$  and  $V_{tot}$  are respectively the inner volume of the dry keel and the expanding keel. To take into account the porosity of the CIL, an effective volume fraction of the dry swelling polymer  $\varphi$  was used which represents the fraction of the keel's inner volume occupied by the CIL in the dry state.

In this way, the water volume fraction could be obtained from this equations by substituting  $b\Delta\alpha$  for  $\Delta\varepsilon$ ;

$$\phi_w = 1 - \frac{\varphi \cdot y}{b \cdot \Delta\alpha + 1 - 2t'} \quad (\text{Eq. 17})$$

Where  $\Delta\alpha$  is the total opening angle, which can be normalized by  $(\alpha_{Dry} - \alpha_{Wet})$  to relate to the opening factor (OF in Figure 30), b is the materials/structure dependent constant linking

$\Delta\varepsilon$  and  $\Delta\alpha$ ,  $y = \frac{y_{cell} - 2t_{wall}}{y_{cell}}$  and  $t' = \frac{2t_{wall}}{y_{cell}}$  where  $y_{cell}$  and  $t_{wall}$  are defined in Figure 33.

Combining Eq. 12 with Eq. 17 and using the pressure vs. opening angle curve obtained by the finite elements simulation, the expected opening as a function of the water activity was calculated through Eq. 11 at 20°C (Figure 33e).

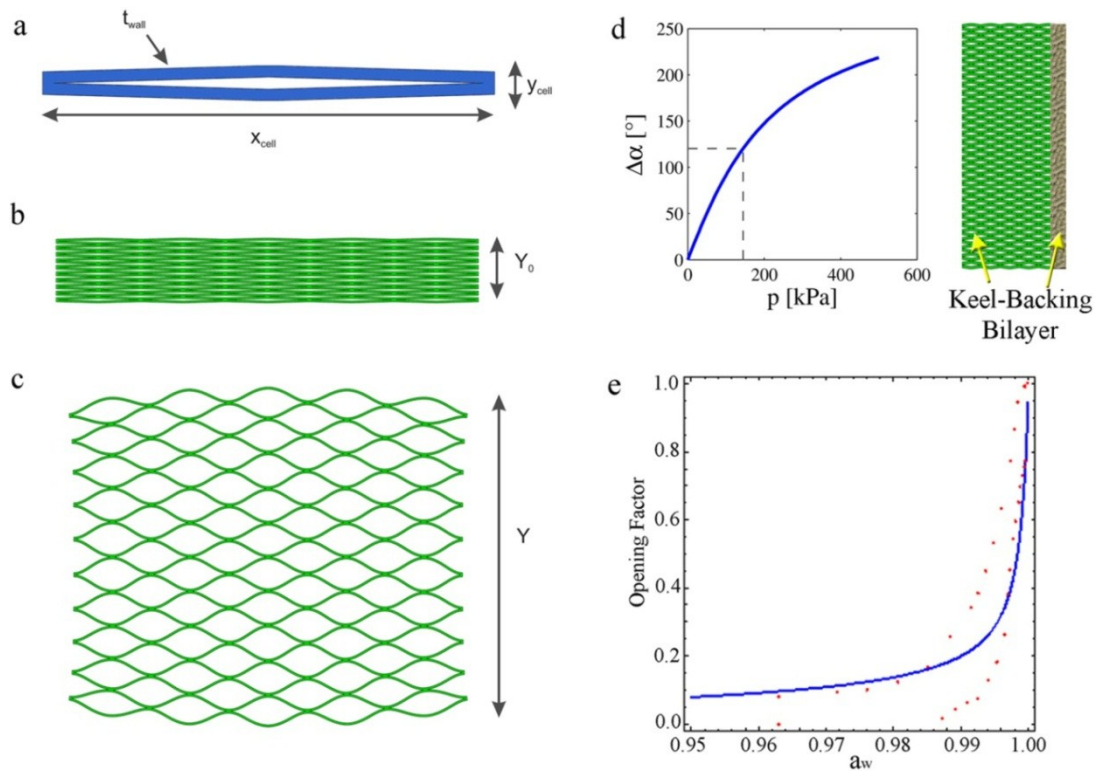


**Figure 33. Simple chemo-mechanical model for keel's actuation.** Left: Finite element simulated deformation of the keel's tissue under hydraulic pressure showing the dependency of the elongation of the keel as a function of the effective mechanical pressure acting in the cells. A representative unit cell (a) has been replicated to create a  $5X_{cell}$ -by- $10Y_{cell}$  array (b). Given the high anisotropy of the microstructure, the experimentally observed value of extension  $Y/Y_0 = 4$  (c) was achieved already at a value of pressure  $p = 150$  kPa. Bending of the keel-backing bilayer ( $\Delta\alpha$ ) upon changes in the mechanical pressure inside the cells, predicted from Timoshenko formula is presented in (d). The grey dotted line locates the value of pressure  $p=150$  kPa at which  $Y/Y_0 = 4$  (fully swollen state). Using Eq.17 and the keel backing curvature curve in (d), the simulated opening vs. water activity ( $a_w$ ), was calculated at 20°C for a CIL effective density  $\phi$  of 0.7 (blue curve) and was found to be in good agreement with the experimental data from PEG-water experiment presented here as red dots (e) (Reprinted from; Razghandi et al. 2014).

The calculated opening factor vs. water activity curve shows a good agreement with the experimental data gained from the PEG-water experiment (Figure 33e). The model predicts

an onset of the actuation and opening of the keels to happen at water activities higher than 98%. At this point, the free energy available to do mechanical work is still quite low, yet it can induce a full actuation only through an elaborate design of the keels to fully exploit small forces, without spending too much energy to deform the cell walls.

To summarize, the chemical model could show how the available free energy from the entropic gain of the system upon free swelling of a model macromolecules inside confined cells (with the geometrical feature resembling the ice plant keel's cells), can generate high enough mechanical pressure inside the cells (~150kpa), which based on the mechanical model, is sufficient to induce a four-fold opening of the model cells, and accomplish a full flexing cycle of the model honeycomb-backing bilayer structure. Through the combined chemo-mechanical model, we could relate the opening angle of the model honeycomb-backing bilayer structure to the volume fraction of the swelling model macromolecule (or CIL) and plot an "opening factor vs. water potential" curve comparable to the one obtained from the PEG-water experiments (Razghandi et al. 2014).

The bilayer actuation mechanism was found in plant actuators where big deflections could be achieved by dimensional amplification using long bilayers and small differential strain such as in wheat awns (Elbaum et al. 2007). However, in the case of the ice plant seed capsule, the same mechanism works with a relatively bulky, non-slender, bilayer structure and a massive differential strain, to produce a remarkable curvature change required for the reversible opening and closing of the seed chambers.

#### **4.6 Origami-like folding/unfolding of the seed capsules**

Beside the flexing movement of the two keel halves, the separation of the keels upon drying adds to the complexity of the folding/unfolding of the seed capsules. The two halves of the keel were found to be touching on their ridges in the wet state and moving apart from each other upon drying (Figure 19, 20). The gap between the two halves in the dry state seems to be a necessary requirement for the packing of the whole seed capsule, as we know that in the initial conformation, the valves are closed during the plant development. The backing tissue was found to have a concave-curved shape in the dry state which converts into a straight plane upon wetting. Figure 19 and 20 show how changes in the curvature of the backing tissue upon wetting/drying cycles enables the two keel halves to move apart and facilitate the tight packing of the septum into the resulted gap. The hydration-dependent changes in the curvature of the backing tissue disappeared upon dissection of the honeycomb cell network from the backing, which suggested that the observed bending of



the backing could be related to the cooperative swelling of the cells in Y-direction and flexing of the keels. However, it should be noted that the separation of the two keel halves upon drying could also to some extent be related to the slight shrinkage of the cells in X-direction (Figure 20).

Simple finite element simulations performed by coworkers on the project (Harrington, Razghandi et al. 2011) proved that the shrinkage of the similar contractile elements (keels) attached on top of a passive plane (backing tissue) could lead to two distinct deformations observed in the biological model system (Figure 34).

The resistance of the passive shell (backing tissue) against the contraction of the two active elements results in the bending and flexing of the bilayer structure as expected from the Timoshenko's principle. Besides, the contraction of the active elements results in the development of elastic stresses in the passive plane. To release these stresses the shell bends in the XZ-plane and in the same direction observed for the backing, though the magnitude of the curvature was found to vary with shape, thickness and elastic properties of both backing and active elements (Harrington, Razghandi et al. 2011). A similar mechanism was reported in other planar structures like plant leaves, where the difference in growth rates leads to formation of differential stresses in the leaf plane, release of which could result in out-of-plane bending and wrinkling of the leaves (Audoly and Boudaoud 2003; Liang and Mahadevan 2009).

A simple paper-folding experiment could demonstrate how the curvature of the backing tissue in the dry state could hinder the unfolding mechanism and somehow locks the seed capsules in the close conformation. Bending the top half of a folded sheet of paper proved to lock the structure in the folded (closed) state (against the gravity), while releasing and straightening the top half resulted in 'unlocking' of the structure and opening of the folded paper (Figure 35).

Hence it could be concluded that for the hygroscopic keel to initiate the flexing movement upon actuation, the backing tissue need to switch from a curved to a plane state. The difference between the finite element and the paper model is that the former allows for the stretching deformation of the backing while the later doesn't, thus depicting the two extreme case of how bending can occur, with the biological system lying probably somewhere between the two mechanisms.

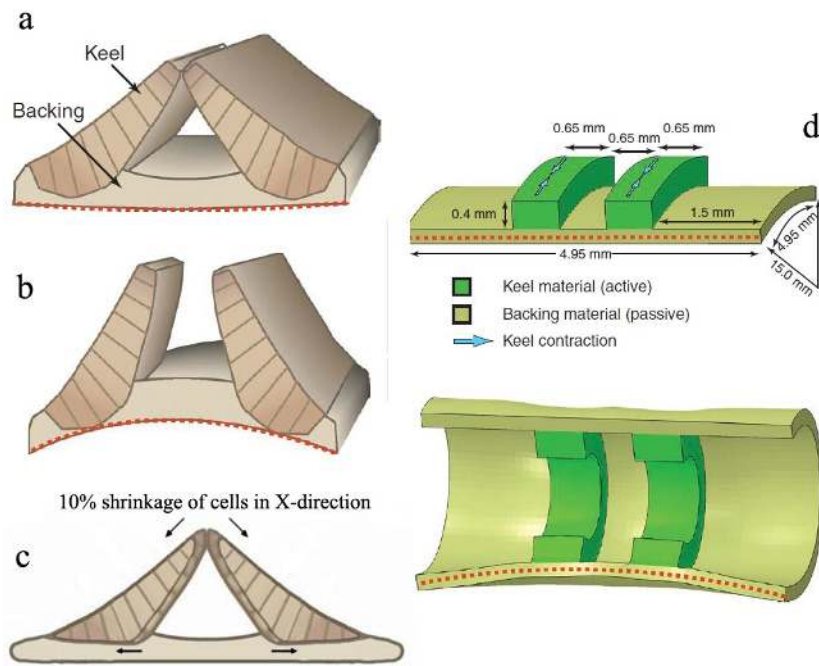


**Figure 34. Mechanism of the flexing and packing of the keels.** Schematics in (a) and (b) illustrate the changes in the curvature of the backing tissue and the separation of the two keel halves in the wet and dry state respectively. The influence of the shrinkage of the cells in the X direction on separation of the keels upon drying is depicted in the figure (c). Finite element simulation of two contractile elements (keels) on top of a passive plane (backing tissue) with geometrical and mechanical features similar to the biological model, performed by coworkers in the project (d), could show how the swelling of the cells in the Y-direction leads to both flexing of the bilayer structure and stress release and bending of the backing tissue in XZ-plane (Re-sketched after; Harrington, Razghandi et al. 2011).

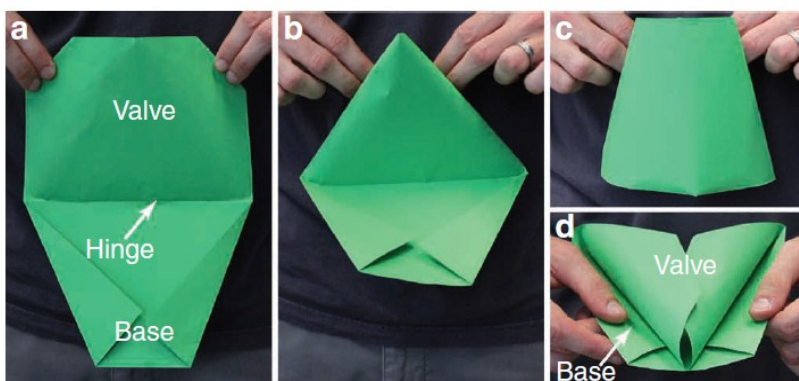


**Figure 35. Paper model for ice plant seed capsule locking mechanism.** Paper origami model (a-d) demonstrate the locking mechanism induced by the backing curvature; when the top half of the folded paper is straight (no bending) it allows the paper to move freely at the hinge (a). Inducing a curvature in the structure by bringing the corners of the top half together (b), results in the upward folding of the bottom half with (c) and (d) showing the folded structure from both sides. The structure was locked in the folded status, and gravity could unfold it only upon releasing the curvature on the top half (Reprinted from; Harrington, Razghandi et al. 2011).

It was also observed that the capsules were locked in a half-open conformation even in the dry state when the drying was accelerated under the vacuum condition, showing the importance of the temporal synergy between the flexing of the keels and bending of the backing. The differential drying of the highly hygroscopic CIL and the less hygroscopic lignified cell walls seems to be a key factor in concerting the temporal mismatch and interplay of the bidirectional movements.

#### **4.7 Ecological adaptation**

In terms of ecology, ice plant strategy to respond only to liquid water and not the changes in the environment relative humidity could be an effective adaptation to its natural habitat. Ice plants usually grow in vast ranges in arid regions (e.g. Namib Desert). In the areas close to the coast belonging to the natural habitat of ice plants in the Namib Desert, the night fog from the cold sea can move up to 100 km inland almost every day, increasing the relative humidity from below 10% during the day up to above 90% (Ebner et al. 2011; Eckardt et al. 2013). A system adapted to movements based on changing air humidity would consequently react every day while a system responding only to liquid water would be more preferred as it can ensure the seed dispersal in the right condition for germination. Although water condensation might happen and still result in opening of the capsule, this can be assumed as a less likely scenario as the fog is limited to few hours and the water condensation might be hindered and the swelling would only occur after sufficient exposure to liquid water (rain) (Razghandi et al. 2014).

## 5 Biomimetic design

As discussed in the previous chapters, adsorption/desorption of water can provide the necessary energy for a variety of actuated stress generation or movement mechanisms in plant kingdom. Passive actuation systems which do not depend on the active role of the living organism are in particular a better candidate for biomimetic transfer and further development of autonomous ‘smart’ systems (Shahinpoor and Thompson 1995; Taya et al. 2003; Fratzl et al. 2008; Reyssat and Mahadevan 2009; Turcaud et al. 2011; Erb et al. 2013; Ma et al. 2013). By applying the same principles observed in the passive actuation systems in plants, various researchers have tried to embed the desired response to specific stimuli by modeling and tailoring various structural features at different hierarchical scales. To show the potential of how the basic principles of plant hydro-actuated movements can inspire the development of new smart systems, Reyssat and Mahadevan utilized the basic mechanism behind the bending movement of the wheat awns and pine cone scales to model and develop a simple bilayer that responds to changes in the surrounding humidity and undergoes a bending movement (Reyssat and Mahadevan 2009). Their flower pellets were made up of an active paper layer with a directional swelling along the leaf axis and a passive polymer film glued to the other side. The flower undergoes a reversible opening and closing upon wetting and drying cycles (Figure 36).

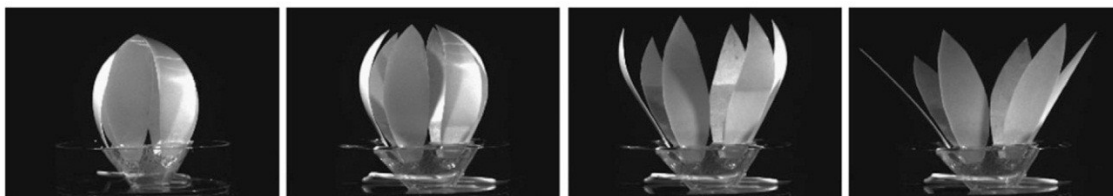


**Figure 36. “Hygromorph model”.** A biomimetic model of a hydro-responsive flower made up of paper–plastic bilayer petals. The “blooming” of the flower can be controlled by humidity so that the petals open when wetted with water and close as they dry (Reprinted with permission from; Reyssat and Mahadevan 2009).

Abstracting from the biological actuators, the source of actuation can be multiple. Any stimuli that can lead to a reversible volume change can be a potential candidate for passive actuation. Some examples are thermal expansion (Que et al. 2001, Park et al. 2001), solvent absorption (water or other proper solvents) (Guiducci 2013) or even magnetic fields as proposed and developed by Erb and colleagues (Erb et al. 2013). By controlling the orientation of inorganic particles inside a swellable polymeric matrix by a weak external magnetic field, they were able to design shape deforming “smart” materials, which can be

programmed to respond differently to the external stimuli according to the required final state or function (Erb et al. 2013). Other abstractions can come from changing the source of heterogeneity. As it can be observed in bending of a paper strip upon wetting, water needs time to diffuse through the paper, so the activation field of water is heterogeneous while the swelling properties are approximately homogeneous. Therefore, in terms of a biomimetic transfer, the question of size and shape is of tremendous importance. Recently, sensitive hydro-actuated polymeric thin films were introduced which can perform a rapid and continuous movement through a slight water exchange with their environment (Ma et al. 2013). A further aspect of these systems studied by Turcaud et al. is that the different arrangement of an expanding and a resisting phase can lead to a variety of responses and performances (Figure 37). Twisting, as an example, can occur when the two phases are no longer arranged along a mirror plane, but around a rotational axis (Turcaud et al. 2011).

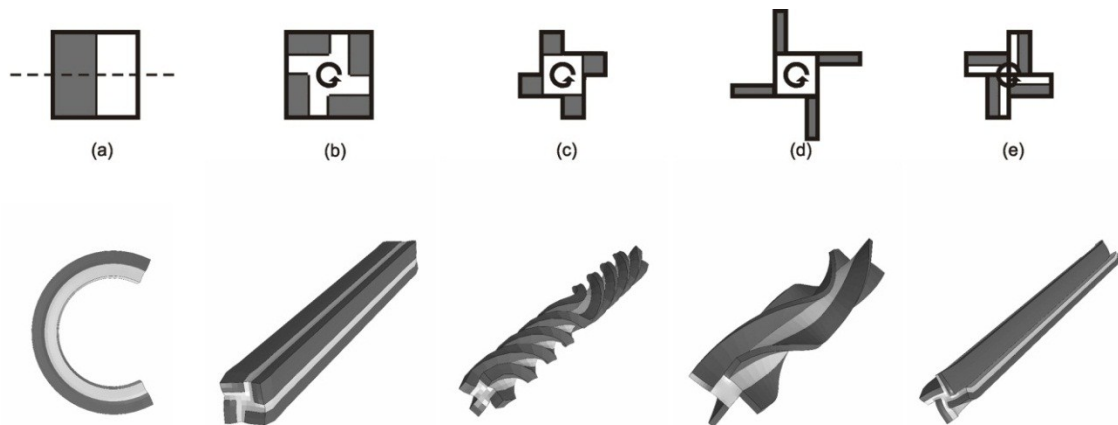


**Figure 37. Actuation patterns simulated for a variety of cross-sectional distributions of the active and passive elements.** (a) Bilayer bending in mirror plane; (b) Closed 4-fold cross section with bilayer unit cell remaining straight; (c) Opened 4-fold cross-section with bilayer showing a large twist; (d) Opened 4-fold cross-section with bigger moment of inertia resulting in less twisting than (c); (e) Opened 4-fold section with differently oriented bilayer unit cell remaining straight (Reprinted from; Turcaud, Guiducci et al. 2011).

The aim of the last part of the thesis is to utilize the abstracted principles behind the passive hydro-actuated movement in ice plant seed capsules to develop biomimetic demonstrators as a proof of concept. Thereby showing the possibility of tailoring and amplifying the initial material's response to external stimuli, through simple yet sophisticated design of the system.

## 5.1 Abstraction of the principles behind ice plant's hydro-actuated movement

The origami-like unfolding of ice plant seed capsules as a sophisticated passive hydro-actuation systems is gaining rising interests in the biomimetic research, with few models already been inspired and developed based on the concepts behind this hydro-actuated system (Ionov 2013; Rafsanjani et al. 2013; Guiducci 2013).

A well-defined extraction and abstraction of the basic principles behind the ice plant passive movement is essential for developing related smart actuation systems. The engine of the investigated actuated movement was found to be the water adsorption and swelling of the highly swellable cellulosic inner layer inside the lumen of the keel cells, yet the relatively complicated movement could only be explained in terms of the sophisticated design at various hierarchical levels of the system (Figure 38).

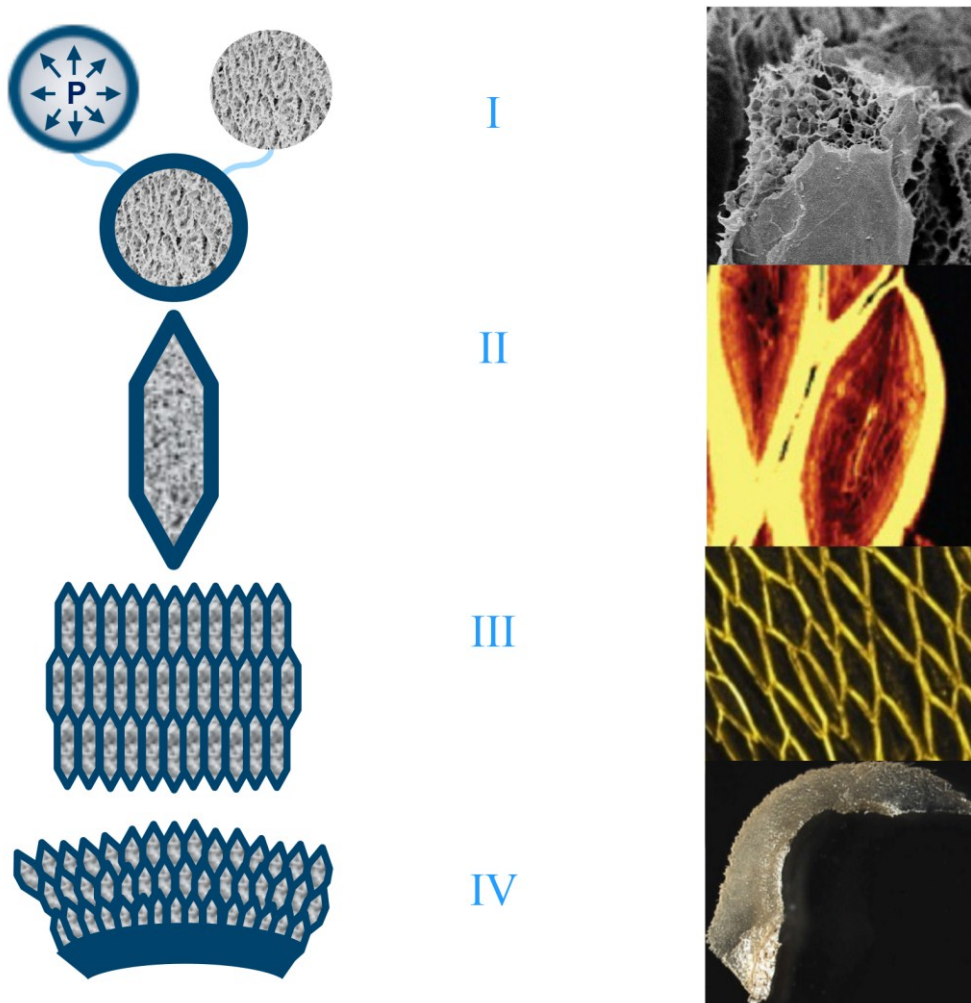


**Figure 38.** Abstraction of the principles behind ice plant hydro-actuation system. Schematics illustrate the actuation principles at different hierarchical level of the system:

**Figure 38 continued:** (I) The first hierarchical level shows the starting point where a highly swellable polymer can play the role of inducing and adjusting the inner pressure inside a confined compartment, leading to an isotropic volume change of the cell (Cryo-SEM image of the cellulosic inner layer). Next level (II), depicts how through tailoring the geometry of the cell one can achieve a desired anisotropic deformation upon changes in the inner pressure through swelling/shrinkage cycles (Raman image of the cells transverse cross-section). (III) illustrates the scaling up of the same concept, where the cooperative anisotropic deformation of individual cells can result in a unidirectional expansion/retraction movement (autofluorescence confocal microscopy image of the keel's honeycomb). (IV) Shows how a unidirectional expansion/extraction can be translated into flexing of the whole honeycomb structure when swelling of the cells in one side is restricted via attachment to an inert backing tissue (Flexing of the keels upon wetting based on the bilayer bending principle).

### ***'Swelling-inflation' strategy***

The first level of abstraction is the concept of utilizing a coupled 'swelling-inflation' strategy to induce a volume change in a confined cell. Ice plant hygroscopic keel cells are an ingenious example of utilizing the swelling/shrinkage of a highly swellable material (CIL) as a passive mean of inducing a passive inflation/deflation inside the lumen of the cells, mimicking the turgor pressure in living cells. By constraining a swellable material into a confined compartment, one can think of the volume changes of the swelling material as alteration of the cell's inner pressure and achieve the desired change in the cell size by tailoring the specific characteristics of the swellable inner layers (composition etc.) and the mechanical response of the cell walls, thus creating a passive hydro-actuation system (Figure 38). The abstracted concept of a 'swelling-inflation' strategy was utilized in the development of the first hydro-actuated demonstrator in chapter 5.2.

### ***Tailoring the anisotropy of swelling***

Another important lesson that can be learned from the ice plant actuation system is the influence of the specific geometrical features of the cells on the final actuated shape of the cell. In the case of the ice plant, the unique ellipsoid-hexagonal shape of the cells, shows an example of how an isotropic swelling/shrinkage of a swellable inner layer inside the lumen of the cell, can be translated into an anisotropic directional deformation of the cells.

Through scaling up the same concept for a single cell into a network of connected cells, one can see how the anisotropic deformation of a single cell is translated into a unidirectional expansion/contraction of the resulting honeycomb structure (Figure 38). By an elaborate design of the cells with various geometrical features and arrangements, one can tailor the response of the cellular structure upon actuation, giving yet another lever in exploring the biomimetic design space (Guidicci 2013). The abstracted idea of utilizing a

cellular structure to tailor the actuated movement was embedded in the design of both proposed biomimetic prototypes in chapters 5.2 and 5.3.

### ***From anisotropic expansion to more sophisticated movements***

The transition from the unidirectional expansion to the flexing movement could easily be modeled as bending of a Timoshenko bilayer (Timoshenko 1925). The cell's swelling gradient from the keel base (restricted to the inert backing tissue) to the keel ridge, results in a flexing of the whole structure as a bending bilayer (Figure 38). Through utilizing such simple models one can envision to translate the simple response of active and passive layers into further movements like bending or twisting through tailoring the architectural design as shown in Figure 37. The abstracted concept of simple bilayer bending elements inspired the design of the autonomously deforming bilayer-honeycomb actuator in chapter 5.3.

## **5.2 Bio-inspired hydro-responsive hydrogel-filled honeycomb actuators**

The first attempt towards a bio-inspired design based on ice plant as a biological model system, was to utilize the concept of 'swelling' as an 'inflation' mechanism in which swelling/shrinkage of a highly swellable material inside confined cells of a honeycomb framework would lead to a unidirectional expansion/contraction of the hydro-actuated honeycomb device.

Highly swellable and pH sensitive super porous poly-acryl-co-acrylamide hydrogels (Gemeinhart et al. 2000) were synthesized inside the cells of a 3D printed polymeric cellular structure (prepared by Dr. James Weaver's group at Wyss Institute, Boston), with geometrical features resembling ice plant keel's honeycomb model previously used in the finite element simulation (more details in the experimental section).

The initial analysis of the free swelling of the hydrogel discs from fully oven-dried weight to fully swollen state after almost a day showed water uptake of about  $20 \text{ gr gr}^{-1}$ , which led to an almost 30 fold increase in the volume of the hydrogel discs. The macroscopic porosity introduced in the hydrogel system in the synthesis process enables higher swelling and shrinking rates through enhancing the diffusion of water into the structure by capillary forces (Gemeinhart et al. 2000). To study the pH sensitivity of the highly swellable hydrogels, the swelling/ shrinkage behavior of the hydrogels in acidic (pH 1.2) and basic (pH 8) solutions were monitored and revealed a  $\sim 30\%$  increase in the swelling from a water uptake of about  $3 \text{ gr gr}^{-1}$  in the acidic solution to a  $4 \text{ gr gr}^{-1}$  water adsorption in the basic medium.



Due to the various problems associated with preparation and characterization of the hydrogel-honeycomb system, such as; (i) not having the necessary control over synthesis of a reliable hydrogel batch with consistent porosity and stiffness, (ii) lack of a proper attachment of the hydrogel into the hydrophobic cell walls and escaping of the swelling hydrogel out of the honeycomb cells (Figure 39), (iii) problems associated with measuring the dry weight of the hydrogel inside the cells and (iv) breakage of the walls of the honeycomb frames before reaching the equilibrium final swelling stages, a precise quantitative analysis of the actuation was not possible.



**Figure 39. Hydro-actuated hydrogel-filled-honeycomb structures.** Swelling of superporous poly-acryl-co-acrylamide hydrogels inside the diamond shape cells of a 3D printed honeycomb structure result in ~65% expansion of the cells along the shorter transverse cross-section direction. The poor control over constraining the hydrogel inside the honeycomb cells, made it difficult to achieve a quantitative analysis of the system.

The preliminary results showed a maximum of ~65% anisotropic expansion of the hydrogel-filled honeycombs measured along the shorter transverse cross-sectional axis of the cells, which was significantly smaller than the 4 fold opening of the ice plant keel's cells. However, qualitatively the deformation of the honeycomb structure upon swelling of the super porous hydrogel inside the cells, was similar to the swelling of the ice plant keel cells, which could show the feasibility of such system as a proof of concept for passive actuated systems based on the constrained swelling of a highly swellaable material inside a confined cellular structure.

Using the same simple principle, similar hydro-responsive or pH sensitive actuation systems with a more pronounced actuated response could be designed and improved through a proper material selection for controlling the swelling and mechanical properties of both hydrogel and the honeycomb framework. Similar studies on the development of

such hydro-responsive actuation systems done by colleagues in different research groups have revealed promising results (Guidicci 2013).

### **5.3 Hydro-actuated bilayer-honeycomb prototype**

#### **5.3.1 Principle of the design at various hierarchical levels**

To detach from the ‘swelling-inflation’ mechanism, while keeping the extracted concepts at higher hierarchical level of the biological model system, we tried to locate the actuation inside the honeycomb walls as shown in figure 40. Getting inspired by the bilayer bending movement principle seen in the flexing of the ice plant keel and other passive hydro-actuated movement in plants (Elbaum et al. 2008; Dawson et al. 1997), the idea was to make a cell with hydro-responsive walls which would change their curvature upon changes in the environment relative humidity.

Figure 40 depicts the principle behind the design of such passive hydro-actuated bilayer honeycomb device at various hierarchical levels. In the lowest level of the hierarchy, the orientation of a none-deforming stiff element inside a softer extendible matrix determines the directionality of the swelling, here resulting in a unidirectional expansion of the “active” layer in the longitudinal direction (I), while a passive layer with random orientation of the stiff elements would have a less pronounced isotropic swelling (Figure 40I).

The bilayer made up of two of such elements attached together would bend upon actuation to compromise between the extending active element and the resistive layer, and by attaching two of such bilayers at their edges with the passive layers facing each other, the actuated-bending of the bilayers would result in opening/closing of a “bilayer-cell” (Figure 40 II-III). Through scaling up and bringing the individual cells into a honeycomb structure, one can achieve a tailorable actuated movement at the macro scale (Figure 40 IV).

At the smallest scales of the design, the goal is to translate the response of the material to an external stimulus into a unidirectional deformation of the active element, which can be satisfied through swelling of a fibre reinforced polymer composite. The higher levels of the hierarchical design are to amplify the initial response of the material in smaller scale, into a tailorable larger macro deformation.

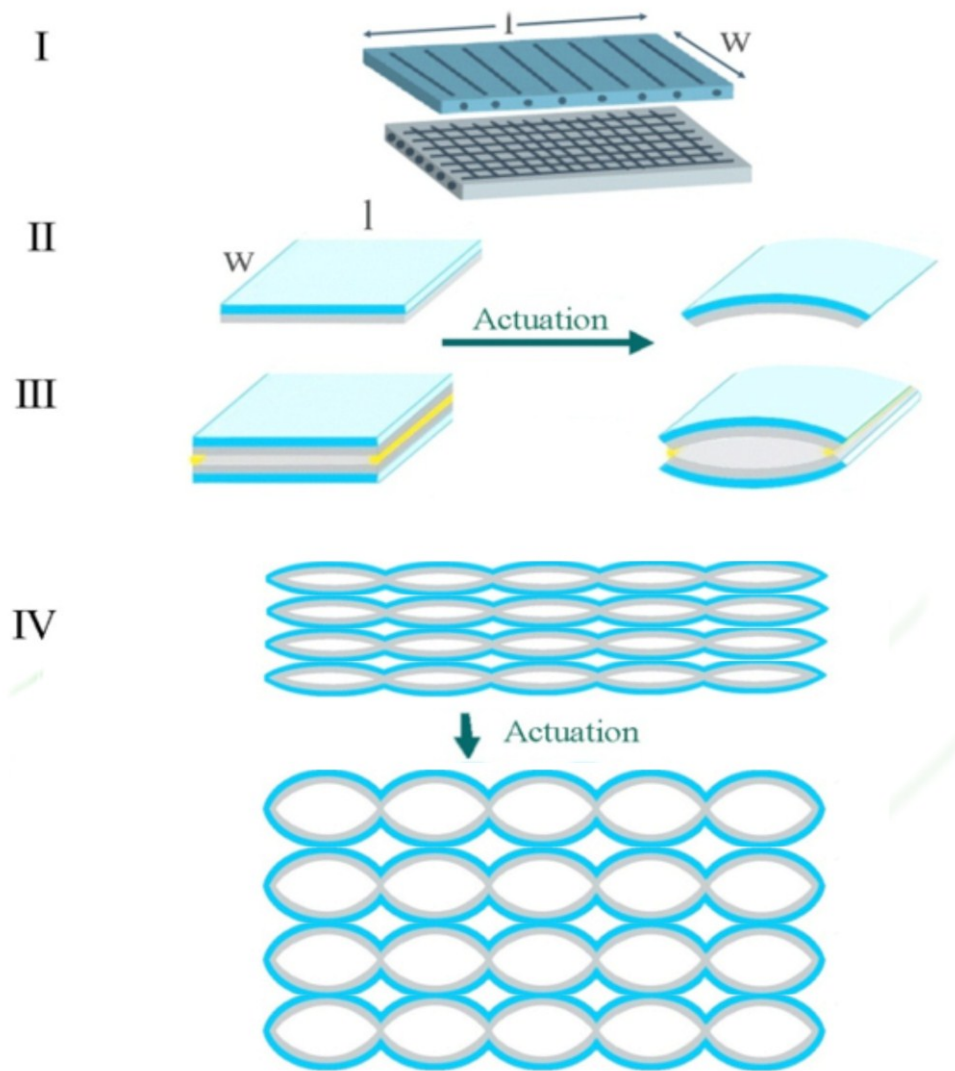


**Figure 40. Schematic illustration of the hydro-actuated bilayer-honeycomb device.** The bioinspired principle behind the actuation mechanism is depicted at various hierarchical levels: (I) Orientation of the fibres inside a swellable matrix determines the directionality and extend of the deformation upon swelling. Here, resulting in an anisotropic expansion of the top (blue) layer in the longitudinal direction  $l$ , while preventing the grey layer with random orientation of the fibres (passive layer) to express such unidirectional swelling. A simple bending bilayer structure can be made out of attaching such an active and passive layer together resisting bottom layer (II), and the fixing two of such bilayers at their edges with the active layers facing outward, would translate the actuated bending of the bilayers into an opening/closing of a “bilayer-cell” (III). Through scaling up such passive hydro-actuated cells into a “bilayer honeycomb”, a tailorable unidirectional movement in macro scale can be achieved (IV).

### 5.3.2 Material selection and characterization

For the material selection procedure, the goal was to stay in the biological realm and have a bio-inspired biomaterial, leading to wood as the first choice for the active element. In first tests on developing a prototype bilayer cell, spruce veneers with various thicknesses were

utilized as the active layer as the direction of the fibres in wood can give the required anisotropy of the swelling. For the passive resistive element, various materials with almost no swelling such as various polymeric films, or materials with more isotropic response such as paper, scotch tape etc. were used. Based on the cooperative response of the two elements in the resulted bending bilayer, and the simplicity of the fabrication and characterization, final hydro-actuated demonstrator was made up of 0,6 mm thick spruce veneers as the active layer, with the spruce cellulose microfibrils running along the bilayer's width ( $w$ , parallel to bilayer-cell axis, Figure 40-I), while a 0.2 mm thick papers with a less anisotropic swelling compared to wood were utilized as the passive/resisting layer. The spatial arrangement of the spruce veneer bilayer is illustrated in Figure 41, with spruce cellulose microfibrils running along the bilayer's width ( $w$ , along the bilayer-cell middle axis). As the fibres in the paper (resistive layer) reorient to some extent along the rolling direction in the production process and give the final paper a relatively anisotropic characteristic, the direction of the paper in the bilayer structure was chosen accordingly and the resistive thick paper layer were cut and laid so that the papers direction with the lower swellability and the higher elastic modulus would lie along the bilayer longitudinal direction ( $l$ ) along the bilayer-cell longer transverse cross-section.

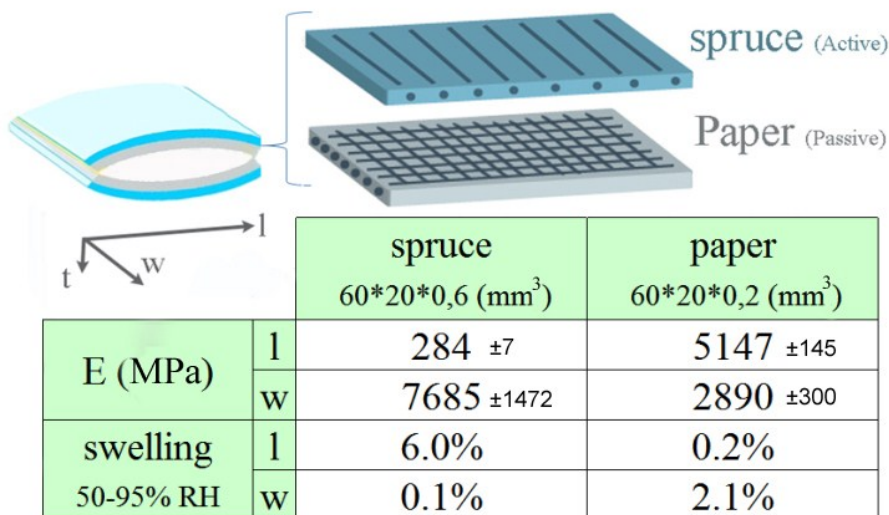


**Figure 41. Characterization of the active and passive elements in the bilayer-cells.** The special arrangement of spruce and paper in the bilayer-cell is illustrated on the top with the bilayers longitudinal axis ( $l$ ) constructing the cell's longer transverse cross-section,  $w$ , representing the bilayers width running parallel to the cells middle axis, and  $t$  presenting the bilayer-cell wall thickness. Elastic modulus of the two layers at 50% relative humidity and their maximum swelling upon wetting are presented in the table. The acquired data were used as input for finite element simulation of the bilayer actuation.

The modulus of elasticity of both, active and passive layers at room condition (25°C, 50% RH), and their maximum swelling upon wetting, were acquired and utilized as an input for finite element simulation of the actuation to be presented and compared in a paper under preparation (Figure 41).

### 5.3.3 Passive hydro-actuation of bilayer-cells and honeycomb

The passive hydro-actuation response of the bio-inspired bilayer-cell were investigated by taking the cells from 50%RH at room temperature and exposing them to high relative humidity in an in-house-built humidity chamber (25°C, ~95%RH). The bilayer-cell's dimensional change upon time of the exposure to the 95% RH is presented in Figure 42. The bilayer-cell starts to open almost immediately after exposure to 95% relative humidity and open up to 4 fold in the short cross-sectional axis (cell width) already in the first 20 minutes of exposure, and reaches its equilibrium maximum 8.5 fold opening state after about 7 hours (with 80% of the opening occurring in the first hour). The cell contraction in the longitudinal direction (cell length) was found to be negligible.

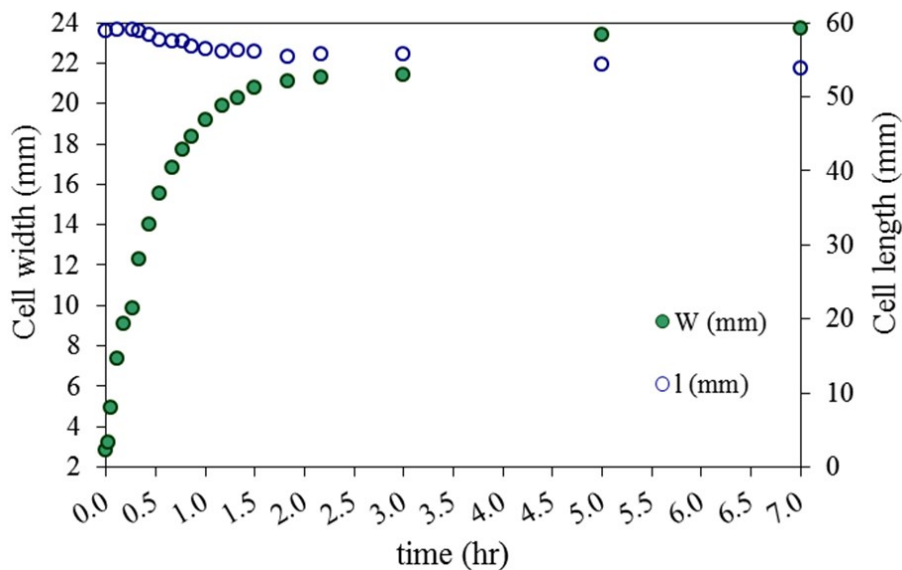


**Figure 42. Deformation of the bilayer-Cell upon actuation.** Starting from 50% relative humidity at room temperature to 95% RH, swelling of the spruce veneers results in bending of the bilayer-cell wall and an 8 fold opening of the cells in the shorter cross-sectional axis ( $w$ ), while the longer cross-sectional axis of the cell ( $l$ ) undergoes only a slight 10% contraction.

To check the reversibility of the actuation, the actuation was done with wetting a bilayer-cell by spraying liquid water on top of the cells and monitoring the opening/closing of the cells upon wetting and the consequent drying cycle at room condition with 25°C and

50%RH (Figure 43). The actuation upon wetting started in half a minute after spraying the water, and continued to an almost 7 fold opening of the cell's in about 10 minute. The cells started to close only minutes after the wetting was stopped and the water desorption and drying of the bilayers continued until the closure to the initial closed state in about half an

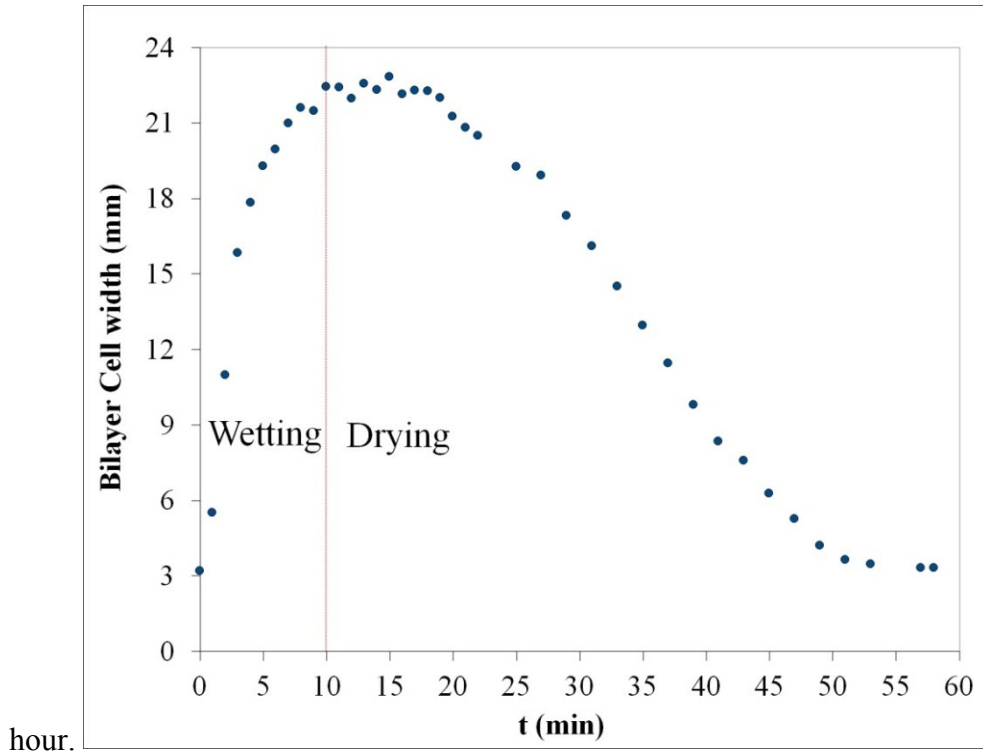


**Figure 43. Reversible actuation of the bilayer-cell upon wetting/drying cycles.** Opening and closing of a bilayer-cell upon wetting and drying at room temperature (50%RH) is plotted as a function of time. The actuation starts immediately after spraying the liquid water with the full opening occurring in less than 15 minutes.

Equilibrium final curvature of actuated bilayers and bilayer-cells upon exposure to 95% RH and in wetting experiment are presented in Figure 44. The bending and equilibrium curvature of the actuated bilayer-cell wall was found to be less than that of the single bilayer (about 80%) probably due to the geometrical and mechanical restrains at the cell hinges.

The actuation measured in terms of changes in the curvature of the bilayers in the cells was almost the same for both wetting and relative humidity experiments, while the equilibrium curvature of the single bilayers measured in 95%RH was found to be almost 20% less than the final curvature of the same bilayer wetted with liquid water. The observed difference between the actuation upon wetting and exposure to high relative humidity can probably be explained by the difference between the changes in the elastic modulus of the active and

passive layers in the two experiments. The changes in the elastic properties of wood polymers upon water adsorption have been related to the breaking of hydrogen bonds by water molecules (Caulfield 1990; Nissan 1990; Englund 2011). The effect is a time-dependent diffusion process, thus the temporal difference between the adsorption process in the two experiments might have a different effect on the deterioration of the mechanical properties of the bilayer, leading to the locking of the bilayer in a different equilibrium actuated state upon exposure to high relative humidity compared to the final equilibrium opening observed in actuation upon wetting.

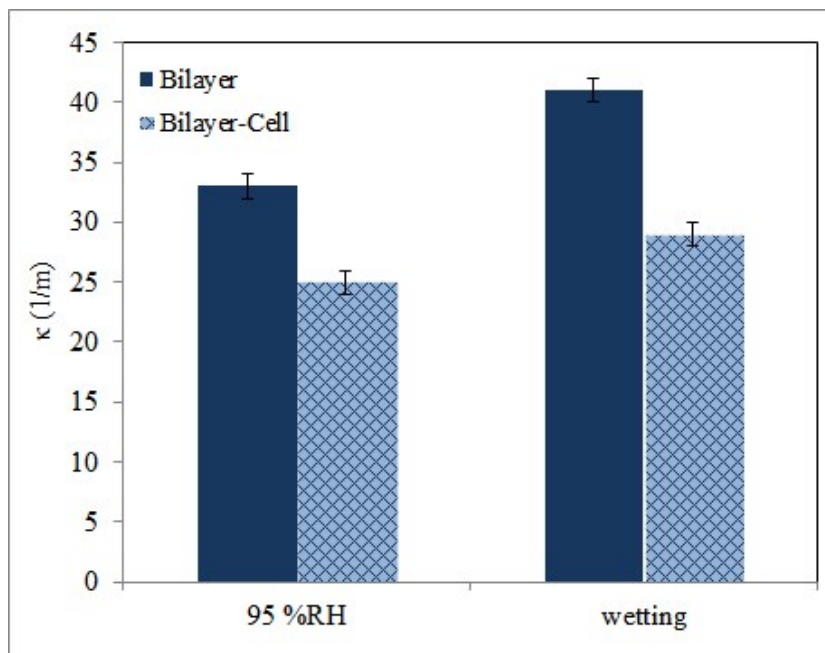


**Figure 44. Single bilayer and bilayer-cell actuation upon wetting and exposure to 95%RH.** Actuation of the single bilayers and bilayer-cells are shown as the final equilibrium curvature,  $\kappa$  (1/m). Bending of the bilayers in the bilayer-cells is less in general probably due to the restriction of the cell hinges. Actuation is more pronounced in case of wetting with liquid water compared to exposure to high relative humidity.

Maximum swelling of the single spruce veneer exposed to 95% RH was measured to be about 6%. However, a rough calculation by putting a 6% strain for the active layer in the simplified version of the Timoshenko's formula (Eq. 7) predicts a significantly higher bending curvature than observed in the actuated bilayers (Figure 44). Hence, it can be concluded that the real water adsorption and swelling of the spruce veneers in the bilayer structure must be significantly lower than that of single veneers, probably due to the smaller available surface area for adsorption in case of the bilayer, as one side of the veneer is covered with the glue attaching the two layers together. The geometrical restriction by the presence of the passive paper layer may also result in different kinetics of diffusion of

the water into the depth of the bilayer, leading to less swelling of the active layer and smaller bending curvature.

Based on the introduced principles and by scaling up the bilayer-cells into a honeycomb structure, an autonomously acting hydro-actuated honeycomb device was constructed as a proof of concept to show how the initial response of the material (5% spruce swelling) can be amplified and translated through a simple yet efficient architecture at various hierarchical level of the system into a unidirectional 4-5 fold expansion and movement at the macro scale (Figure 45-46). It is worth noting that, for the honeycomb actuation experiments done in the 95% relative humidity climate room, the actuation time to the equilibrium full opening state was significantly longer than the equilibrium actuation time of the bilayer-cells in the smaller in-house-built humidity chamber.

The core idea of the proposed design is to translate the initial response of the material into a tailorable amplified deformation/movement at the macro scale. The expansion can be enhanced to some extent by increasing the bending curvature and optimizing length, thickness and mechanical properties of the active and passive layer. One can take the same principles further and design structures with more sophisticated movements such as bending, twisting etc. By attaching a passive layer to one of the edges of the bilayer-honeycomb structure, one can restrict the expansion of that side and achieve various flexing movements similar to that observed in ice plant keels. Bending can also be achieved through restricting the expansion of the honeycomb via covering one side of the honeycomb cells with a passive substrate. In this mode, two of such bending structures (bilayer-honeycomb + backing substrate) can be used as the building block to construct a bigger cell (or even honeycomb) through a similar concept used to make the initial bilayer-cell (Figure 40 II-IV), and conceptually one can think of further amplification of the response through design of higher levels of hierarchy on top of each other.

In general, using the same basic design principles extracted from the biological model system, one can tailor various aspects of the actuated movement by varying different features of the system to develop “smart” actuation devices with a variety of possible applications from facades and roofing systems to biomedical engineering etc.



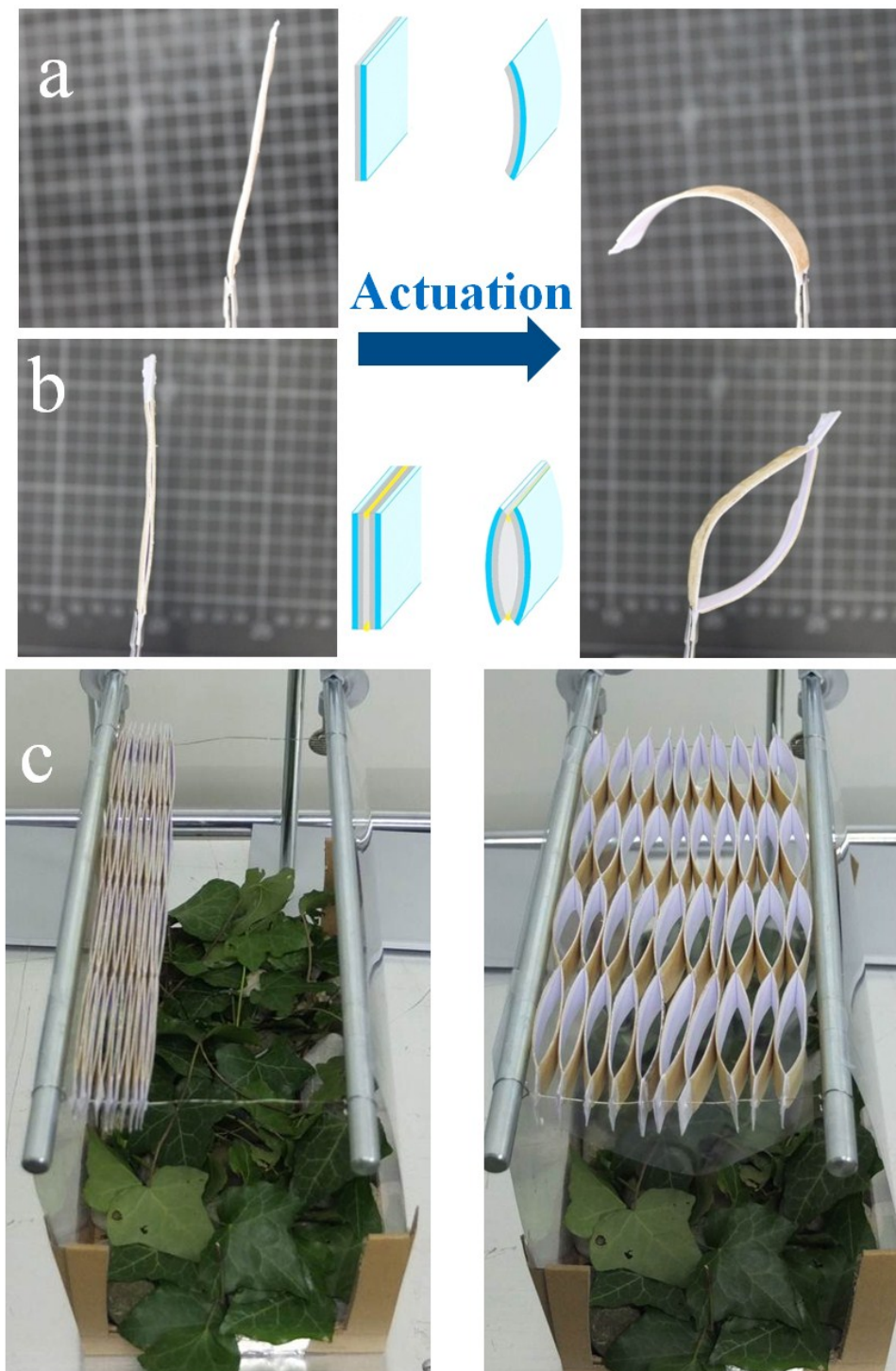


**Figure 45. Passive hydro-actuation in bilayer-cell and bilayer honeycomb prototypes.** Initial (left) and final actuated (right) state of the passive hydro-actuation systems upon changing the relative humidity from 50 to 95% are depicted at various hierarchical level of the design; a) A bilayer made up of spruce veneer (active layer) glued to a thick paper (passive layer), bends upon anisotropic swelling of the spruce veneer in the direction perpendicular to the cellulose fibrils orientation. b) Two of such bilayers attached together on their edges, constructs a cell-like structure which can open/closes upon changes in the relative humidity. c) Scaling up the bilayer-cell into a hydro-actuated honeycomb device as a prototype roofing system that can expand up to 5 fold and close the roof upon actuation.

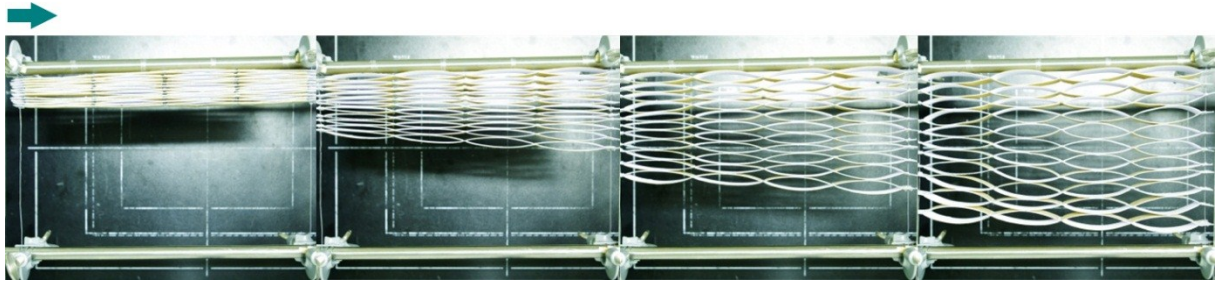


**Figure 46. Passive hydro-actuation of bio-inspired bilayer-honeycomb device.** Sequential images of bilayer-honeycomb opening upon 0, 2, 4 and 16 hours of exposure to 95% relative humidity room (from left to right).

The hydro-actuated bilayer honeycomb device can also in principle generate forces along the shorter transverse cross-section of the cells. The force generated by a single bilayer-cell upon exposure to 95%RH was monitored by restricting its actuated movement by a load cell placed on top of its middle point (where the maximum bending occurs). The maximum force generated by the bilayer-cell upon actuation was measured to be about 2N.

The results shows the feasibility of utilizing such simple bilayer-cell design for force generation, although one has to consider limitations in the reversibility of such systems due to the viscoelastic behavior of wood. Through scaling up the cells into a well design honeycomb structure and a proper material selection, one can think of improving the simple design-concept for practical applications as lifting systems such as passive hydro-actuated flooring system for storage of hydro-sensitive goods, etc.

## 6 Summary and conclusion

The focus of the present thesis is on understanding the underlying principles for passive hydro-actuated unfolding of the ice plant seed capsules and utilizing the extracted principles behind this actuation system for the development of passive actuated devices as a proof of concept.

From actuation based on the reversible/ irreversible changes of the cells shape and size driven by the active changes of the cell turgor pressure, to passive actuation based on the anisotropic swelling of the secondary cell wall layers, plants have evolved variety of smart mechanisms to utilize water to actuate a specific movement or stress generation in their organs. Some species of Aizoaceae also known as **ice plants**, utilize a ‘**swelling-inflation**’ **mechanism** to actuate an origami-like unfolding of their seed containing capsules and release the seeds upon exposure to liquid water. The swelling of a **highly swellable cellulosic inner layer (CIL) inside the lumen of the cells**, was found to be the engine of the actuation as it provides the required pressure for passive inflation/deflation of the cells even after cell’s death. The specific **cellular structure** of the CIL containing hygroscopic tissue, with the “**eye-like**” shape cells, dictates an **anisotropic deformation** in the shorter transverse cross-section of the cells upon water adsorption and swelling of the cellulosic inner layer (CIL), which results in a **unidirectional expansion** of the **honeycomb structure**. The attachment and restriction of the two hygroscopic tissues (keels halves) to an inert **backing tissue**, introduces a **swelling gradient**, from the cells at the keel base restricted to the backing tissue, to the free cells at the keels ridge. The differential swelling at different height of the keels leads to the **bending of the keel-backing “bilayer”**, which results in the unfolding of each of the five seed containing valves in ice plant seed capsule. It was found that unlike other known plant hydro-actuation systems, ice plant actuation can only occur in presence of **liquid water** and not upon changes in relative humidity. Sorption isotherm acquired by thermogravimetric analysis showed that even at relative humidity as high as 85%, hygroscopic keels can adsorb only about 15 wt.% water which was not enough to initiate the actuation, and exposure to liquid water was necessary for the actuation to occur. Thermogravimetric analysis of CIL water sorption revealed that, up to 40 wt.% moisture content the adsorption is enthalpy driven and is the result of the adsorption of the first layers of water molecules onto the network of the cellulose chains, which was found to be insufficient to initiate the actuation. The water adsorption after this moisture content and up to about 350 wt.% was found to have an **entropic nature** and to

be the **mechanically working** water responsible for the four fold swelling of the cells and flexing of the keels.

A simple **chemo-mechanical model** could describe how the relatively small available energy from the entropic gain of the system upon swelling of the CIL can be translated into the desired deformation at the macro scale, through an elaborate design at higher hierarchical level of the system.

A thorough study of the **morphology of the cellulosic inner layer** by scanning electron microscopy revealed that CIL has a **highly porous** structure that can exhibit a significant swelling only through exploiting the entropic gain from being exposed to liquid water. This was speculated to probably serve as an adaptation to prevent the opening to occur upon humidity changes in the environment and ensure the seed release and germination in the right condition. It was also concluded that, in comparison to various other swelling agents, water with high hydrogen bonding power ( $\delta h$ ) and low molecular volume is the most effective medium for swelling of the cellulosic inner layer and actuation of the keels.

By **transferring the extracted underlying principles** behind the hydro-actuated movement of the ice plant seed capsule into simple models, we could detach from the biological system and provide two different concepts for design of such passive actuated honeycomb devices as biomimetic prototypes:

#### **Hydro-actuated hydrogel-filled-honeycomb devices.**

This prototype resembles the mechanism observed in the biological model, where a unidirectional expansion of the honeycomb framework could be achieved through a **coupled ‘swelling-inflation’** mechanism. Here swelling of a highly porous hydrogel inside the cell lumen of a honeycomb frame provides the required pressure to open the cells in the shorter transverse cross-sections, resulting in a unidirectional expansion of the cellular structure.

#### **Hydro-responsive bilayer-honeycomb demonstrator.**

By building the honeycomb walls from two layers with different swelling properties, we could bring the actuation inside the honeycomb frame, so that the differential swelling of the two layers upon actuation would result in bending of the cell walls and, in consequence, in a unidirectional expansion of the bilayer-honeycomb structure.

## 7 Outlook

The reported work led to a better understanding of the underlying mechanism for hydro-actuated opening of the ice plant seed capsules, and how abstraction of these principles can lead to the development of bio-inspired autonomous devices. Potential future research directions can be listed as follows;

As for better understanding of the **biological model system**:

- A more thorough study of the CIL composition.
  - Although the Raman studies showed the presence of a mainly cellulosic non-lignified layer inside the cell's lumen, a more thorough compositional study of the CIL via sugar analysis etc., may help to gain a better understanding of the nature of the swellable macromolecules and their interaction with water.
- Investigation of the hydro-actuated seed dispersal in other ice plant species.
  - Various Aizoaceae species show a similar hydro-actuated unfolding of their seed capsule, with anatomical differences like fruit size, number of the seed containing valves etc., which would be worth studying to gain a more comprehensive understanding of the biological system.

As for further exploration of the **Biomimetic design**;

- Better attachment in the hydrogel-honeycomb system.
  - In our preliminary work on the hydrogel-honeycomb system, the attachment of the hydrogel macromolecules to the 3D-printed honeycomb was relatively poor. A proper material selection for the framework and the hydrogel can lead to a better attachment and a proper analysis of the hydro-actuated deformation.
- Exploring the possibility of utilizing other environmental stimuli.
  - Water with high hydrogen-bonding power ( $\delta_h$ ), was found to be the most suitable swelling medium for the cellulosic system. However, the chemo-mechanical model showed that the entropic gain of the swelling of a model macromolecule can be sufficient to induce the pressure required for the inflation of the cells and a actuation of the systems, provided that the design principles at higher hierarchical levels of the cells and the keel are followed. Hence, one can think of the possibility of detaching from water-cellulose coupled systems, and design of a similar system that can exploit the swelling of different polymeric materials in

response to other suitable swelling agents to inflate the cells and actuate the desired movement.

- The hydrogel system showed a promising pH sensitivity which could be utilized to tailor the actuation to be responsive to a certain pH. A more thorough material selection for the swellable inner layer can lead to development of autonomous systems that can be tailored to be responsive to pH, other solvents, temperature etc.
- The same principle can be applied to the bilayer-honeycomb actuators. The key playing factor in the bending of the bilayer structures is the differential strain response of the two layers to an external stimuli. A thorough material selection of the active and passive layers in the bilayer-cell structure, may lead to the design of autonomous bilayer-honeycomb devices with response to other external stimuli such as temperature etc.
- Further simulation and experiments for exploring the possibility of more sophisticated movements.
  - By considering each hydrogel-containing (or bilayer) cell as an actuation building block, one can think of exploring various design concepts by varying the arrangement of the “active” and “passive” cells to achieve more complex movements of the honeycomb structure, such as bending, twisting etc.
  - Besides varying the cells as the actuation building blocks, one can also think of restricting various sides of the honeycomb with an inert layer, and build bending bilayer structure at a higher hierarchical level to amplify the initial response of the material even further.

## Bibliography

Aizenberg, J. and P. Fratzl (2009). "Biological and Biomimetic Materials." *Adv. Mater.* 21(4): 387-388.

Aizenberg, J., A. Tkachenko, et al. (2001). "Calcitic microlenses as part of the photoreceptor system in brittlestars." *Nature* 412(6849): 819-822.

Arzt, E., S. Gorb, et al. (2003). "From micro to nano contacts in biological attachment devices." *Proceedings of the National Academy of Sciences* 100(19): 10603-10606.

Audoly, B. and A. Boudaoud (2003). "Self-Similar Structures near Boundaries in Strained Systems." *Physical Review Letters* 91: 086105.

Bacic A., Harris, P. J., Stone B. A. (1998). In: *Carbohydrates. Structure and Function. The biochemistry of plants.* New York: Academic Press. .

Barth, F. (1998). *The Vibrational Sense of Spiders. Comparative Hearing: Insects.* R. Hoy, A. Popper and R. Fay, Springer New York. 10: 228-278.

Barthlott, W. and C. Neinhuis (1997). "Purity of the sacred lotus, or escape from contamination in biological surfaces." *Planta* 202(1): 1-8.

Barton, A. F. M. (1990). *Handbook of Polymer-Liquid Interaction Parameters and Solubility Parameters.* Boca Raton, FL., CRC Press.

Berger, A. (1908). *Mesembrianthemmen und Portulacaceen. Beschreibung und Anleitung zum Bestimmen der wichtigsten Arten, mit kurzen Angaben über die Kultur.* Stuttgart, Ulmer.

Bhushan B. (2009). "Lessons from nature- an overview." *Philos Trans Roy Soc A* 367: 1445-1486.

Bhushan, B. (2009). "Biomimetics: lessons from nature—an overview." *Philosophical Transactions of the Royal Society A: Mathematical, Physical and Engineering Sciences* 367(1893): 1445-1486.

Bhushan, B. and R. Sayer (2008). *Gecko Feet: Natural Attachment Systems for Smart Adhesion-Mechanism, Modeling, and Development of Bio-Inspired Materials.* Applied Scanning Probe Methods X. B. Bhushan, M. Tomitori and H. Fuchs, Springer Berlin Heidelberg: 1-61.

Bolus, H. M. L. (1928). *Notes on Mesembrianthemnm and Some Allied Genera,* Cape Town.

Bond, J., L. Donaldson, S. Hill, K. Hitchcock (2008) "Safranine fluorescent staining of wood cell walls." *Biotech. Histochem.* 83: 161–171.

Bowling, A. J. and K. C. Vaughn (2009). "Gelatinous Fibers Are Widespread in Coiling Tendrils and Twining Vines." *American Journal of Botany* 96(4): 719-727.

- Brown, N. E. (1921). *Mesembryanthemum* and some new genera separated from it. *Gardeners' Chronicle*.
- Brunauer S., Emmett, P. H., Teller E. (1938). "Adsorption of gases in multimolecular layers." *Journal of the American Chemical Society* 60: 309-319.
- Burgert, I. (2006). "Exploring the micromechanical design of plant cell walls." *American Journal of Botany* 93(10): 1391-1401.
- Burgert, I., M. Eder, et al. (2007). "Tensile and compressive stresses in tracheids are induced by swelling based on geometrical constraints of the wood cell." *Planta* 226(4): 981-987.
- Burgert, I. and P. Fratzl (2009). "Actuation systems in plants as prototypes for bioinspired devices." *Philosophical Transactions of the Royal Society A: Mathematical, Physical and Engineering Sciences* 367(1893): 1541-1557.
- Burgert, I. and P. Fratzl (2009). "Plants control the properties and actuation of their organs through the orientation of cellulose fibrils in their cell walls." *Integrative and Comparative Biology* 49(1): 69-79.
- Burgert, I., J. Keckes, et al. (2002). "A Comparison of Two Techniques for Wood Fibre Isolation - Evaluation by Tensile Tests on Single Fibres with Different Microfibril Angle." *Plant Biology* 4(1): 9-12.
- Burgert I., Fratzl P., (2007). *Mechanics of the expanding cell wall. Plant cell monogr (5) The expanding Cell*. V. K. Verbeelen JP. Berlin, Heidelberg: Springer-Verlag: 191–215.
- Cai, J., S. Kimura, et al. (2008). "Cellulose aerogels from aqueous alkali hydroxide-urea solution." *Chemosuschem* 1(1-2): 149-154.
- Campbell N. A., Thomson, W. W. (1977). "Multi vacuolate motor cells in *mimosa pudica*." *Annals of Botany* 41(176): 1361-1362.
- Çarçabal, P., R. Jockusch, et al. (2005). "Hydrogen Bonding and Cooperativity in Isolated and Hydrated Sugars: Mannose, Galactose, Glucose, and Lactose." *J. Am. Chem. Soc.* 127(32): 11414-11425.
- Carpita, N. C. and D. M. Gibeaut (1993). "Structural models of primary cell walls in flowering plants: consistency of molecular structure with the physical properties of the walls during growth." *The Plant journal : for cell and molecular biology* 3(1): 1-30.
- Caulfield, D. F. (1990). Effect of moisture and temperature on the mechanical properties of paper. *Solid mechanics advances in paper related industries. Proceedings of National Science Foundation workshop, Syracuse, NY, USA.*
- Chen, Z., C. Majidi, et al. (2011). "Tunable helical ribbons." *Applied Physics Letters* 98(1): 011906.
- Clair, B., T. Alm eras, et al. (2011). "Maturation stress generation in poplar tension wood studied by synchrotron radiation microdiffraction." *Plant physiology* 155(1): 562-570.



- Clair, B., J. Gril, et al. (2008). "Characterization of a gel in the cell wall to elucidate the paradoxical shrinkage of tension wood." *Biomacromolecules* 9(2): 494-498.
- Clair, B., J. Ruelle, et al. (2006). "Tension wood and opposite wood in 21 tropical rain forest species 1. Occurrence and efficiency of the G-layer." *Iawa Journal* 27(3): 329-338.
- Clair B., Ruelle, J., Thibaut B. (2003). "Relationship between growth stresses, mechano-physical properties and proportion of fibres with gelatinous layer in chestnut (*Castanea Sativa* Mill.)." *Holzforschung* 57, 2: 189-195.
- Cleland, R. (1971). "Cell Wall Extension." *Annual Review of Plant Physiology* 22(1): 197-222.
- Cohen, J. A., R. Podgornik, et al. (2009). "A Phenomenological One-Parameter Equation of State for Osmotic Pressures of PEG and Other Neutral Flexible Polymers in Good Solvents." *Journal of Physical Chemistry B* 113(12): 3709-3714.
- Collins (2004). *Optimisation mechanics in nature*, WIT press.
- Cosgrove, D. (2000). "Loosening of plant cell walls by expansins." *Nature* 407(6802): 321-326.
- Cosgrove, D. (2005). "Growth of the plant cell wall." *Nat Rev Mol Cell Biol* 6(11): 850-861.
- Currey, J. (2006). "Bones : structure and mechanics.", Princeton, NJ: Princeton University Press.
- Dawson, J., J. F. V. Vincent, et al. (1997). "How pine cones open." *Nature* 390(6661): 668-668.
- Dent, R. W. (1977). "A Multilayer Theory for Gas Sorption." *Textile Research Journal* 47(3): 188-199.
- Donaldson, L. A., J. Grace, G. M. Downes (2004). "Within-tree variation in anatomical properties of compression wood in radiata pine." *IAWA J.* 25: 253–271.
- Dunlop, J. and P. Fratzl (2010). "Biological Composites." *Annual Review of Materials Research* 40(1): 1-24.
- Ebner, M., T. Miranda, et al. (2011). "Efficient fog harvesting by *Stipagrostis sabulicola* (Namib dune bushman grass)." *Journal of Arid Environments* 75(6): 524-531.
- Eckardt, F. D., K. Soderberg, et al. (2013). "The nature of moisture at Gobabeb, in the central Namib Desert." *Journal of Arid Environments* 93: 7-19.
- Eckelt, J., R. Sugaya, et al. (2008). "Pullulan and dextran: Uncommon composition dependent Flory-Huggins interaction parameters of their aqueous solutions." *Biomacromolecules* 9(6): 1691-1697.

- Elbaum, R., S. Gorb, et al. (2008). "Structures in the cell wall that enable hygroscopic movement of wheat awns." *Journal of Structural Biology* 164(1): 101-107.
- Elbaum, R., L. Zaltzman, et al. (2007). "The role of wheat awns in the seed dispersal unit." *Science* 316(5826): 884-886.
- Elices, M. (2000). "Structural biological materials design and structure-property relationships.", New York: Pergamon.
- Emons, A., H. Höfte, et al. (2007). "Microtubules and cellulose microfibrils: how intimate is their relationship?" *Trends in Plant Science* 12(7): 279-281.
- Engelund E. T., Thygesen, L. G., Svensson S. H., Callum A. (2013). "A critical discussion of the physics of wood–water interactions." *Wood Science and Technology* 47(1): 141-161.
- Engelund E., Thygesen, L. H. P. (2010). "Water sorption in wood and modified wood at high values of relative humidity. Part 2: Appendix. Theoretical assessment of the amount of capillary water in wood microvoids." *Holzforschung* 64(3).
- Engelund, E. T. (2011). Wood-water interactions, Linking molecular level mechanisms with macroscopic performance. Department of civil engineering. DTU Civil engineering, Technical University of Denmark. PhD Thesis.
- Erb, R., J. Sander, et al. (2013). "Self-shaping composites with programmable bioinspired microstructures." *Nature communications* 4.
- Fagerberg W. R., Howe, D. G. (1996). "A quantitative study of tissue dynamics in Venus's flytrap *Dionaea muscipula* Droseraceae. II. Trap reopening." *American Journal of Botany* 83(7): 836-842.
- Fagerberg W.R. , D. Allain (1991). "A quantitative study of tissue dynamics during closure in the traps of Venus's flytrap *Dionaea muscipula* (Ellis)." *American Journal of Botany* 78: 647-657.
- Fantner, G., E. Oroudjev, et al. (2006). "Sacrificial bonds and hidden length: unraveling molecular mesostructures in tough materials." *Biophysical journal* 90(4): 1411-1418.
- Federle, W., W. J. P. Barnes, et al. (2006). "Wet but not slippery: boundary friction in tree frog adhesive toe pads." *Journal of The Royal Society Interface* 3(10): 689-697.
- Fengel, D. and G. Wegener (1984). *Wood—chemistry, ultrastructure, reactions*. Berlin, Germany, De Gruyter.
- Firn, R. D. and A. B. Myers (1989). "Plant movements caused by differential growth--unity or diversity of mechanisms?" *Environmental and experimental botany* 29(1): 47-55.
- Forterre, Y. and J. Dumais (2011). "Generating Helices in Nature." *Science* 333(6050): 1715-1716.
- Forterre, Y., J. M. Skotheim, et al. (2005). "How the Venus flytrap snaps." *Nature* 433(7024): 421-425.

- Fratzl, P. (2003). "Cellulose and collagen: from fibres to tissues." *Current Opinion in Colloid & Interface Science* 8(1): 32-39.
- Fratzl, P. (2007). "Biomimetic materials research: what can we really learn from nature's structural materials?" *Journal of the Royal Society, Interface / the Royal Society* 4(15): 637-642.
- Fratzl, P. and F. Barth (2009). "Biomaterial systems for mechanosensing and actuation." *Nature* 462(7272): 442-448.
- Fratzl, P., I. Burgert, et al. (2004). "On the role of interface polymers for the mechanics of natural polymeric composites." *Phys. Chem. Chem. Phys.* 6(24): 5575-5579.
- Fratzl, P., R. Elbaum, et al. (2008). "Cellulose fibrils direct plant organ movements." *Faraday Discussions* 139(0): 275-282.
- Fratzl, P., H. S. Gupta, et al. (2004). "Structure and mechanical quality of the collagen-mineral nano-composite in bone." *J. Mater. Chem.* 14(14): 2115-2123.
- Fratzl, P. and R. Weinkamer (2007). "Nature's hierarchical materials." *Progress in Materials Science* 52(8): 1263-1334.
- Fromm, J. and S. Lautner (2007). "Electrical signals and their physiological significance in plants." *Plant, Cell & Environment* 30(3): 249-257.
- Fry, S. C., R. C. Smith, et al. (1992). "Xyloglucan endotransglycosylase, a new wall-loosening enzyme activity from plants." *The Biochemical journal* 282 ( Pt 3): 821-828.
- Garside, S. and S. Lockyer (1930). "Seed dispersal from the hygroscopic fruits of *Mesembryanthemum carpanthea* (*Mesembryanthemum*), pomeridiana N. E. Br." *Annals of Botany* 44(175): 639-655.
- Gemeinhart, R. A., J. Chen, et al. (2000). "pH-sensitivity of fast responsive superporous hydrogels." *Journal of Biomaterials Science-Polymer Edition* 11(12): 1371-1380.
- Gibson, L. J. and M. F. Ashby (1988). *Cellular solids structure & properties*. Oxford etc., Pergamon Press.
- Gierlinger, N. & M. Schwanninger (2006). "Chemical imaging of poplar wood cell walls by confocal Raman microscopy." *Plant Physiology* 140; 1246-1254.
- Gorb, S. (2009). *Functional Surfaces in Biology: Adhesion Related Phenomena Volume 2*, Springer.
- Gorb, S. (2012). *Adhesion and friction in biological systems*, Springer.
- Goswami, L., J. W. C. Dunlop, et al. (2008). "Stress generation in the tension wood of poplar is based on the lateral swelling power of the G-layer." *Plant Journal* 56(4): 531-538.

- Guiducci L. (2013). Passive biomimetic actuators: the role of material architecture. Mathematisch-Naturwissenschaftlichen Fakultät. Potsdam Universität. PhD Thesis.
- Gupta, H., J. Seto, et al. (2006). "Cooperative deformation of mineral and collagen in bone at the nanoscale." *Proceedings of the National Academy of Sciences* 103(47): 17741-17746.
- Hansen, C. M. (1969). "The Universality of the Solubility Parameter." *Ind. Eng. Chem. Prod. Res. Dev.* 8, No. 1: 2-11.
- Harrington, M. J., K. Razghandi, et al. (2011). "Origami-like unfolding of hydro-actuated ice plant seed capsules." *Nature Communications* 2:337.
- Hart, J. W. (1990). *Plant tropisms and other growth movements*. London etc., Unwin Hyman.
- Haupt, W. (1977). *Bewegungsphysiologie der Pflanzen*. Stuttgart, Germany, Thieme Verlag.
- Hetherington, A. and I. Woodward (2003). "The role of stomata in sensing and driving environmental change." *Nature* 424(6951): 901-908.
- Hodick, D. and A. Sievers (1989). "On the Mechanism of Trap Closure of Venus Flytrap (*Dionaea-Muscipula* Ellis)." *Planta* 179(1): 32-42.
- Huber, J. A. (1924). *Zur Morphologie von Mesembrianthemum*, *Botanisches Archiv*.
- Iino M., Long, C., Wang, X. (2001). "Auxin- and abscisic acid-dependent osmoregulation in protoplasts of *Phaseolus vulgaris* pulvini. ." *Plant and cell physiology* 42(11): 1219-1227.
- Ionov, L. (2013). "Bioinspired Microorigami by Self-Folding Polymer Films." *Macromol. Chem. Phys.* 214(11): 1178-1183.
- Jeronimidis, G. and A. G. Atkins (1995). "Mechanics of Biological Materials and Structures: Nature's Lessons for the Engineer." *Proceedings of the Institution of Mechanical Engineers, Part C: Journal of Mechanical Engineering Science* 209(4): 221-235.
- Jin, H., Y. Nishiyama, et al. (2004). "Nanofibrillar cellulose aerogels." *Colloids and Surfaces a-Physicochemical and Engineering Aspects* 240(1-3): 63-67.
- Kamat, S., X. Su, et al. (2000). "Structural basis for the fracture toughness of the shell of the conch *Strombus gigas*." *Nature* 405(6790): 1036-1040.
- Keckes, J., I. Burgert, et al. (2003). "Cell-wall recovery after irreversible deformation of wood." *Nat Mater* 2(12): 810-813.
- Kerner A., Oliver, F. W. (1894). *The Natural History of Plants; their forms, growth, reproduction, and distribution*. .

- Kerstens, S., W. Decraemer, et al. (2001). "Cell Walls at the Plant Surface Behave Mechanically Like Fiber-Reinforced Composite Materials." *Plant Physiology* 127(2): 381-385.
- Kimura, M., T. Hatakeyama, et al. (1974). "DSC study on recrystallization of amorphous cellulose with water." *J. Appl. Polym. Sci.* 18(10): 3069-3076.
- Knippers, J. and T. Speck (2012). "Design and construction principles in nature and architecture." *Bioinspiration & Biomimetics* 7(1): 015002.
- Kovalenko, V. I. (2010). "Crystalline cellulose: structure and hydrogen bonds." *Russian chemical reviews* 79(3): 231-241.
- Lakes, R. (1993). "Materials with structural hierarchy." *Nature* 361(6412): 511-515.
- Lanvermann, C., R. Evans, et al. (2013). "Distribution of structure and lignin within growth rings of Norway spruce." *Wood Science and Technology* 47(3): 627-641.
- Levin, S., H. Muller Landau, et al. (2003). "The Ecology and Evolution of Seed Dispersal: A Theoretical Perspective." *Annual Review of Ecology, Evolution, and Systematics* 34(1): 575-604.
- Liang, H. and L. Mahadevan (2009). "The shape of a long leaf." *Proceedings of the National Academy of Sciences* 106(52): 22049-22054.
- Lloyd, C. and J. Chan (2008). "The parallel lives of microtubules and cellulose microfibrils." *Current opinion in plant biology* 11(6): 641-646.
- Lockhart, J. A. (1965). "An analysis of irreversible plant cell elongation." *Journal of theoretical biology* 8(2): 264-275.
- Lockyer (1932). "Seed dispersal from hygroscopic *Mesembryanthemum* fruits, *Bergeranthus scapigerus*, Schw., and *Dorotheanthus bellidiformis*, N.E.Br, with a note on *Carpanthea pomeridiana*, N.E.Br." *Ann. Bot.* 46: 323-342.
- Ma, M., L. Guo, et al. (2013). "Bio-Inspired Polymer Composite Actuator and Generator Driven by Water Gradients." *Science* 339(6116): 186-189.
- Martone, P., M. Boller, et al. (2010). "Mechanics without Muscle: Biomechanical Inspiration from the Plant World." *Integrative and Comparative Biology*: icq122.
- Mäthger, L., E. Denton, et al. (2009). "Mechanisms and behavioural functions of structural coloration in cephalopods." *Journal of the Royal Society, Interface / the Royal Society* 6 Suppl 2(Suppl 2): S149-S163.
- Mattheck, C. (1998). *Design in nature : learning from trees*, Springer-Verlag.
- Mattheck, C. and K. Bethge (1998). "The Structural Optimization of Trees." *Naturwissenschaften* 85(1): 1-10.

McCann M. C., Roberts, K. (1991). *The cytoskeletal basis of plant growth and form*, New York: Academic Press.

Mellerowicz, E. J. and T. A. Gorshkova (2012). "Tensional stress generation in gelatinous fibres: a review and possible mechanism based on cell-wall structure and composition." *Journal of Experimental Botany* 63(2): 551-565.

Mellerowicz, E. J., P. Immerzeel, et al. (2008). "Xyloglucan: The Molecular Muscle of Trees." *Annals of Botany* 102(5): 659-665.

Meyers, M., P.-Y. Chen, et al. (2008). "Biological materials: Structure and mechanical properties." *Progress in Materials Science* 53(1): 1-206.

Michielsen, K. and D. G. Stavenga (2008). "Gyroid cuticular structures in butterfly wing scales: biological photonic crystals." *Journal of the Royal Society, Interface / the Royal Society* 5(18): 85-94.

Moon, R., A. Martini, et al. (2011). "Cellulose nanomaterials review: structure, properties and nanocomposites." *Chem. Soc. Rev.* 40(7): 3941-3994.

Moran, N. (2007). "Osmoregulation of leaf motor cells." *FEBS Letters* 581(12): 2337-2347.

Morillon, R., D. Liénard, et al. (2001). "Rapid movements of plants organs require solute-water cotransporters or contractile proteins." *Plant physiology* 127(3): 720-723.

Nissan A. H., Batten, G. L. (1990). "On the primacy of the hydrogen-bond in paper mechanics." *Tappi Journal* 73: 159-164.

Nobel (1970). *Introduction to Biophysical Plant Physiology*, W H Freeman.

Okuyama, T., H. Yamamoto, et al. (1994). "Growth stresses in tension wood: role of microfibrils and lignification." *Annales des Sciences Forestières* 51(3): 291-300.

Ortiz, C. and M. Boyce (2008). "Bioinspired Structural Materials." *Science* 319(5866): 1053-1054.

Paredez, A., C. Somerville, et al. (2006). "Visualization of Cellulose Synthase Demonstrates Functional Association with Microtubules." *Science* 312(5779): 1491-1495.

Paris, O., I. Burgert, et al. (2010). "Biomimetics and Biotemplating of Natural Materials." *MRS Bulletin* 35: 219-225.

Park, J.S., L. L. Chu, et al. (2001). "Bent-beam electrothermal actuators Part II: Linear and rotary microengines". *Journal of Microelectromechanical Systems* 10 (2): 255–262.

Postek, M., A. Vladár, et al. (2011). "Development of the metrology and imaging of cellulose nanocrystals." *Measurement Science and Technology* 22(2): 024005.

Que L., J. S. Park et al. (2001). "Bent-beam electrothermal actuators Part 1: Single beam and cascaded devices." *Journal of microelectromechanical systems* 10(2): 247-254.

- Raabe, D., C. Sachs, et al. (2005). "The crustacean exoskeleton as an example of a structurally and mechanically graded biological nanocomposite material." *Acta Materialia* 53(15): 4281-4292.
- Rafsanjani, A., D. Derome, et al. (2013). "Swelling of cellular solids: From conventional to re-entrant honeycombs." *Applied Physics Letters* 102(21): 211907.
- Raven, P. H., R. F. Evert, et al. (1999). *Biology of plants*. New York, Freeman and Company.
- Razghandi, K., L. Bertinetti, et al. (2014). "Hydro-actuation of ice plant seed capsules powered by water uptake." *Journal of Bioinspired, Biomimetic and Nanobiomaterials* 3(3): 169-182.
- Reiterer A., L. H., Tschegg H., Fratzl P. (1999). "Experimental evidence for a mechanical function of the cellulose microfibril angle in wood cell walls." *Philosophical Magazine, Part A* 79: 2173-2184.
- Reyssat, E. and L. Mahadevan (2009). "Hygromorphs: from pine cones to biomimetic bilayers." *Journal of the Royal Society Interface* 6(39): 951-957.
- Rho, J. Y., L. Kuhn-Spearing, et al. (1998). "Mechanical properties and the hierarchical structure of bone." *Medical engineering & physics* 20(2): 92-102.
- Roelfsema and R. Hedrich (2005). "In the light of stomatal opening: new insights into 'the Watergate'." *New Phytologist* 167(3): 665-691.
- Salmén, L. (2002). *Proceedings of 1st International Conference of the European Society of Wood Mechanics*, Lausanne, Switzerland, EPFL.
- Salmen, L. and J. Fahlen (2006). Reflections on the ultrastructure of softwood fibers. *Cellulose Chem. Technol.* 40, 3/4: 181-185.
- Saxena, I. M. and R. M. Brown (2000). "Cellulose synthases and related enzymes." *Current Opinion in Plant Biology*: 523-531.
- Schmid, W. (1925). "Morphologische, anatomische und entwicklungsgeschichtliche Untersuchungen an *Mesembryanthemum pseudotricatellum* Berger." *J. Naturf. Gesellsch. Zurich* 70.
- Schreiber, N., N. Gierlinger, et al. (2010). "G-fibres in storage roots of *Trifolium pratense* (Fabaceae): tensile stress generators for contraction." *Plant Journal* 61(5): 854-861.
- Shahinpoor, M. and M. S. Thompson (1995). "The Venus-Flytrap as a Model for a Biomimetic Material with Built-in Sensors and Actuators." *Materials Science & Engineering C-Biomimetic Materials Sensors and Systems* 2(4): 229-233.
- Sheppard, S. E. (1933). "The structure of xerogels of cellulose and derivatives." *Trans. Faraday Soc.* 29(140): 77-85.

- Shimomura (2010). "The new trends in next generation biomimetics material technology: learning from biodiversity." *SciTechnol Trends Quart Rev.* 37: 53–75.
- Sibaoka, T. (1991). "Rapid plant movements triggered by action potentials." *The botanical magazine, Shokubutsu-gaku-zasshi* 104(1): 73-95.
- Skaar, C. (1988). *Wood-water relations*. Berlin, Springer.
- Skotheim, J. and L. Mahadevan (2005). "Physical Limits and Design Principles for Plant and Fungal Movements." *Science* 308(5726): 1308-1310.
- Speck, T. and O. Speck (2008). *Process sequences in biomimetic research*. Design and Nature IV, Algarve, Portugal, WIT Press.
- Steinbrinck, C. (1883). "uber einige Friichtgehause, die ihre Samen infolge von Benetiung freilagen." *Ber. d. deutsch bot. Ges.* 1.
- Sundar, V., A. Yablon, et al. (2003). "Fibre-optical features of a glass sponge." *Nature* 424(6951): 899-900.
- Taiz, L. (1984). "Plant Cell Expansion: Regulation of Cell Wall Mechanical Properties." *Annual Review of Plant Physiology* 35(1): 585-657.
- Taya, M., A. Almajid, et al. (2003). "Design of bimorph piezo-composite actuators with functionally graded microstructure." *Sensors and Actuators A: Physical* 107(3): 248-260.
- Teraoka, I. (2002). *Polymer solutions an introduction to physical properties*. New York, Wiley.
- Thompson, D. A. (1992). *On Growth and Form*, Cambridge University Press.
- Thompson, J., J. Kindt, et al. (2001). "Bone indentation recovery time correlates with bond reforming time." *Nature* 414(6865): 773-776.
- Thygesen L., Engelund, E. T., Hoffmeyer P. (2010). "Water sorption in wood and modified wood at high values of relative humidity. Part I: Results for untreated, acetylated, and furfurylated Norway spruce." *Holzforschung* 64(3).
- Timoshenko, S. (1925). "Analysis of bi-metal thermostats." *Journal of the Optical Society of America and Review of Scientific Instruments* 11(3): 233-255.
- Tirrell, D. A. (1994). *Hierarchical structures in biology as a guide for new materials technology*, National Academy Press. Washington. DC.
- Toriyama, H. and M. J. Jaffe (1972). "Migration of Calcium and Its Role in the Regulation of Seismonasty in the Motor Cell of *Mimosa pudica* L." *Plant physiology* 49(1): 72-81.
- Treloar, L. R. G. (2005). *The physics of rubber elasticity*. Oxford, Oxford University Press.



Turcaud, S., L. Guiducci, et al. (2011). "An excursion into the design space of biomimetic architected biphasic actuators." *International Journal of Materials Research* 102(6): 607-612.

Uehlein, N. and R. Kaldenhoff (2008). "Aquaporins and plant leaf movements." *Annals of botany* 101(1): 1-4.

van der Sman, R. G. M. and M. B. J. Meinders (2011). "Prediction of the state diagram of starch water mixtures using the Flory-Huggins free volume theory." *Soft Matter* 7(2): 429-442.

Veytsman, B. A. and D. J. Cosgrove (1998). "A model of cell wall expansion based on thermodynamics of polymer networks." *Biophysical journal* 75(5): 2240-2250.

Vincent, J. (1990). *Structural biomaterials*, Princeton University Press.

Vincent, J. and D. Mann (2002). "Systematic technology transfer from biology to engineering." *Philosophical transactions. Series A, Mathematical, physical, and engineering sciences* 360(1791): 159-173.

Volkov, A., T. Adesina, et al. (2008). "Kinetics and mechanism of *Dionaea muscipula* trap closing." *Plant physiology* 146(2): 694-702.

Vukusic, P. and R. Sambles (2003). "Photonic structures in biology." *Nature* 424(6950): 852-855.

Wallenberger F. T., Weston, N. E. (2003). *Natural fibers, plastics and composites*. London, UK., Springer.

Wegst, U. G. K. and M. F. Ashby (2004). "The mechanical efficiency of natural materials." *Philosophical Magazine* 84(21): 2167-2186.

Weiner, S. and H. D. Wagner (1998). "THE MATERIAL BONE: Structure-Mechanical Function Relations." *Annual Review of Materials Science* 28(1): 271-298.

Zwaag, S. (2007). *Self healing materials an alternative approach to 20 centuries of materials science*. International Conference on Self Healing Materials, Springer.

## List of Figures

- Figure 1. Natural vs. Engineering materials.
- Figure 2. Biomimetic approaches.
- Figure 3. Classification of plant and fungal movements.
- Figure 4. Inflation's principle.
- Figure 5. Structure of the natural cellulose chains in the plant cell wall.
- Figure 6. Simple schematic of plant primary cell wall architecture and composition.
- Figure 7. Simple schematic of secondary cell wall architecture and composition.
- Figure 8. A typical sorption isotherm for wood.
- Figure 9. Stomatal movement.
- Figure 10. The Venus flytrap hydro-actuated movement.
- Figure 11. Anisotropy of swelling in the secondary cell wall.
- Figure 12. Passive hydro-actuated bending of the pine cone scales.
- Figure 13. Hydro-driven movement of wild wheat awns.
- Figure 14. Principles behind actuated-deformation of bi-layer structures.
- Figure 15. Proposed mechanisms for tensile stresses generation in tension wood fibres.
- Figure 16. First anatomical illustration of the ice plant seed capsule.
- Figure 17. Experimental set up for hydro-actuated stress generation in bilayer-cells.
- Figure 18. Ice plant seed capsule hierarchical morphology.
- Figure 19. Detailed analysis of keel movement.
- Figure 20. Separation of the two keels upon drying.
- Figure 21. Variation of the size of the keel's cells in wet open state.
- Figure 22. Composition and morphology of hygroscopic keel cells.
- Figure 23. Cryo-SEM micrographs of a cell transverse cross-section in swollen state.
- Figure 24. Cryo-SEM micrographs of a cell in swollen state.
- Figure 25. Cryo-SEM micrographs of keel's cell in swollen state.
- Figure 26. Cryo-SEM micrographs of CIL in higher magnification.
- Figure 27. Effect of enzymatic removal of cellulosic inner layer (CIL) on cell's actuation.
- Figure 28. Water adsorption-desorption isotherm in TGA.
- Figure 29. Keel water loss in TGA.
- Figure 30. Keel actuation in various PEG-water concentrations.
- Figure 31. Role of different solvent parameters in actuation of the ice plant keel.
- Figure 32. Simplified model of the hygroscopic keel's cells.
- Figure 33. Simple chemo-mechanical model for keel's actuation..
- Figure 34. Mechanism of the Flexing and Packing of the keels.
- Figure 35. Paper model for ice plant seed capsule locking mechanism.
- Figure 36. "Hygromorph model".
- Figure 37. Actuation patterns simulated for a variety of cross-sectional distributions of the active and passive elements.
- Figure 38. Abstraction of the principles behind ice plant hydro-actuation system.
- Figure 39. Hydro-actuated hydrogel-filled-honeycomb structures.
- Figure 40. Schematic illustration of the hydro-actuated bilayer-honeycomb device.
- Figure 41. Characterization of the active and passive elements in the Bilayer-cells.
- Figure 42. Deformation of the Bilayer-Cell upon actuation.

Figure 43. Reversible actuation of the bilayer-cell upon wetting/drying cycles.

Figure 44. Single bilayer and Bilayer-cell actuation upon wetting and exposure to 95%RH.

Figure 45. Passive hydro-actuation in bilayer-cell and bilayer honeycomb prototypes.

Figure 46. Passive hydro-actuation of bio-inspired bilayer-honeycomb device.

- Different movies have been made to show various aspect of the hydro-actuated movements at different hierarchical levels of both the biological model system and the developed prototype, which can be provided upon request.

## Acknowledgements

Foremost, I would like to express my gratitude to my doctoral advisor Ingo Burgert for supporting me during this period with his valuable guidance. I am thoroughly grateful for the opportunity to nurture under his supervision which provided me with an optimum flexibility within a structured plan. I would like to thank Peter Fratzl not only for the valuable scientific discussions we had, but also for providing a novel concept of leadership, under which scientists from various disciplines could work together in a cooperative and friendly environment.

I would also like to thank Michaela Eder, who gracefully accepted me into her group in MPIKG during the last phase of my project, and was always there for me with a smile on her face supporting me with any problem I had. I would like to specially thank Matt Harrington who was working on the project before I joined the group. I'm grateful to him for leading me through the first phase of the project during which I learnt a lot from him and his contributions in understanding the biological system. I also want to give my warm thanks to Luca Bertinetti for his support and guidance, helping me with a lot of patience and enthusiasm through various experiments, calculations etc.

I highly appreciate the collaboration with Sebastien Turcaud and Lorenzo Guiducci, and want to thank them for their contribution with finite element simulations and fruitful discussions, which ended up in various joint conference presentations and joint papers. I would also like to thank Markus Rüggeberg who was a great help not only during our work together in MPI, but also in my time as a PhD guest at ETH Zurich.

I also highly appreciate the support from Susann Weichold, Ingrid Zenke, Annemarie Martins, Antje Reinecke, Birgit Schonert and Gabriele Wienskol and all the colleagues from the workshop, who were always there to help with any problem concerning various experiments, materials etc. and a big thank you to Kerstin Gabbe for her great help concerning organizational matters. Warm thanks to all my colleagues and friends at the MPIKG and ETHZ, who made this period an enjoyable time with many wonderful memories that I will carry on for the rest of my life.

Thanks to all my friends who were there for me all along, from Berlin, to Zurich, to Stockholm, to Vancouver, to Tehran.

Finally, I would like to close this thesis with a big thank you "Hug" to my parents; Nothing in my life could have been possible without your support and love, Merci.

# Curriculum Vitae

Khashayar Razghandi

28th March 1983, Tehran, Iran

## Contact

Max Planck Institute of Colloids and Interfaces, Department of Biomaterials

Am Mühlenberg 1, 14476 Potsdam-Golm, Germany.

Khashayar.razghandi@mpikg.mpg.de

Khashayar.razghandi@gmail.com

+49 (0)17670875464

## Education

- PhD Candidate; Material Science and Engineering  
Max-Planck-Institute of Colloids and Interfaces, Biomaterials Department.  
(ETH Zurich, Institute for Building Materials, Switzerland.)  
Technical University of Berlin, Germany.  
Thesis: “Passive hydro-actuated unfolding of ice plant seed capsules as a concept generator for autonomously deforming devices.”
- M.Sc. Applied Polymer Science Jan. 2010  
M.L.U Halle, Germany.  
Thesis: “Electrospinning of PVA/PHB blend nanofibres as a scaffold for skin tissue engineering”
- B.Sc. Material Sci. & Eng., Industrial Metallurgy Sep. 2007  
Sharif University of Technology (SUT), Tehran, Iran.  
Thesis: “Equal channel angular pressing (ECAP) of Aluminum alloys”

## List of publications

- "Origami-like unfolding of hydro-actuated ice plant seed capsules", Nature Communications, 2011, 2: 337, M. J. Harrington, K. Razghandi, F. Ditsch, L. Guiducci, M. Rueggeberg, J. W. C. Dunlop, P. Fratzl, C. Neinhuis & I. Burgert.
- “Hydro-actuation of ice plant seed capsules powered by water uptake”, Journal of Bioinspired, Biomimetic and Nanobiomaterials, 2014, 3(3): 169-182, K. Razghandi, L. Bertinetti, L. Guiducci, J. W. C. Dunlop, C. Neinhuis, P. Fratzl and I. Burgert.
- Book chapter: “Hydro actuated plant devices.” In: Coupled fluid-elastic systems (eds. R. Guyer & A. Kim), Wiley, in press. K. Razghandi, S. Turcaud, I. Burgert.

- “Bio-inspired hydro-actuated Honeycomb Devices”, K. Razghandi, L. Guiducci, L. Bertinetti, S. Turcaud, J. Weaver, P. Fratzl, I. Burgert & J. W. C. Dunlop (In preparation).
- “Nanofibers from Blends of Polyvinyl Alcohol and Polyhydroxy Butyrate As Potential Scaffold Material for Tissue Engineering of Skin”, *Biomacromolecules*, 2010, 11 (12): 3413–3421. A. Sh. Asran, K. Razghandi, N. Aggarwal, G. H. Michler, T. Groth.

### *Conference contributions*

- Keynote speaker, Workshop “Moving Without Muscles”, Sept 2013, Grenoble, France.
- Conference Talk, EUROMAT, European Congress and Exhibition on advanced Material and Processes, Sept. 2013 Seville, Spain.
- Conference Talk & Poster, DGM, Bio-inspired Materials, International School and Conference on Biological Materials Science, 2012 Potsdam, Germany.
- Conference Talk & Poster, EUROMAT, European Congress and Exhibition on advanced Material and Processes, 2011 Montpellier, France.
- Conference Talk & Poster, COST Action FP0802 Thematic workshop Mixed numerical and experimental methods applied to the mechanical characterization of bio-based materials, 2011, Vila Real, Portugal.